

# Investigations on $\text{NO}_x$ emissions from a turbulent non-premixed bluff body stabilized flame.

Neel Kumar

Master of Science Thesis





# Investigations on $\text{NO}_x$ emissions from a turbulent non-premixed bluff body stabilized flame.

MASTER OF SCIENCE THESIS

by

Neel Kumar

In partial requirement for the degree of Master of Science in Mechanical  
Engineering at the Delft University of Technology, The Netherlands.

To be defended publicly on Friday August 27, 2021 at 9:00.

Supervisors:

Prof. Dr. Dirk Roekaerts  
Ir. Joey Telussa

Thesis committee:

Prof. Dr. Dirk Roekaerts	TU Delft
Ir. Joey Telussa	A.de Jong BV
Dr. ir. Mark Tummers	TU Delft
Dr. Domenico Lahaye	TU Delft

An electronic version of this thesis is available at <http://repository.tudelft.nl/>

Faculty of Mechanical, Maritime and Materials Engineering (3mE) · Delft University of  
Technology

The work in this thesis was completed with the support of TU Delft and A. de Jong BV. Their cooperation is hereby gratefully acknowledged.



Copyright © Process and Energy Department  
All rights reserved.



---

# Abstract

In this thesis work, we strive to describe and apply the modelling methodology for simulating a turbulent jet diffusion flame stabilized behind a bluff body by applying flamelet generated manifold (FGM) model and steady diffusion flamelet model for predicting the pollutant emissions from the flame.

The flame under consideration is a CH<sub>4</sub>/H<sub>2</sub> (1:1) bluff-body stabilized flame known as HM1. The numerical calculations of the flow physics has been completed by using a commercial CFD code namely Ansys Fluent 19-R3, where the computational domain is assumed to be two dimensional and axis-symmetric in nature due to the cylindrical symmetry of the burner with an structured grid for meshing. The turbulence is modelled by using a two equation Reynolds averaged Navier Stokes model, namely the standard  $k-\epsilon$  model with a modification in the  $C_{\epsilon 1}$  from 1.44 to 1.60. The chemical mechanism used in the project was the GRI 2.11 mechanism developed by the Gas Research Institute, USA. Next, post-processing tools like the Reactor Network Model (RNM) and Ansys NO<sub>x</sub> post-processor were used as an alternative, possibly a better way to obtain the NO species concentrations.

The acquired results from the simulation are thoroughly analysed and were compared to earlier results on the HM1 flame in the literature and validated by using the experimental data documented by the University of Sydney in collaboration with the TNF Workshop. The results showed that the steady diffusion flamelet performed better than the FGM model and was in acceptable agreement with the experimental data, although some under-prediction and overpredictions were reported for NO and OH species. In regard with the post-processing tools the RNM model performed better than the Ansys NO<sub>x</sub> post processor.



---

# Table of Contents

<b>Preface</b>	<b>ix</b>
<b>Acknowledgements</b>	<b>xi</b>
<b>1 Introduction</b>	<b>1</b>
1-1 State of affairs . . . . .	1
1-2 Research motivation and method. . . . .	6
1-2-1 Research Question. . . . .	7
1-3 Structure of thesis. . . . .	7
<b>2 Literature Survey and state of art.</b>	<b>9</b>
2-1 Combustion . . . . .	9
2-1-1 Fundamentals of combustion . . . . .	9
2-1-2 Turbulent Combustion . . . . .	13
2-1-3 Chemical kinetics . . . . .	15
2-2 Emissions . . . . .	16
2-2-1 Carbon monoxide . . . . .	16
2-2-2 Nitrogen oxides . . . . .	17
2-3 Chemical mechanisms . . . . .	19
2-4 Jet flame modelling . . . . .	20
2-4-1 Introduction . . . . .	20
2-4-2 Developments in numerical modeling of HM1 flame . . . . .	21
2-4-3 Summary of strong and weak points of the selected papers . . . . .	24
2-4-4 Conclusions and Recommendations . . . . .	26
2-5 Reactor Network Modeling . . . . .	26
2-5-1 Introduction . . . . .	26
2-5-2 Chemical reactor network (CRN) modeling – A basic outline. . . . .	28
2-5-3 Elements of CRN . . . . .	29
2-5-4 Developments in hybrid CFD-CRN approaches for prediction of NO <sub>x</sub> emission. . . . .	37
2-5-5 CRN solvers. . . . .	44
2-5-6 Conclusions. . . . .	45

<b>3</b>	<b>Theory</b>	<b>47</b>
3-1	Turbulence model . . . . .	47
3-2	Models for turbulence-chemistry interactions . . . . .	49
3-2-1	Steady diffusion flamelet model . . . . .	49
3-2-2	Flamelet generated manifold model . . . . .	51
3-3	Reactor Network Model theory . . . . .	52
3-4	Ansys NO <sub>x</sub> post-processor theory . . . . .	53
<b>4</b>	<b>Test case</b>	<b>55</b>
4-1	Introduction . . . . .	55
4-2	Measurement technique . . . . .	56
4-3	CFD set-up . . . . .	58
4-4	Grid independence study . . . . .	61
<b>5</b>	<b>Results</b>	<b>63</b>
5-1	Observations of the Results. . . . .	63
5-1-1	Velocity Field . . . . .	63
5-1-2	Temperature and Mixture Fraction. . . . .	67
5-1-3	Major species profiles. . . . .	71
5-1-4	Minor species profiles . . . . .	74
5-1-5	Performance of post-processing tools on NO <sub>x</sub> predictions. . . . .	79
5-2	Discussion and analysis . . . . .	87
5-2-1	Performance of combustion models . . . . .	87
5-2-2	Performance of post-processing tools . . . . .	87
<b>6</b>	<b>Conclusion and recommendations</b>	<b>89</b>
<b>A</b>	<b>FGM transport equations</b>	<b>91</b>
	<b>Glossary</b>	<b>99</b>
	List of Acronyms . . . . .	99
	List of Symbols . . . . .	99

---

# List of Figures

1-1	Importance of combustion in industries.[58]	2
1-2	Greenhouse gas emissions per economic sector[59]	3
1-3	Greenhouse gas emissions by economic sector[59]	4
1-4	Greenhouse gas emissions by gas.[59]	4
2-1	General classification of combustion.	11
2-2	Basic types of flames.	12
2-3	NO production with Fenimore prompt mechanism[57].	19
2-4	Types of turbulent jet flames.	20
2-5	Different model formulations for HM1 in literature.	21
2-6	Boundary conditions in literature of HM1	23
2-7	Different applications of CRN approach [32].	27
2-8	Diagram of a Perfectly Stirred Reactor [57].	28
2-9	Diagram of a Plug Flow Reactor [57].	29
2-10	Main elements of the conventional combustor[49].	30
2-11	Standard CRN construction algorithm using the component modeling approach[32].	31
2-12	Evolution of combustion modeling.	37
2-13	Schematic description of the glass melting furnace.[25]	38
2-14	Reactor network considered by Falcitelli et al.[25]	39
2-15	Reactor network considered by Nguyen and Park[28]	40
2-16	Numerical procedure proposed by Cuoci et al.[5]	41
2-17	Details of the investigated flames.	41
2-18	Schema chart for AGNES tool [45]	44
4-1	Image of HM1 flame. [41]	55

4-2	Representation of the bluff-body burner [41]	56
4-3	Radial profiles for scalar data validation. [15]	57
4-4	Representation of computational domain	58
4-5	Enlarged view of mesh	59
4-6	Breakdown of the numerical simulations	60
4-7	Grid independence test	62
5-1	Radial profiles of U-component of velocity.	64
5-2	Contours for streamlines for velocity	65
5-3	Contour for velocity vector	65
5-4	Contour for velocity magnitude.	65
5-5	Radial profiles of V-component of velocity.	66
5-6	Radial profiles of the mean temperature	67
5-7	Contour of temperature for FGM model.	68
5-8	Contour of mixture fraction for FGM model.	68
5-9	Radial profiles of the mean mixture fraction.	69
5-10	Radial profiles of rms of the mixture fraction.	70
5-11	Radial profiles of H <sub>2</sub> O mass fraction.	71
5-12	Contour of CO <sub>2</sub> for FGM model.	72
5-13	Contour of CO <sub>2</sub> for SDF model.	72
5-14	Radial profiles of CO <sub>2</sub> mass fraction.	73
5-15	Contours of CO for FGM model	74
5-16	Contours of CO for SDF model	74
5-17	Radial profiles of CO mass fraction.	75
5-18	Radial profiles of OH mass fraction.	76
5-19	Contour of NO for FGM model	77
5-20	Contour of NO for SDF model	77
5-21	Radial profiles of NO mass fraction.	78
5-22	Temperature profile by RNM tool.	79
5-23	NO profile by RNM tool.	79
5-24	Radical profiles of NO mass fractions with RNM model.	80
5-25	Radical profiles of CO mass fractions with RNM model.	81
5-26	Contours of NO mass fraction predicted by RNM for SDF model as baseline	82
5-27	Contours of CO mass fraction predicted by RNM for SDF model as baseline	82
5-28	NO profiles with RNM tool for SDF model	83
5-29	CO profiles with RNM tool for SDF model	84
5-30	Radical profiles of NO mass fractions with RNM model and NO <sub>x</sub> post processor.	85

---

# List of Tables

2-1	General fuel classification for combustion. . . . .	10
4-1	Geometrical dimensions . . . . .	58
4-2	Mesh characteristics. . . . .	58
4-3	Mesh quality. . . . .	59
4-4	Grid resolutions for Richardson extrapolation. . . . .	62



---

# Preface

On January 2021, I joined the research and development department of A. de Jong BV, The Netherlands, for conducting my master thesis work on emission prediction from a bluff body stabilized flame, particularly the HM1 flame, this study was initiated to generate a standard procedure for emission calculations that can be than replicated and applied to the calculations of emissions from the in-house industrial burners manufactured by A. de Jong BV.

During the period of the thesis work I received invaluable and inestimable support and guidance from Prof. Dirk Roekaerts and Mr. Joey Telussa, I am grateful to my supervisors Prof. Roekaerts and Mr. Telussa for introducing me to the topic of turbulent combustion in general and emissions predictions using FGM and chemical reactor networking (CRN) in particular and helping me to understand CRN models for the non-premixed turbulent flames. I pay my sincere acknowledgment to Mr. Mark Senden and the entire management team of A. de Jong BV, for giving me the opportunity to conduct the project in their organization. I would also like to express my gratitude to Prof. Arvind Gangoli Rao and Mr. Rishikesh Sampat for their advice and guidance on constructing CRNs by using AGNES software for Sandia D flame.

This document presents the literature research needed to understand the background of the thesis project and then setting priorities on the domain of interest to tackle the problem of emissions quantification produced by bluff body stabilized flame in a systematic and effective way. The document is divided into 6 chapters. The first chapter present the comprehensive view of industrial combustion systems taking the burner technology as the focal point, because that is the potential domain where this thesis finds its application on the other hand the second and third chapter present the state of art of theoretical and modeling aspects of combustion science that are vital for the thesis project. Together these three chapters functions as the constitution for the thesis project.

Later, in the forth chapter we present our test case, that is the HM1 flame, in this chapter the applied methods and modeling approaches are also presented in detail with a special interest on emission predictions by using FGM and CRN methods, the entire modeling study was performed on Ansys Fluent 19 R3 software. Chapter 5 deals with the acquired CFD and CRN results from the test case and chapter 6 constitutes the end of the thesis project, where we present the our conclusions from the thesis project and then propose some recommendations

on the modeling approach that can be of value for the similar studies or can be favored while extending this study to more complex industrial burners.

Neel Kumar

Delft, The Netherlands

August 23, 2021

---

# Acknowledgements

I would like to take this opportunity to pay my gratitude to people that have been cardinal to the successful completion of the thesis project.

First of all I would like to express my sincere gratitude towards Prof. Dr. Dirk Roekaerts and Ir. Joey Telussa for guiding me through the research activities needed for the thesis project. During the period of thesis we came across many challenges on multiple fronts of software, theory and resources, but we tenaciously continued to work towards the project while finding alternatives and improvising the resources.

I would also like to thank Ir. Ramon Winkel for his support on post-processing steps needed for calculation of  $\text{NO}_x$  concentrations and the entire fraternity of A. de Jong BV. During the thesis period my father Dr. Vipin Kumar and my mother Manisha Kumar acted as pillars of motivation and encouragement for me also my friends specially Mr. Cristopher Morales Ubal and Mr. Ivan Ban also played a very important role in boosting my morale and motivation as this thesis work was performed in the COVID-19 pandemic thus support of friends and family was very vital for personal mental well being.

Delft, University of Technology  
August 23, 2021

Neel Kumar



“If you are out to describe the truth, leave elegance to the tailor.”

— *Ludwig Eduard Boltzmann (1844-1906)*



---

# Chapter 1

---

## Introduction

This chapter presents the formal background and motivation of the thesis work in an incisive manner with the intent to get familiarized with the domain of combustion technology in general and emission predictions in particular.

### 1-1 State of affairs

Historically, combustion technology was one of the pillars for industrial revolution that led to economic growth and betterment of humanity, till now the domain of combustion science and technology remains relevant and active in the scientific community for developing better products and energy systems. Fundamentally, the science of combustion is complex and complicated by many factors as it is a highly nonlinear phenomenon and incorporates the coupling of fluid dynamic and detailed chemical mechanisms, which makes even simple combustion studies very daunting[1].

Combustion technology has an immense effect on our daily lives both directly and indirectly, from the cooking stoves that we use for preparing our food to the vehicles we drive for commuting and the products we utilize for sustaining our lives like electronics, sanitary ware, chemicals (bulk, fine or specialty chemicals) all depends on the process of combustion either for getting manufactured, processed or getting powered (usually electronics). Thus industry depends excessively on combustion process; figure 1 shows the importance of combustion in respective industries. The major domains of applications of combustion are also depicted in table 1,



**Figure 1-1:** Importance of combustion in industries.[58]

Industry	Operation
Metal melting	Steel making Brass melting Bronze melting Aluminum melting
Metal heat treating	Aluminum heat treating Brass heat treating Iron heat treating Steel heat treating Copper annealing Copper heat treatment
Drying	Paint drying Meat smoking Coffee roasting Varnish cooking
Calcining	Cement making
Clay Firing	Clay burning Brick making
Non metallic materials making	Glass making Glass annealing
Textile manufacturing	Drying operation Finishing operation
Paper and Printing Chemicals	Drying operation Glycol Reboiler operation Freeze Protection Tank Heating

Table-1, Common industrial combustion applications.



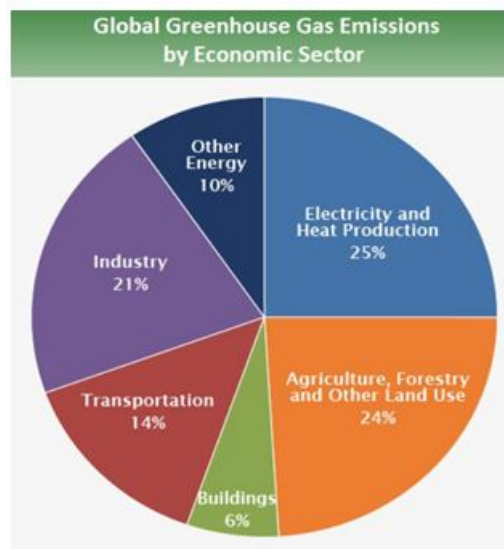


Figure 1-3: Greenhouse gas emissions by economic sector[59]

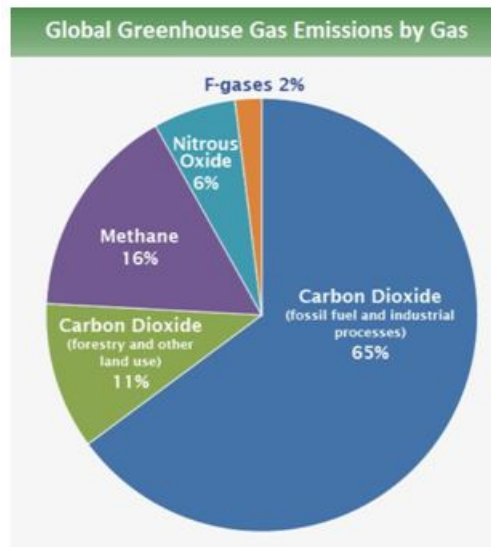


Figure 1-4: Greenhouse gas emissions by gas.[59]

Thus, from the above paragraphs we can state that the industrial combustion systems have an important role to play in greenhouse gas emissions, thus efforts must be taken to mitigate the emissions from the combustion systems, for doing this we have to put efforts in developing a strategy to produce novel/better systems, for this we can allude to the report published by the U.S. department of energy (DOE), titled as Industrial Combustion Vision: A Vision by and for the Industrial Combustion Community,[58] From the report we only consider the topics related to burner research and development as the thesis work is confined to burner systems. From the report of DOE, we conclude that the goals envisioned in the year 2000 are still not achieved completely, thus we can make efforts to achieve them by using new design tools/procedures.

For research and development in burner systems, it will be wise to handle the product development in stages, as investigating a industrial burner right off would not be a systematic and efficient way to contribute towards research and development efforts due to very complex nature of the industrial burner and lack of experimental data for validation step. Thus we propose to consider the partially premixed bluff- body stabilized flame as a test case for our research on improving the emission predictions capabilities by considering the available simulation tools and techniques in the market, by this we would contribute towards accessing the emission prediction capabilities of the tools and techniques; here tools are the softwares used by the users to simulate combustion systems and techniques are the computational models like turbulence models, combustion models etc.

## 1-2 Research motivation and method.

After the regulatory and governmental bodies revised the emission regulations in the Netherlands[24], the energy sector particularly the industrial burner manufacturers became more attentive and responsive to address the needs to curb emissions from the burners. The main motivation of the project comes from the effort to address these needs to develop better burner technology capable of adhering to governmental regulations.

Thus to respond to the above needs, the research and development activities required to advance the burner technology can be divided into 6 classifications namely – environmental quality, process improvement, fuel flexibility, health, safety, and reliability, energy efficiency and materials[40]. We are more interested in the environmental quality classification and thus intend to develop a robust technique/procedure to accurately and economically predict the emissions which will also assist in understanding the combustion process within the burner resulting in design advancement of burners. The methodology for the project is elucidated below.

The objective of the thesis work is to develop an emission prediction method that is reliable, fast and economical. From literature and industrial product development perspective, the emission prediction is a complicated problem as it involves the coupling of complex flow physics and chemical reaction mechanisms.

Thus, there is dire need to develop a modelling approach with lower computational cost, better chemistry analysis and fast result acquisition, to satisfy this we need to make advancements from a fundamental level, i.e. analyzing the fundamental building blocks of the computational models. For, modelling the reacting flows we need to consider two main ingredients in the computational models that are; turbulence model and combustion model, further to capture the coupling of flow physics and chemical mechanisms we have to include the interaction of turbulence and chemical mechanisms and this association is represented in a computational model by turbulence-chemistry interaction. Thus to effectively model the reacting flows with a focus on emission predictions, we have to understand and carefully implement the turbulence-chemistry interactions in our simulations.

One of the approaches to satisfy these objectives is to use a robust combustion model to predict the thermo-chemical properties of the flame, coupled with a post-processing techniques like chemical reactor networks (CRN),  $\text{NO}_x$  post-processor etc. As this approach has already shown promising results in the aerospace sector for emissions predictions from aircraft gas turbines thus we are interested to develop this methodology for emissions prediction in burner systems also.

For the project, the CFD study will be carried out on a bluff-body stabilized flame with two different combustion models, namely the steady diffusion flamelet model and the flamelet generated manifold (FGM) model. Then we use two different post-processing tools available in Ansys Fluent software to predict  $\text{NO}_x$  emissions. Here, we will use reactor network model (RNM) and  $\text{NO}_x$  post processor model to post-process our CFD simulations. The RNM

model is a inbuilt CRN generation tool in Ansys Fluent that models the combustion system (under study) into a system of ideal PSR reactors that takes the inputs like mass flow rate, temperature of fuel etc. from the CFD setup and then predicts the emissions characteristics of the combustion process, By this we will be able to capture detailed chemistry with fast acquisition of results. Also this will give us the opportunity to conduct sensitivity analysis.

### 1-2-1 Research Question.

While there has been several extensive work were combustion models have been used to simulate the bluff-body stabilized flame but this study focuses on comparing the two popular combustion models for partially pre-mixed flames namely FGM model and steady diffusion flamelet model with steady state RANS simulation to predict  $\text{NO}_x$  emissions from the flame, by this we aspire to propose a "best practice" for modelling bluff-body stabilized flames in particular and practical industrial re-circulating flows in general. Thus the following research questions has been framed for the purpose of this thesis project:

1. Which combustion models should be used to get the most reliable results for the turbulence-chemistry interaction for a bluff-body stabilized flame?
2. Does using a detailed chemical mechanism corresponds to better emission prediction results ?
3. Does the predictions of NO species calculated by CFD simulations improve if we include post-processing tools like RNM or  $\text{NO}_x$  post-processor in the simulations?

## 1-3 Structure of thesis.

The structure of the thesis describes the general plan of action that is employed to systematically approach the research questions described above. The approach is as follows; in the first chapter the state of affairs of combustion technology is covered with a brief background about the current domains available for further development with concise explanations of the test case and modelling techniques that will be employed to simulate the test case.

In the second chapter the state of art and the literature that is referred is articulated. The third chapter deals with the theoretical aspects of the thesis project where the computational models used for simulation are discussed further, the fourth chapter deals with the full description of the test case, on the other hand the fifth chapter consists of the results that are obtained from the modelling with the corresponding verification and validation of the results. Chapter six which is also the last chapter touches on the concluding remarks and recommendation from the project.



# Literature Survey and state of art.

## 2-1 Combustion

As, it can be referred from chapter one, combustion technology is not a new domain of research. Substantial amount of research has been done and completed on combustion technology. In this chapter, we try to elucidate the basic theory of combustion science, more advanced theoretical treatment on combustion will be presented in chapter 3.

### 2-1-1 Fundamentals of combustion

Combustion is a chemical reaction in which fuel and oxidant reacts to produce chemical products usually accompanied by heat release but heat release may or may not accompany light emission[31], Typically combustion is exothermic and oxidative in nature but it can be endothermic reaction also for instance in case of pyrolysis where solid fuels are utilized. In the chemical reaction the atoms of the reactants are conserved but the molecules are not conserved, i.e. when the reactants molecules react a rearrangement of atoms takes place resulting into product molecules with no creation or destruction of atoms[31].

Thus, we can infer that there are 3 main components of a combustion process, namely fuel, oxidizer and the reaction products. Basically the fuel species consists of carbon and hydrogen atoms referred as hydrocarbons and the oxidizer species generally consists of oxygen and nitrogen atoms[39]. The combinations of fuel and oxidizer species are termed as reactants, these reactants are exposed to an ignition source which supplements the oxidation of fuel resulting in combustion outside the burner. If the reactants also vaporize during combustion then we observe a “flame”, due to the flame, heat is liberated which inturn supplies adequate energy to overcome the activation energy barrier for initiating combustion and also makes the chemical reaction self contained.

Type of fuel	Examples
Gaseous fuels	Natural gas, Liquid Petroleum Gas, coal gas, syngas etc.
Liquid fuels	Petroleum, Kerosene, Diesel etc.
Solid fuels	Lignite, Wood, Anthracite etc.

**Table 2-1:** General fuel classification for combustion.

Broadly fuels are classified as solid, liquid and gaseous fuels. Commonly used fuels of each category are tabulated in table 2-1.

Selection of fuel is done on the basis of its availability, cost and inherent properties; one of the foremost property is the calorific value of the fuel, it is defined as the amount of energy liberated from burning one kilogram of the fuel[1]. The calorific value dictates the required flow rate of the fuel inside the burner, which is then introduced to an appropriate amount of oxidizer to instigate combustion. Atmospheric air is the standard oxidizer used in burners however properties like moisture and temperature can be manipulated by using appropriate equipment like pre-heater etc for increasing performance standards of the burners. In the burners the mass flow rate of both the fuel and oxidizer should be maintained throughout the operation cycle to ensure complete combustion usually for methane as a fuel, 1 kg/s of methane and 17 kg/s of air has to be maintained for complete combustion.

Thus the quantity of available fuel and oxidizer is a critical factor in combustion thus it needs to be properly determined, we generally use mole numbers to properly quantify the amount of species reacted of fuel and oxidizer[31]. One mole of substance corresponds to  $6.023 \cdot 10^{23}$  particles and is related to Avogadro's number as  $N_a = 6.023 \cdot 10^{23} \text{ mol}^{-1}$ . Now, as the mass quantification standard is framed, we can deal with the stoichiometry of the chemical reaction. Commonly used concepts in stoichiometric studies are explained below as –

- Mass fraction :- The mass fraction  $y_i$  defined as the ratio of mass of the species to the total mass, depicted as  $y_i = \frac{m_i}{\sum m_i}$
- Molar mass:- The molar mass is the mass of one mol of species. Example molar mass of carbon is 12 g/mol
- Mole fraction:- The mole fraction can be defined as the ratio of the mole number  $a_i$  of species to the aggregated mole number  $a = \sum a_i$
- Density :- Density is an intensive property of a system it is defined as the ratio of mass to the volume of the system. The SI unit of density is  $\text{kg}/\text{m}^3$

Now, after the basic concepts of stoichiometry have been established we can utilize them for describing and defining the concept of equivalence ratio. As, from the above paragraphs we discussed that the mass flow rate of fuel and oxidiser is one of the vital factor which determines the nature of the combustion process and its outcome. Thus, these mass flow rates are usually described as air to fuel ratio or fuel to air ratio, apart from this there is a more standard way of defining these quantities by using the equivalence ratio. The equivalence ratio is the ratio of the actual air or fuel quantity to the stoichiometric air or fuel quantity.

Thus, if fuel to air ratio is considered, the corresponding equivalence ratio can be defined as,

$$\phi = \frac{\left(\frac{m_{fuel}}{m_{air}}\right)}{\left(\frac{m_{fuel}}{m_{air}}\right)_{st}} \quad (2-1)$$

Thus, in a similar way if air to fuel ratio is considered then the corresponding equivalence ratio will be;

$$\lambda = \frac{\left(\frac{m_{air}}{m_{fuel}}\right)}{\left(\frac{m_{air}}{m_{fuel}}\right)_{st}} \quad (2-2)$$

The main objective of using equivalence ratio is to compare the proportion of fuel to air or vice versa. Based on the equivalence ratio we can classify the mixture of air and fuel into three categories namely[31]:-

- Fuel- rich, if equivalence ratio is greater than 1 ,  $\phi > 1$
- Fuel -lean, if equivalence ratio is less than 1 ,  $\phi < 1$
- Stoichiometric, if equivalence ratio is equal to 1 ,  $\phi = 1$

### **Classification of combustion.**

Due to the intrinsic complex nature of combustion process, the classification of the phenomenon becomes a strenuous task but it can be illustrated by the below figure in a concise manner.

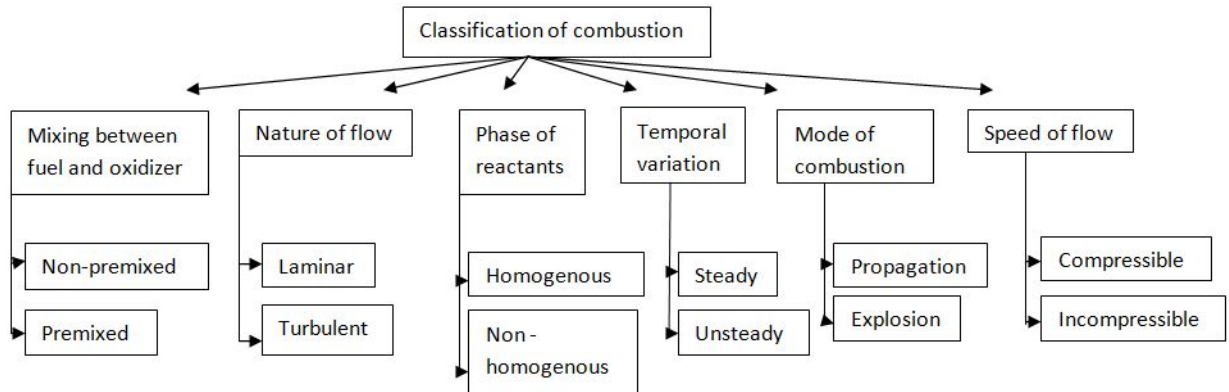


**Figure 2-1:** General classification of combustion.

As, this thesis project is devoted on burner systems, thus we limit our scope to classification of flames and not to the entire discipline of combustion. Flame classification can be initiated from the juncture where the mixing of fuel and air takes place, when reactant mixture is in proper proportions it is termed as flammable, when such a flammable mixture is supplied into the combustion chamber and introduced to a localized ignition source it results into a combustion reaction. Depending on the geometry and configuration of the combustion chamber

a ‘volumetric reaction’ can be initiated over the complete chamber volume concomitantly [2].

The boundary conditions of the reaction along with the composition of reactants and combustion chamber pressure dictates the intensity of reaction and the propagation speed of this chain reaction[2]. In a large combustion chamber, the localized ignition source will initiate the reaction only in a small region of the combustion chamber, this localized reaction zone is termed the flame.

The generated flame will then propagate into the combustion chamber with a speed, manducating the available reactant mixture inside the combustion chamber, based on the speed of the flame it can be classified as supersonic or subsonic also termed as detonation and deflagration respectively.

If the reactant mixture is fed into the burner and ignition source is introduced at the outflow port location then a stationary flame will be developed at a close proximity to the outflow port[2]. This is termed as premixed combustion. Flame speed and its corresponding temperature are important attributes of this type of combustion.

On the other hand, if fuel and oxidizer are supplied into the combustion chamber from different ports then, they will mix together due to mass diffusion and convection processes. When the ignition source is introduced to this mixture, the combustion reaction will only be initiated at locations where the fuel and air are in proper proportions, thus flame will be formed at specific locations. These types of flames are termed as non-premixed flames. In this situation the rate of chemical reaction is usually high[2].

Thus, from the above discussion we can conclude that due to difference in the mixing scheme of fuel and oxidizer, the flames can be broadly classified as premixed and non-premixed and further each of this classification can have laminar and turbulent flow behaviour. The figure below concludes the classification of flames.

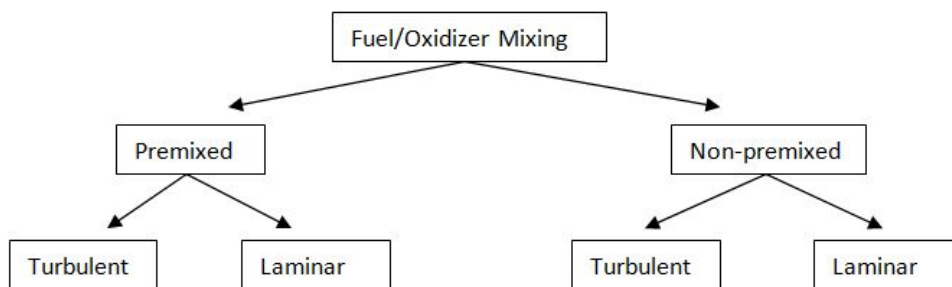


**Figure 2-2:** Basic types of flames.

Now, each category of flame type can be further discussed as:-

- Laminar premixed flames; In laminar premixed flames, the mixing between fuel and air is achieved before combustion process and the fluid flow is laminar in nature. The flame propagates with a speed known as laminar burning velocity or flame speed ( $v_L$ ) and this velocity depends on the mixture composition, pressure and initial temperature [31].

The laminar burning velocity should be higher than the velocity of the unburnt reactant mixture, else the flame will blow off [31].

- Turbulent premixed flames; In turbulent premixed flames, the mixing between air and fuel is achieved before combustion but after the ignition the flame propagates bearing turbulence. However, if the turbulence intensity of the flame is low then it can be approximated as an ensemble of laminar premixed flames [31].
- Laminar non-premixed flames; In laminar non-premixed flames the mixing of fuel and air occurs simultaneously with combustion process and the flow has a laminar nature. These flames can be further segmented as laminar counterflow and laminar coflow non-premixed flames [31].
- Turbulent non-premixed flames; In case of turbulent non-premixed flames the flame depicts turbulent behaviour. These types of flames are usually used in industrial combustion systems.

## 2-1-2 Turbulent Combustion

Turbulent combustion is the phenomenon that is at the epicenter of modern propulsion and energy systems and it is also critical for the development of future low-carbon energy systems. Thus, its understanding becomes important for practical reasons for developing safe, economical and efficient energy systems.

As, we already documented the flame definition and its classifications we can bring about the dynamical phenomenon that it poses, when the flame is produced it propagates into the furnace or freely propagates (unbounded flame) in environment with an acceleration associated with it, while propagation it interacts with the flow inside the furnace/environment and as a result of this interaction it modifies the temperature, density and viscosity of the flow, due to this interaction turbulence is generated and is termed as flame generated turbulence. Now, once turbulence is established in the flow it produces its own response to the flame by altering the flame structure and its speed of propagation.

To better understand the above described phenomenon we have to understand the crux of turbulence. A flow becomes turbulent at fairly large Reynolds numbers. Turbulence can be described as local fluctuations in the properties of fluid like density, pressure etc, thus these properties are represented as averages and are described as contributions from the mean and fluctuating parts [46]. If we take example of velocity in a turbulent flow it can be denoted as,

$$v = \bar{v} + v' \quad (2-3)$$

Where,  $\bar{v}$  represents the mean contributions and  $v'$  represents the fluctuating contributions. Further, we can define the turbulence intensity (I) as, the ratio of root mean square of fluctuations to mean component of the variable (here, velocity), thus denoted as:-

$$I = \sqrt{\bar{v}'^2} / \bar{v} \quad (2-4)$$

The numerator term in eq.2-4, is also written as  $u_{rms}$ , larger the value of  $u_{rms}$  indicates larger level of turbulence[46]. Although, computing turbulence intensity is not adequate to describe turbulent combustion, as the vital concern is to know the distribution of turbulence energy based on the length scales over the fluid flow field. The turbulence fluctuations can be ranging from the largest scales known as integral length scale ( $l_t$ ) to the smallest scales known as Kolmogorov length scale ( $\eta_k$ ).

For the case of isotropic and homogeneous turbulence, the turbulence energy cascade dissipates the energy from the largest scales to smallest scales and this dissipation of kinetic energy  $k$  is denoted as the ratio of kinetic energy,  $u'(r)^2$  to time scale  $\frac{r}{u'(r)}$ , given by:-

$$\epsilon = \frac{u'(r)^2}{\frac{r}{u'(r)}} = \frac{u'(r)^3}{r} \quad (2-5)$$

During the energy cascade the Reynolds number decreases from  $Re_t$  to close to unity[46]. Through this we can find the smallest scale present in the turbulent flow i.e. the Kolmogorov scale, presented as:-

$$Re_k = Re(\eta_k) = \frac{u'_k \eta_k}{\nu} = \frac{\epsilon^{1/3} (\eta_k)^{4/3}}{\nu} = 1 \quad (2-6)$$

Where,  $\nu$  corresponds to kinematic viscosity and  $u'$  is the characteristic velocity. Thus, we can write the expression for Kolmogorov scales as:-

$$\eta_k = (\nu^3 / \epsilon)^{1/4} \quad (2-7)$$

Similarly, the Reynolds number for the integral scale  $l_t$  is given by:-

$$Re_t = Re(l_t) = u' l_t / \nu \quad (2-8)$$

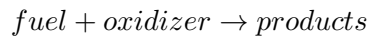
Now, by using relations 2-5,2-7 and 2-8, we can get the ratio of largest length scale to the smallest length scale as [46]:-

$$\frac{l_t}{\eta_k} = \frac{u'^3 / \epsilon}{(\nu^3 / \epsilon)^{1/4}} = (Re_t)^{3/4} \quad (2-9)$$

After, reviewing the length scales we can consider the effects of turbulence on the flames, In this case we will encounter two kind of flames, (a) turbulent premixed and (b) turbulent non-premixed flames. Detailed description of these flames will be provided in chapter 3, particularly turbulent non-premixed flames, where we will consider the modeling aspects of these flames.

### 2-1-3 Chemical kinetics

The study of rates of chemical reaction are dealt in the domain of chemical kinetics. In general combustion reaction can be described as -



The combustion process involves a chain of reactions with production of large amount of intermediate products, due to this complex process the accurate chemical details of the oxidation of fuels is not available in a concise form. The general form of a reaction mechanism with a collection of elementary reaction can be written as -

$$\sum_{i=1}^{N_s} v'_{ij} S_i = \sum_{i=1}^{N_s} v''_{ij} S_i$$

Where,  $v'_{ij}$  and  $v''_{ij}$  represents the forward and backward stoichiometric coefficients of species  $i$  in reaction  $j$  and  $S_i$  denotes the species  $i$  and  $N_s$  is the total number of species. Also for this equation we will have forward and backward reaction rate coefficients[39]. These reaction rate coefficients can be written by using Arrhenius equation as -

$$k = AT^n e^{-E_a/R_u T}$$

Where,  $E_a$  defined as the activation energy.  $A$ ,  $n$  and  $E_a$  are called the rate constants and need to be specified for every reaction in a given mechanism.

#### Residence time

A important factor which effects the chemical kinetics in the combustion chamber is the residence time. The residence time is related to the reactant fluid which is present in the combustion chamber and it can be defined as the total time spend by the reactant fluid inside a control volume (which can be a combustion chamber). Mathematically it can defined as :-

$$\tau = \frac{\rho V}{\dot{m}} \quad (2-10)$$

Where,

- $\tau$  is the residence time
- $\rho$  is the density of the reactant mixture
- $V$  is the control volume
- $\dot{m}$  is the mass flow rate of the reactant mixture

### Reaction time

The reaction time of a chemical reaction can be defined as the time taken for a significant concentration change of a species in the reaction. For a species 'n', the reaction time can be defined as:-

$$\tau_{reaction} = \frac{[n]}{d[n]/dt} \quad (2-11)$$

Where,

- $\tau_{reaction}$  is the reaction time.
- $[n]$  is the concentration of  $n^{th}$  species.
- $d[n]/dt$  is the concentration change rate of  $n^{th}$  species.

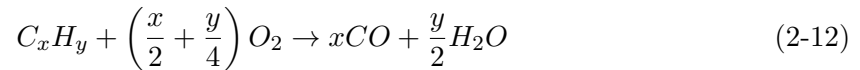
## 2-2 Emissions

Due to the combustion of reactant mixture, combustion products are formed. These combustion product/s are usually termed as flue or exhaust gas/es. These emissions that are discharged as exhaust gases are generally harmful to the environment in various ways, for instance carbon dioxide which is one of the major compound emitted increases the global warming, NO species on the other hand contribute to lung cancer, colorectal cancer and also contribute to complications in functioning of human heart.

In this section we will briefly describe the emissions mechanisms of the dominant compounds of exhaust gas namely carbon monoxide and NO species. This study will provide a comprehensive understanding on emission chemistry which will complement us to form strategies to control the concentration/s of the compounds of emissions for developing better energy systems.

### 2-2-1 Carbon monoxide

In case of complete combustion of reactant mixture, the products produced will be carbon dioxide and water, however when this combustion is incomplete carbon monoxide is produced[57]. This reaction can be represented as a two step global mechanism as:-



In the first reaction of the above mechanism, due to rapid oxidation CO and  $H_2O$  are produced, it is followed by the second reaction in which CO is oxidized into  $CO_2$ . However, the complete oxidation of CO to  $CO_2$  is not properly represented in this reaction. This oxidation reaction is slow but the oxidation rate can be increase by introduction of hydrogen species [57]. Water is the most common hydrogen containing compound which is used for oxidizing CO, the reaction can be represented as :-





The reaction (2-14) serves as an initiating step and does not have significant contribution in the formation of  $CO_2$  [57]. The important reaction leading to the production of  $CO_2$  is (2-16) which is also the chain propagating step, which produces the hydrogen radicals that reacts with oxygen to produce OH and oxygen radicals, these radicals again react with CO and O radicals resulting in the oxidation of  $CO_2$ . Thus, reaction 2-16, is the most important step in this mechanism and from the kinetic analysis of this reaction we can state two important observations of CO oxidation [57]-

- In case of insufficient supply of oxygen, the CO production increases.
- In the case of low residence time with high temperature lead to an increase in CO production.

### 2-2-2 Nitrogen oxides

Although, nitric oxide is a minor species in the combustion but it is important to study it due to its contribution to air pollution and health hazards associated with it. In our case, the fuel used in combustion will be 50 percent by volume of  $CH_4$  and 50 percent by volume of  $H_2$ , thus inherently it does not contain nitrogen. In fuels that are devoid of nitrogen, nitric oxide is formed by three chemical mechanisms by involving nitrogen from the air, these mechanisms are:-

#### Zeldovich or thermal mechanism

The thermal mechanism takes place in high temperature combustion for a wide range of equivalence ratios [57]. The Zeldovich mechanism can be represented as two chain reactions depicted as :-



It can be extended by addition of a reaction with OH as :-



The forward and backward rate coefficients for the above three reactions can be listed as [57] :-

$$k_{rxn1,f} = 1.8 \cdot 10^{11} \exp[-38,370/T(K)]$$

$$k_{rxn1,r} = 3.8 \cdot 10^{10} \exp[-425/T(K)]$$

$$k_{rxn2,f} = 1.8 \cdot 10^7 T \exp[-4680/T(K)]$$

$$k_{rxn2,r} = 3.8 \cdot 10^6 T \exp[-20,820/T(K)]$$

$$k_{rxn3,f} = 7.1 \cdot 10^{10} \exp[-450/T(K)]$$

$$k_{rxn3,r} = 1.7 \cdot 10^{11} \exp[-24,560/T(K)]$$

These three reaction (i.e. 2-18,2-19,2-20) described above are termed as extended Zeldovich mechanism. This mechanism can be coupled with the fuel chemistry through the  $O_2$ , O and OH species but it can be uncoupled for processes where the fuel combustion gets completed before production of NO, in this case, provided that the time scales are sufficiently long, we can assume that the concentrations of  $N_2, O_2$ , O and OH have equilibrium values and steady state is acquired by N atoms [57]. From these assumptions NO formation analysis becomes easier. Also, if we impose another assumption stating that the NO concentrations are less than the equilibrium values then the reverse reaction can be avoided, this will give us a rate expression as:-

$$\frac{d[NO]}{dt} = 2k_{rxn1,f}[O]_{eq}[N_2]_{eq} \quad (2-21)$$

As, the activation energy for the reaction 2-18, is large i.e. 319,050 kJ/kmol therefore, there is a strong dependence on temperature for this reaction. Thus, the Zeldovich mechanism is only relevant for high temperatures it becomes irrelevant at temperatures below 1800 K [57]. On comparing with the time scales of fuel oxidation process, the NO has a slower formation rate, thus generally thermal NO is formed in the post-flame gases.

### Fenimore or prompt mechanism

Fenimore mechanism is relevant in rich combustion processes. It was discovered by Fenimore that some amount of NO species were rapidly formed by laminar premixed flames around their flame-zone, before they (the NO species) could be formed by the Zeldovich mechanism. Fenimore termed these NO species as "prompt NO". Generally, in Fenimore mechanism the hydrocarbon radicals react with the nitrogen species to form amines or cyano compounds [57], which leads into the formation of NO, the Fenimore mechanism can be represented as :-



In this mechanism the reaction (2-22) is the rate limiting step in the mechanism. But if the equivalence ratios are less than 1.2, then the chemical mechanism can be depicted as :-



If the equivalence ratios are bigger than 1.2 then the chemistry becomes more complex. As recorded by Miller and Bowman the above reaction scheme is not rapid and NO is transformed to HCN, obstructing NO production[36]. Figure (2-3) shows the Fenimore prompt mechanism, in this figure we can observe that the coupling of prompt mechanism with Zeldovich mechanism actually inhibits the production of NO.

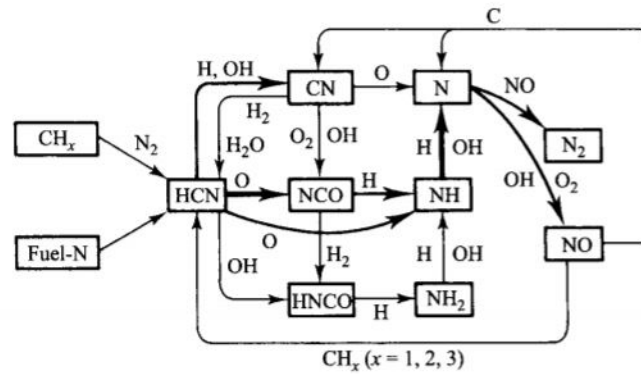


Figure 2-3: NO production with Fenimore prompt mechanism[57].

### $N_2O$ - intermediate mechanism

$N_2O$  - intermediate mechanism has relevance in the formation of NO in a fuel-lean, low temperature combustion process, for equivalence ratios less than 0.8 ( $\phi < 0.8$ ) [57]. The mechanism can be represented in three steps depicted as :-



This mechanism is important in formulating NO control strategies for lean premixed combustion processes.

## 2-3 Chemical mechanisms

As stated previously, combustion is not a single step elementary reaction it consists of multiple number of reactions and species. Reactions that take place while combustion process are compiled as a mechanism file. Gas reaction rate coefficients are measured experimentally for all the reactions which depend upon the temperature, pressure and branching ratio. The mechanism file consist of three separate files namely:-

1. Transport data file
2. Element/species data file
3. Thermodynamic data file

Ansys Fluent software imports the chemical mechanisms in CHEMKIN format and uses these three data files for numerical simulation. As, our fuel consists of methane and hydrogen

thus, we will consider chemical mechanisms for methane and hydrogen. Generally there are two popularly used mechanisms for methane combustion namely, GRI Mech. 3.0 and Leeds mechanism[32]. GRI-Mech 3.0 consists of 53 species and 325 reactions with associated rate and thermodynamic data.

## 2-4 Jet flame modelling

### 2-4-1 Introduction

In this section we attempt to present the past studies that have been completed in the domain of jet modeling, particularly the modeling of bluff-body stabilized flame namely HM1. However, a detailed account of HM1 flame will be presented in chapter 4 of the thesis report; in this section the research methodologies of other authors on modelling HM1 flame are presented.

Turbulent jet flames, have proven to be a very vital component in turbulent combustion research, they act as a perfect test case to analyze the fundamental issues in combustion science like turbulence-chemistry interactions, radiation effects etc from the numerical combustion models used for simulating reacting flows. In the current study we have selected a bluff-body stabilized flame as our test case, but the reader should be aware that in literature there are multiple types of turbulent jet flames, for illustration of the major types of jet flames, refer to figure 2-4.

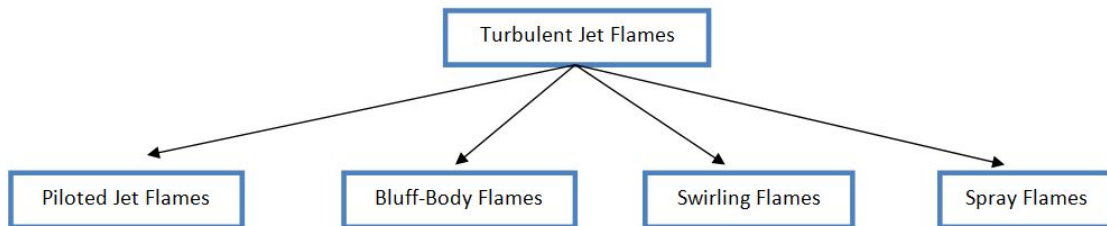


**Figure 2-4:** Types of turbulent jet flames.

The major types of turbulent jet flames can be categorized as piloted, bluff-body, swirl and spray flames, but further fragmentation/categorization can be done within each type of the flame by introducing different chemistry of the fuel and by changing the dimensions of the burner's inlet. In the next section we will discuss the recent developments in numerical modelling for HM1 flame.

### 2-4-2 Developments in numerical modeling of HM1 flame

Although, the experimental studies on HM1 are well established and dates back to 1998, when Dally et al. [11], first studied the HM1 by doing experimental investigations, the numerical investigation of HM1 still poses challenges on design engineers. Here we focus only on the most relevant numerical studies on HM1 published since 2005. By doing this we will be able to formulate a “plan of action” for modelling the HM1 flame. For better illustration of the literature of HM1, we also present an overview by tabulating the details of relevant publications.

Model	Submodel	NOx model	Kinetic scheme	Remarks	Reference
Transported PDF	Monte Carlo Joint PDF velocity, scalar, frequency	Included in MC PDF algorithm	19 species ARM	--	K. Liu et al, 2005
Steady laminar flamelet	Steady flamelets in mixture fraction space (Flame Master), beta-pdf	Transport equation	Reduced Peters, GRI2.11, GRI3.0, San Diego	RSM, upstream extended domain	Ravikanti et al, 2009
Chemical reactor network (CRN)	Flamelet as underlying flame prediction, Kinetic postprocessing using KPPSMOKE	From CRN	Polimi_C1C3	Comparison with Fluent NOx post processor	Stagni et al, 2014
Laminar reaction rates	SAGE-solver	SAGE-solver	GRI3.0	--	Di Mauro, 2021
FGM	Counterflow solved in mixture fraction space, beta-pdf	From FGM	CRECK	--	Di Mauro, 2021

**Figure 2-5:** Different model formulations for HM1 in literature.

In 2005, Liu et al. [14], presented results obtained using the transported PDF method, also called Monte Carlo particle method for turbulence-chemistry interaction. In this approach (not yet mentioned in the literature review above), the turbulent fluctuations in the thermochemical composition are represented in a set of notional particles evolving with the flow and participating in mixing and reaction. Also fluctuations in the velocity fields are represented as particle properties. The model provides closure of the chemical mean source term since each particle has its own chemical source term and the mean can be obtained by averaging over particle properties. The simulations used an augmented reduced mechanism (ARM) which is based on GRI 2.11 mechanism. Nevertheless the computational cost is high since reaction proceeds in every particle. Good agreement with experiments was obtained, which is the reason to include it in the selected articles.

In 2008, Ravikanti et al.[16] investigated the HM1 flame by using non-adiabatic laminar flamelet model, by which they accounted the radiative heat loss and the effect of radiation

on the predictions of  $\text{NO}_x$  emissions. The chemical mechanism used by them was GRI 2.11 mechanism, as the non-adiabatic model can be further fragmented into non-adiabatic model with single (NADS) and multiple scalar dissipation rates (NADM) based on the variation in scalar dissipation in flamelet calculations. The authors compared the performance of both of these non-adiabatic flamelet models on predicting scalar concentrations. They used Reynolds stress transport model and modified  $k-\epsilon$  model for turbulence closure and then the predictions of the RSM and modified  $k-\epsilon$  model were compared. The CFD code used was an in-house software based using the finite volume method. The authors reported that the performance of the non-adiabatic flamelet models were in similar agreement with the adiabatic flamelet model thus they concluded that the radiation models have a minuscule effect on the overall results and with respect to turbulence models RSM performed better than modified  $k$ -epsilon in  $\text{NO}$  mass fraction predictions.

However, later in the same year (2008), Ravikanti et al.[17] published one more numerical investigation on the HM1 flame, in this study they used Reynolds stress transport model to represent the turbulence effects, the employed combustion model was laminar flamelet model. The main focus of this study was to observe the effects of chemical mechanisms on the results, thus the authors used four chemical mechanisms to do a comparative study keeping the combustion model as laminar flamelet model. Out of the four chemical mechanisms, one mechanism was a reduced chemical mechanism, namely Peters mechanism and the other three mechanisms belong to the class of detailed chemical mechanism namely GRI 2.11, GRI 3.0 and San Diego mechanisms. The result showed that overall, laminar flamelet model gives very good results with respect to the experimental data and the GRI 2.0 mechanism performed better than other mechanisms for  $\text{NO}$  mass fraction predictions.

In 2014, Stagni et al[10] proposed the use of their chemical reactor network model software KPPSMOKE, to post-process the CFD results of HM1 flame for predicting the  $\text{NO}_x$  concentrations. In this study the authors used Ansys Fluent (version 13.0) as the CFD software with the skeletal version of POLIMI-C1C31201 as their chemical mechanism for CFD simulations. The combustion model used was steady flamelet combustion model. The turbulence effects were modelled by using modified  $k-\epsilon$  model. After this the simulations were performed by using Ansys post-processor and unsteady flamelet model and KPPSMOKE software to compare the results of  $\text{NO}_x$  concentrations. The reported results showed a good numerical performance of KPPSMOKE software in predicting  $\text{NO}_x$  emissions, although the  $\text{NO}_x$  predictions of KPPSMOKE were not in full agreement to the experimental data but were better than the  $\text{NO}_x$  concentrations reported with CFD predictions and predictions from Ansys  $\text{NO}_x$  post-processor.

In 2019, Verma et al [13], investigated the HM1 flame by employing a three dimensional mesh with the flamelet generated manifold (FGM) model as their combustion model and the turbulence was modelled by using three RANS models namely the modified  $k-\epsilon$  model, the SST  $k-\omega$  model and the generalized  $k-\omega$  model (GEKO), the CFD software used was Ansys Fluent 2019-R1, the chemical mechanism used for this study was GRI 3.0 mechanism. They concluded that GEKO model with coefficients as  $C_{SEP}=2$ ,  $C_{NW}=1$ ,  $C_{MIX}=0.35$ ,  $C_{JET}=0.9$ , predicted better profiles of velocity and recirculation zone in the HM1 flame as compared with other models. Next, they compared the results with experimental data and reported

Models	Transported PDF	Steady laminar flamelet	CRN KPPSMOKE	Laminar rates	Flamelet Generated Manifold
Reference	Liu 2005	Ravikanti 2009	Stagni 2014	Di Mauro 2021	Di Mauro 2021
BC Fuel Jet Bulk velocity Imposed profile of mean and second moments	118 m/s Based on experimental data	118 m/s	118 m/s	118 m/s Imposed fully developed profile	118 m/s
BC bluff body Velocity Thermal	Slip	No-slip	No-slip Fixed temp	No-slip Adiabatic	No-slip Adiabatic
BC Air coflow Bulk velocity Imposed Profile	40 m/s	40 m/s	40 m/s	40 m/s Fully developed	40 m/s Fully developed
Remarks	Mentioned low sensitivity to slip or no-slip at bluff-body		Temperature value to be checked		

**Figure 2-6:** Boundary conditions in literature of HM1

good agreement with experimental data. They did not report  $\text{NO}_x$  predictions.

The most recent study on numerical modelling of HM1 flame was reported by Mauro et al. [8] in 2021, in which the authors report on studies made using the CFD code CONVERGE. They used standard two equations  $k-\epsilon$  model and the Speziale-Sarkar-Gatski Reynolds Stress Model for modelling turbulence with SAGE and FGM models as their combustion model with GRI 3.0 and CRECK chemical mechanisms. Then the authors did an examination by comparing the  $\text{NO}$  mass fraction results from simulations using standard wall function and enhanced wall treatment. The authors compared SAGE/GRI 3.0 mech. with FGM/CRECK combustion model by employing two approaches for near-wall regions. The results reported that the FGM/CRECK combustion model performed better than SAGE/GRI 3.0 mech. and overall the standard wall function approach showed better results than enhanced wall treatment.

Figure 2-6, illustrates the boundary conditions that have been used in the simulations of HM1 listed above.

### 2-4-3 Summary of strong and weak points of the selected papers

Based on a preliminary analysis of the papers the following strong and weak points of the articles can be pointed out:

#### K. Liu et al [14]

##### Strong

1. The joint velocity scalar frequency PDF approach is the most comprehensive representation of turbulent fluctuations in RANS context.
2. It is the most accurate one among the PDF approaches.
3. Boundary conditions were implemented using all available experimental information. The chemical source term is stored in a table generated during run time (ISAT).
4. Presented a comprehensive error analysis.
5. In summary: the best available result using PDF approaches.

##### Weak

1. No real weakness.
2. Reduced mechanism is used. Track record of ARM2 for  $\text{NO}_x$  predictions is not elaborated.
3. Improvements could come from the combination of more detailed chemistry and alternative micromixing models.

#### Ravikanti et al.[17]

##### Strong

1. This paper is the final one of a series, incorporating many insights gained on flamelet model strengths and weaknesses. This is their final choice, including second moment closure (RSM) for good prediction of velocity field, the selection of GRI 2.11 mechanism for  $\text{NO}_x$  predictions and the use of an extra equation for  $\text{NO}_x$ .
2. Influence of turbulent fluctuations in  $\text{NO}_x$  formation source term is taken into account.
3. In summary: the best possible results using steady flamelet modeling.

##### Weak

1. No real weakness.
2. A more extensive error analysis would be valuable.

#### A. Stagni et al.[10]

##### Strong

1. Based on extensive previous work on CRN methodology. Includes detailed description of the CRN solution methods.
2. Comparison between different chemical mechanisms is presented in the study, confirming good performance of GRI 2.11.
3. Comparison with the ANSYS Fluent  $\text{NO}_x$  post-processor results.
4. In summary: the best available result using CRN methodology.

**Weak**

1. The limitations of the steady flamelet model providing the basic flame structured may still be present in the final results.
2. Limitations due the choice for  $k-\epsilon$ ,  $C_{\epsilon 1}=1.6$ .

**A. Di Mauro et al. [8]****Strong**

1. The non-reacting case was studied first providing insight in the flow patterns. This motivates the selection of the turbulence model.
2. FGM is interesting because it is expected to be more accurate than steady flamelet and comparable to unsteady flamelet.
3. The comparison with SAGE shows the weakness of not including fluctuations.

**Weak**

1. Remaining limitations due the choice for  $k-\epsilon$ ,  $C_{\epsilon 1}=1.6$ .
2. The FGM approach is not clearly explained. The equation given in the paper seems for premixed flamelets only. Which flamelets were used? Was differential diffusion included?
3. The reason to use both standard and enhanced wall functions on the same grid is not clear.
4. The results of the two wall function approaches are not really consistent. Standard wall functions give somewhat better velocity field. But the enhanced wall function gives better temperature field. This discussion on wall treatment should have been elaborated with information on  $y^+$  value.
5. The suggestion to choose a different model constant  $C_{\epsilon 1}$  in the two wall treatments is ad hoc because the term containing this model constant is controlling phenomena far from the wall. One model constant cannot be tuned to optimise predictions both far away and close to the wall.
6. Remarkable that SAGE and FGM results provide almost the same mean temperature field. This would need further explanation.
7. Indications on axial location of radial profiles and the displayed experimental data points do not seem to agree with the other works.

## 2-4-4 Conclusions and Recommendations

Different mainstream modeling approaches to turbulent combustion have been applied to the HM1 flame. What remains to be done is to bring all results together in a comparative analysis providing direct comparison of the results. By making new figures the results can be directly compared. Only then a firm analysis of the remaining discrepancies between model and experiments and between models is possible.

The papers on PDF methods (Liu et al.[14]) and on flamelet models (Ravikanti et al. [17]) present the best possible results in the selected modeling approach.

The paper on CRN (Stagni et al. [10]) is excellent in the application of CRN, but may still not be the final answer when it comes to coupling an underlying less detailed turbulent combustion modeling to a kinetic post processor and furthermore for better  $\text{NO}_x$  prediction it should be extended so as to include in a better way the mean  $\text{NO}_x$  formation rate.

The paper on FGM model by Verma et al.[13] is unclear on some points and the study should be repeated with clear definition of flamelet equations, analysis of role of wall boundary conditions and also a better way the mean  $\text{NO}_x$  formation rate, including influence of turbulent fluctuations.

### Recommendations

1. The value of the CRN approach should be studied in more detail.
2. Working with Ansys Fluent the following work program is proposed (in order of priority):
  - Study the relative performance of obtaining  $\text{NO}_x$  from flamelet/FGM directly, from Fluent  $\text{NO}_x$  post-processor or from Fluent CRN option.
  - Study the relative performance of steady flamelet model and FGM.
  - Study the impact of the turbulence model ( $k-\epsilon$ ,  $C_{\epsilon 1}=1.6$  or RSM)
3. Because of the proven performance of GRI mech 2.11 for  $\text{NO}_x$  predictions it will be taken as chemical mechanism. When possible and useful, reduced mechanisms will also be used. (DRM19 based on GRI mech 2.11, ARM1 and ARM2 based on GRI mech 2.11)

## 2-5 Reactor Network Modeling

### 2-5-1 Introduction

The objective of this section is to present a review on the progress of the chemical reactor network (CRN) approach with its recent applications in combustion systems; here the structure of CRN will be dealt along with the recent approaches of CRN construction, along with the available CRN solvers. The section concludes with an efficiency analysis of the CRN approach in relation to emission prediction.

Due to strict emission legislations and a global initiative to reduce air pollutants, the use of a robust emission prediction tool becomes a necessity for development and testing of combustion systems. In the past the design, development, and performance analysis of combustors

were aided by experiments and empirical correlations which made the processes of design and performance analysis very expensive[6]. After the advent of computers, numerical simulations became a popular practice for the design and development process with less time and cost associated; still, these numerical approaches have limitations in simulating the reactive flows in practical combustion systems like furnaces with accurate flow physics and detailed chemistry[32].

One of the major limitation of the present numerical simulations are its inability to predict detailed chemistry or chemical kinetics of the combustion process, due to this proper emission analysis and further thermal performance studies of the industrial combustion system becomes difficult.

To counter this limitation of detailed chemistry analysis for emission predictions, the chemical reactor network (CRN) approach was developed that was able to predict detailed chemical kinetics in a combustor thus aided emission predictions in a very significant way[20]. In CRN approach a network of ideal reactors in constructed and then solved for obtaining the concentrations of the minor species in a constant volume[32]. CRN is one of the most efficient and low-cost computational tool in the market for predicting detailed chemistry[53]. Apart from emission predictions, CRN is also capable to analyze the static stability of the combustion process and it is also used in developing reduced-order chemical mechanisms[3], these applications make CRN an important tool in the combustion modeling process, figure 2-7, pictorially shows different domains of possible applications of CRN.

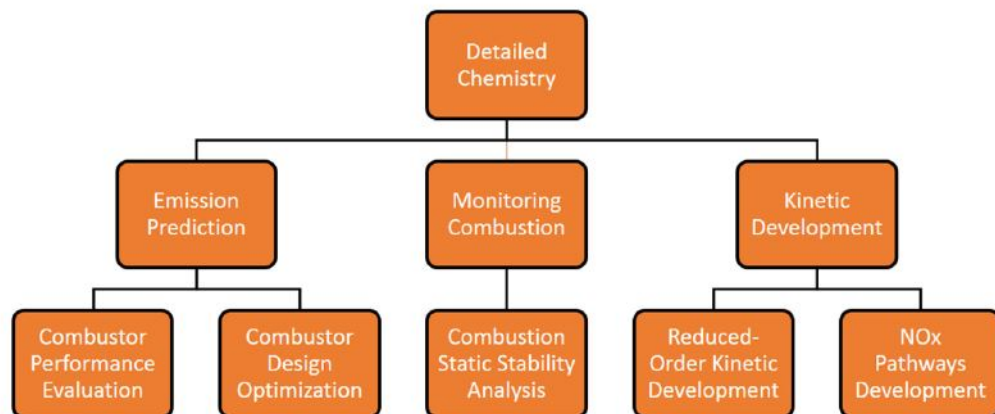


**Figure 2-7:** Different applications of CRN approach [32].

### 2-5-2 Chemical reactor network (CRN) modeling – A basic outline.

CRN approach is a methodology for modeling the combustion process in a combustor. Basically in CRN approach, the combustor volume is divided into several regions then these regions are modeled as ideal reactors. The flow field and chemical kinetics dictates the designation of the category of chemical reactor employed (e.g. PSR, PFR etc) and its interconnections with other subsequent reactors.

From the literature it is noted that CRN has acceptable accuracy in predicting detailed chemical kinetics of a combustion process at low costs with moderate to low predictions of the flow field inside the combustor. In CRN the category of reactor and its connections in CRN are dependent on the flow field and each reactor is interconnected with subsequent reactor through a parameter of the flow field. After a network of these reactors is constructed, a relevant combustion mechanism is introduced in the CRN. After this the governing equations of the reactor network is solved which gives the concentration of species and output temperatures of the reactors as the solution[32].

The CRN can be constructed by using four types of ideal reactors, namely – perfectly stirred reactor (PSR), partially stirred reactor (PaSR), mixing only reactor (MIX) and plug flow reactor (PFR). Now we can discuss each of these reactors in-detail below:-

- Perfectly stirred reactor (PSR)

In a PSR it is assumed that it undergoes fast and extreme mixing, thus in this system the flow field is completely turbulent with high mixing rates thus the chemical rates becomes insignificant[32]. Thus the chemical kinetics of the combustion process serves as a controlling factor of the combustion rate in the mixture[57].

As the mixture is assumed to be perfectly mixed thus the combustion process is not dependent on the flow parameters which let us to drop the equation for the conservation of momentum in the formulation[32]. Furthermore, the equation of energy, mass and species transport are time –independent which results in describing a PSR by a set of nonlinear algebraic equations which can be solved using Newton-Raphson method[57]. Below, the figure describes the schematic view of a PSR.

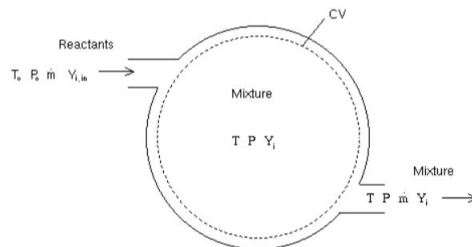


**Figure 2-8:** Diagram of a Perfectly Stirred Reactor [57].

- Plug flow reactor (PFR)

In this type of reactor a steady, one-dimensional and in-viscid ideal gas flow is assumed. It is also assumed that all the reactants entering the reactor are converted into the products due to absence of axial mixing. Due to these assumptions the nonlinear three-dimensional equations are converted into ordinary differential equations.

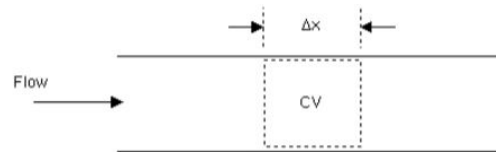


**Figure 2-9:** Diagram of a Plug Flow Reactor [57].

- MIX configuration.

MIX stands for an element in which the entering streams are uniformly mixed without the chemical reaction.

- Partially stirred reactor (PaSR)

PaSR reactors are used to capture the effects of flow perturbations or flow field disturbances in the CRN.

### 2-5-3 Elements of CRN

This section presents the fundamental elements needed to construct a CRN model; basically there are two major steps in construction of CRN model. The first step is to obtain the flow characteristics of the combustor, which can be done by using experimental methods, empirical methods or by computational fluid dynamic modeling approaches and the second step is to construct CRN model based on the acquired flow field, for doing this also we have simple empirical approaches to very detailed mathematical algorithms (which will be discussed in this section). This section discusses the above mentioned steps in detail with help of the available literature on the subject of CRN modeling.

#### 1. Flow field modeling

In the literature, there are three methods that are extensively used to calculate the flow field inside the combustor of interest. These methods are explained below:-

##### (a) Network approach

The network approach is a quasi one-dimensional method consisting of network elements. The network elements are created on the basis of the combustor design/-geometry [43]. These elements are interconnected to other corresponding elements

by nodes and each element is mathematically described by empirical equations. Once, all the governing equations of the elements are compiled, they can be solved as a system of linear equations by methods of linear algebra for obtaining physical parameters like temperature, pressure, mass flow and species concentration profiles inside the combustor, thus aiding us to calculate the flow field characteristics.

One of the main advantages of this approach is that it can provide detailed information about the internal flow field of the combustor[32], but the disadvantages of this method is the accuracy of the results and its inability to calculate the temperature distribution and flame stability in the regions of combustor having localized high temperatures[47].

Thus, this method presents a trade-off between accuracy and the computational cost in the flow field calculation. We would recommend this method to be used in the conceptual design phase of product development.

(b) Component modeling approach

The component modeling approach is the second approach by which we can calculate the one dimensional flow field in the combustor. In this approach the internal flow field of the combustor is divided into sections, these sections are connected to the corresponding section by stream parameters. The governing equation of each section is solved to extract the flow field which in-turn aids to extract flow properties of each 'zone'. In this approach the discretization of combustor volume is not completely user defined[32].

The main advantage of this approach is that it is very modular in application, thus the components can be arranged in multiple ways to get the optimized configuration of the combustion chamber. The components are described by models that can be empirical, semi-empirical or physical correlations. Figure below, shows the main elements that are utilized in the modeling of the combustion chamber.

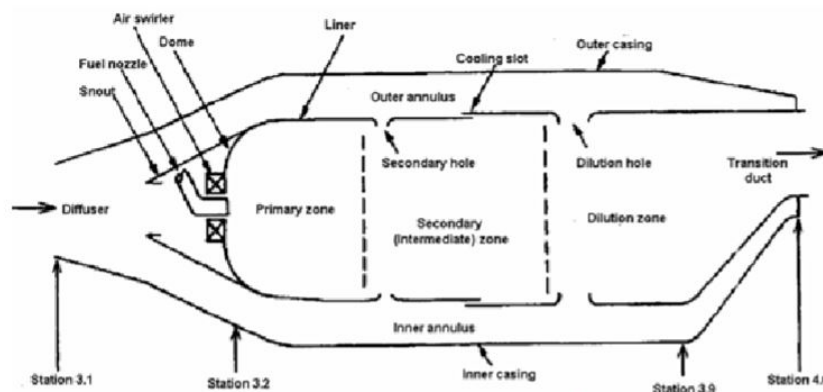
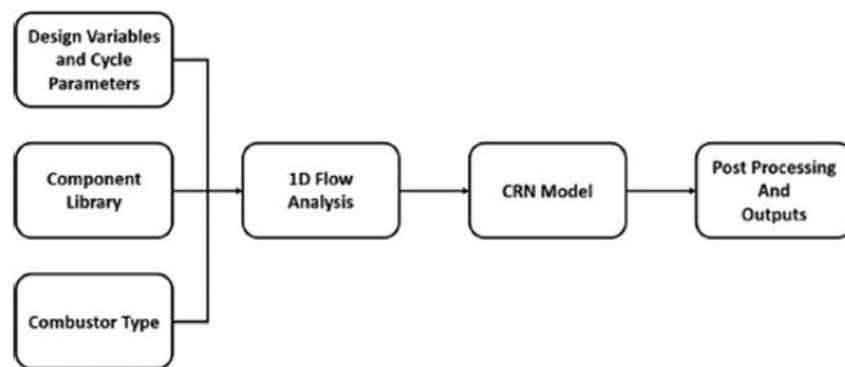


Figure 2-10: Main elements of the conventional combustor[49].

The elements of a conventional combustor consist of diffuser, injector, primary, secondary and dilution zones. The elements are the fundamental building blocks

required to model the flow field using component modeling approach. This approach is extensively applied in the preliminary design phase, for determining the optimized combustion geometry and combustion chamber dimensions[49]. It is also applied to analyze the configuration of the combustor in the design and off-design conditions.

Rezvani et al in 2009[49], presented a study in which the authors presented a semi-analytical emissions prediction method where they used component modeling approach to calculate the flow field inside an advanced gas turbine combustor and then used this extracted flow field to construct a CRN for pollutant emission analysis by using a standard algorithm described in figure below:-



**Figure 2-11:** Standard CRN construction algorithm using the component modeling approach[32].

Flow field characteristics like velocity vectors, temperature and species concentrations are the primary splitting criteria for constructing a CRN model by utilizing the component modeling approach[32]. Also, constructing CRN by utilizing component modeling approach is less computationally costly as compared to CFD-CRN approaches.

(c) Computational fluid dynamics modeling approach

The third approach for flow field modeling is by using CFD approach. Due to better access and increase in the computational power of the computers, CFD approach became an effective and reliable tool to model flow field inside the combustors. Although, CFD codes are considered as a competent and robust tool to predict the reactive flow field in combustors, they have limitations when detailed chemical reactions are introduced in the flow analysis, thus making the CFD methods inadequate for studying detailed chemical kinetics for the combustion process.

Thus, CFD codes are integrated with other post processing tools (like- KPP, Cantera etc.) to generate CRN models, thus making CFD methods as a robust tool to provide flow field characteristics required for generating CRNs.

The development of CRN models has tremendously improved by the help of CFD methods[32], as the CFD methods provide detailed information on the residence

time distribution and turbulent mixing for the reactive flows [32][29], this has led to the development of CFD-CRN algorithms[27]. The application of CFD-CRN algorithms have aided significantly in the prediction of minor species of the combustion process, especially in the prediction of NOx emissions in various industrial combustion systems like glass melting furnaces, gas boilers and coal-fired boilers[38].

Within CFD approaches for combustion modeling, the selection of correct turbulence models and combustion models is a very vital part for getting correct flow field results. Thus we present a general overview on the turbulence and combustion models:-

i. Turbulence modeling

Direct numerical simulation (DNS) is the most advanced simulation technique for solving turbulence, It solves the complete range of the spatial and temporal scales of turbulence in the Navier-Stokes equations, thus the whole computational domain is simulated from the integral scale to the Kolmogorov microscales. Due to this the computational cost of the simulation is very high even for flows in simple geometries with low Reynolds number[32].

The other approach for turbulence modeling is by using the large eddy simulation (LES) method. This method solves the larger, highly anisotropic eddies in the turbulent flow, while the smaller eddies are described by using a simple eddy-viscosity isotropic turbulence model[32], thus only the larger eddies are simulated while the smaller eddies are modeled. In literature, LES approaches have been used for simulating transient turbulent reactive flows[61][54].

Due to high computation costs involved with the above two turbulence models they are not very attractive for modeling the flow field of the industrial combustion systems; as a consequence these approaches (Direct Numerical Simulation (DNS) and LES) are deemed unsuitable for CFD-CRN studies for emissions prediction.

However, the Reynolds averaged Navier-Stokes (RANS) turbulence models are extensively used to calculate the flow field in the combustor at comparatively low computational costs. The RANS turbulence models are capable to predict the main flow field characteristics in an accurate and reliable manner[32]. Thus RANS models are generally used in CFD-CRN studies for emissions prediction.

ii. Combustion modeling

Combustion models are needed for predicting the species concentrations and flame structure of the combustion process. Generally, In a CFD simulation the number of species used is often limited to main reactants and products species to reduce the complexity and runtime of the simulations[51].

The chemical kinetics used in CFD simulations are generally limited to primary reactions with limited species rather than detailed chemical mechanisms, thus multiple step chemical kinetics is reduced to global kinetics where the in-

intermediate reactions are neglected[32].

As, in industrial combustion systems we encounter turbulent combustion, thus turbulent combustion models are used in CFD simulations to extract flow field and allied results. The most common models employed in simulating turbulent reactive flows are eddy breakup model (EBU), eddy dissipation model (EDM), finite rate /EDM, eddy dissipation concept (EDC) and flamelet based models (flamelet model, FGM)[32]. The models can be ranked according computation cost: the EDC model is the most expensive followed by flamelet/FGM and EDM[4]. This is because EDC using the detailed chemistry during the turbulent flow calculation whereas flamelet/FGM only used detailed chemistry in a pre-processing phase and EDM is using very simple chemistry.

In EBU model, the turbulent reaction rate for products is described as an average with turbulent mixing rate to model the combustion process, neglecting the chemical reaction rate. The EBU model is not so robust in modeling the lean and rich regimes of the combustion process[32].

The EDM model is used to simulate all types of combustion process i.e. turbulent pre-mixed and turbulent non pre-mixed combustion inside the combustor. The model assumes that the chemical reaction rates are higher than turbulent mixing rate [32] and the turbulent mixing rate controls the fast reaction rates. Also, the kinetics in the model is defined by one or two step mechanisms.

The finite-rate/EDM combines the EDM model with the finite-rate chemistry, by this combination the model is able to calculate the reaction rate with EDM and kinetic rates by using finite-rate chemistry[32]. This model is used to simulate turbulent reactive flows in a variety of combustors. However, while using this model the user has to adjust the constant coefficients of reactants and products, also to initiate the combustion reaction there is a need to introduce some products upfront and turbulence-chemistry interaction cannot be captured by this model. The EDC model is a improved version of EDM model for finite rate chemistry[32]. The EDM model is well suited for modeling with high steps reaction mechanisms. The EDC model has been applied to simulate premixed, non-premixed and partially premixed combustion processes.

The flamelet based models (flamelet model and flamelet generated manifold FGM model) are based on the assumption that the local state in any flame can be represented as flamelets which are flame states observed in representative laminar flames [30]. They can be used for diffusive, premixed or partially premixed flames, using proper selection of flamelets. This model is not directly suitable for slow reaction and non-equilibrium effects like ignition, extinction and slow chemistry. This in principle also puts limitations on the ability to predict  $\text{NO}_x$  formation[33].

In this work new simulation results using flamelet model and FGM will be presented. More information on the theory is provided in the Theory chapter.

## 2. CRN construction approaches

Based on the present literature there are three methods which are generally used to construct a CRN model (these approaches are described below). The choice for application of these approaches depends on the flow field input that is present with the designer, if we are dealing with simple geometries of the combustor with simple flow fields without re-circulation zones and multiple inlets then combustor can be divided into several zones represented by ideal reactors, in these cases we may apply empirical methods like component modeling or network modeling methods to calculate the flow field with CRN construction by “chemical reactor network without detailed geometry data”. But if complex combustor geometries are considered with complex flow field patterns including recirculation zones than we have to consider more complex methods to generate CRN by using “Approaches based on flow-field patterns” or by using “Systematic approaches”, to get a better overview of these approaches, we have listed them below as:-

### (a) Chemical reactor networks without detailed geometry data.

As, explained above this approach is used when we are considering a simple combustor geometry with simple flow field. In this approach the designer has to divide the flow field inside the combustor based on the velocity, temperature data by his/hers own ability and knowledge, usually the primary and secondary zones of combustion in the combustor are modeled by using PSRs and the PFRs represent the dilution zone of the combustion process.

Rizk et al in 1999[50], used this approach to model the diffusion flame for predicting the NO<sub>x</sub> emissions. The researchers divided the combustor flow field into several zones and each zone was represented by an ideal reactor. A parallel configuration of PSR was used to simulate the primary zone and the downstream combustion process was simulated by a series of PFRs. They concluded that the NO<sub>x</sub> emissions predicted by this approach were in good agreement with the experimental data.

Charest et al in 2006[22], used a simplified network of reactors to model the combustion process with a well stirred reactor (WSR) and a PFR for estimating the lengths of the primary and secondary zones and also estimating the pollutant emissions. The results obtained by this approach were compared with the CFD simulations of the combustion chamber and they concluded that the results were not in good agreement with each other, significant discrepancies existed in the concentrations of the pollutants.

### (b) Approaches based on the flow-field patterns.

This approach for CRN construction is used in the cases where we encounter complex combustor geometries and complex flow fields. The CRN model is constructed based on the flow field pattern in the combustor such as flame, post flame and recirculation zones, thus based on the flow field patterns the splitting of combustor volume into homogeneous zones takes place. Usually, CFD results on flow field are considered to construct CRN in this approach.

Novoselov et al in 2006[29], used this approach based on CFD flow field results and compared their results with two experiments. In this study they made significant efforts to model the injector and the main zones of the combustion process i.e. the flame, post flame and re-circulation zones. The resultant CRN model consisted of 31 ideal chemical reactors.

Lebedev et al in 2009[33], proposed a simplified strategy to predict the NO<sub>x</sub> emissions from a diffusive flame by using a simple CRN model, they also used CFD results to construct CRN model, mixture fraction and temperature field were used to divide the combustor volume into several homogeneous zones namely:- flame front zone, fuel rich zone and mixing zone. The NO<sub>x</sub> emission results were verified by using three different chemical mechanisms for methane.

In recent times this approach was used by Wang et al in 2016[60], to investigate the pollutant emissions from a combustor, particularly they investigated the effects of pressure on the pollutant emissions. The fuel used in combustion was syngas and concentration of species and temperature field were used to discretize the combustion zone into five homogeneous zones.

(c) Systematic approaches.

This approach is the most advanced method to create CRN model so far. The systematic approaches use mathematical algorithms to create CRNs based on the flow field that is calculated generally by CFD codes. These algorithms can discretize the flow field based on the user's criteria, this criteria is known as 'partitioning criteria'. Researchers have used many different partitioning criteria over the years to construct CRNs, thus there is no standard partitioning criteria for CRN generation and also the choice of criterion depends on the geometry and flow field of the combustor. Figure, represents the different types of partitioning criteria used by the researchers over time.

Falcitelli et al[25] were the pioneers in proposing an algorithm for constructing CRN from the CFD results. This proposed algorithm required multiple inputs from the CFD simulation, namely the temperature, mass fraction of fuel, O<sub>2</sub>, N<sub>2</sub>, CO<sub>2</sub>, H<sub>2</sub>O, CO, H<sub>2</sub>, H, O, OH, density, and specific mass flow vectors[32]. The working procedure of the algorithm can be stated as follows:-

- i. Algorithm starts with the calculation of the local stoichiometry by taking the ratio of the total mass of oxygen available and the oxygen required for complete oxidation to carbon-oxide and water.
- ii. After, this the flow field is classified based on the temperature field and stoichiometry.
- iii. Then, the regrouping of the classified cells takes place.
- iv. To account for mixing properties, an extra criterion of unmixedness index is introduced.
- v. Then the calculation of the volume of individual reactor, the operational temperature and the mass exchanged between the reactors is completed.

This algorithm has been verified on various industrial combustion systems like full-scale steam generator, boiler and glass furnaces[32].

After this study, Faravelli et al in 2003[26], proposed a new algorithm to extract CRNs there algorithm is known as SFIRN. Cuoci et al in 2007[23], while investigating the NO<sub>x</sub> emissions from a combustor used CFD method and a post processing tool called as kinetic post-processes (KPP) to predict the pollutant emission, In this study they used an algorithm to coarsen the CFD grid for grouping the cells into different zones, and then they carried out a sensitivity analysis to study the effects of mesh coarsening on the KPP results. They concluded that the resolution of CFD results had a major impact on the KPP results on pollutant concentrations [32].

#### 2-5-4 Developments in hybrid CFD-CRN approaches for prediction of NO<sub>x</sub> emission.

The usage of ideal chemical reactors for modeling combustion process was first initiated by S.L. Bragg in 1953 [21]. An improvement in the approach came with modeling the combustor volume as zones also known as “zonal combustion modeling”. Zonal modeling was used by Rubin et al[42] for evaluating the emissions produced by a gas turbine combustor. The figure below shows the evolution of combustion modeling, based on current trends.

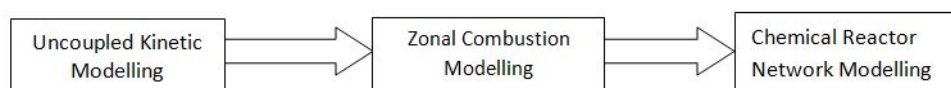


**Figure 2-12:** Evolution of combustion modeling.

After, the zonal modeling, direct applications of ideal chemical reactor network for combustion modeling emerged into the literature[25], but the CRN development method differed amongst the researchers, here we concentrate only on the CRN construction strategy, where the post-processed results of CFD simulations were used for the development of a chemical reactor network to predict the pollutant emissions particularly  $NO_x$  from the combustor.

The initial work following this strategy were initiated by Faravelli, Bua et al [56] in the year 2001 where they discussed a novel approach for predicting NO<sub>x</sub> formation from a industrial furnace connected to a boiler, where they obtained the flow and temperature fields in the furnace by using CFD model and then used SFIRN (Simplified Fluid dynamic by Ideal Reactor Network) approach to simplify the complex fluid behavior inside the furnace for construction of network of ideal reactors, this approach was able to predict the kinetic and fluid dynamics description of the industrial furnace in a detailed way.

An important milestone of the study by Faravelli, Bua et al (2001)[56] was that it proposed a methodology to couple the fluid-dynamic and combustion reactions in an effective and systematic way. As, in general emission studies the predictions of combustion byproducts whose concentrations are in ppms or even ppbs is very difficult to capture and thus requires the designer to apply detailed kinetic models to predict them but if we apply detailed models with the CFD codes then the computational cost becomes very high with CFD-combustion model integration issues thus making the result reporting unfeasible.

One of this pollutant byproduct is NO<sub>x</sub> which has concentrations in ppms or even ppbs in a general industrial combustion system. Prediction of NO<sub>x</sub> can be decoupled from the CFD simulations, this is due to the differences in time scales and also as the minor species have a very marginal effect on the main combustion process, thus global temperature and flow field remains unchanged, thus as a consequence we can apply a detailed kinetic model for the NO<sub>x</sub> formation mechanism that can be later coupled with the CFD results for emission predictions.

In the same year of 2001, Falcitelli, Pasini and Tognotti [25] proposed an integrated methodology for predicting NO<sub>x</sub> emissions from industrial combustion systems, here the test case was a glass furnace with two firing ports, each having three barrel burners. The reactive mixture consisted of natural gas and air, figure 2-13, shows the diagram of the furnace geometry. Two configuration of the furnace were considered in this study with 5 and 10 MW of thermal load.

The most important part of this study was that it was capable to handle industrial combustion systems having complex flow dynamics with multiple inlet streams and internal re-circulating flows, having an additional advantage of predicting minor species other than NO<sub>x</sub>. The flow field was calculated by CFD simulation by using IPSE code (Developed by ENEL S.p.A.) and the NO<sub>x</sub> concentrations were predicted by using a novel RNA (Reactor Network Analysis) methodology.

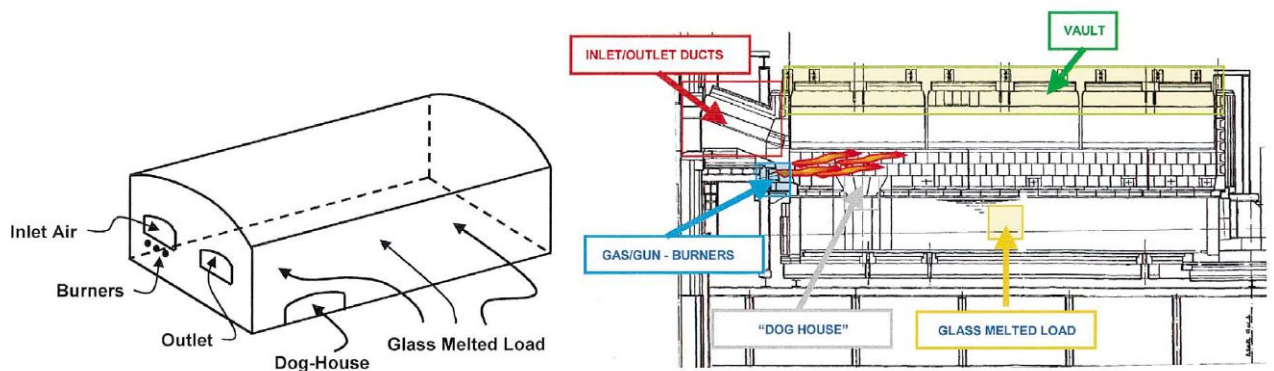


**Figure 2-13:** Schematic description of the glass melting furnace.[25]

For the CFD study, the finest possible grid was taken of 21525 nodes and the boundary conditions for radiative heat transfer were employed, here radiation was solved by using discrete ordinates method, same as derived by Truelove (1987) and the adopted combustion model was based on ‘quasi-global’ scheme (Westbrook and Dryer,1984) together with single irreversible reaction of the fuel (CH<sub>4</sub>) and oxygen to form CO and H<sub>2</sub>, with a detailed oxidation mechanism of CO/H<sub>2</sub> with 8 species and 9 reactions

Furthermore, the reactor network was extracted by RNA method based on the temperature and stoichiometry ranges and the furnace was modeled as 12 zones by ideal chemical reactors, the reactor network extracted can be shown as:-

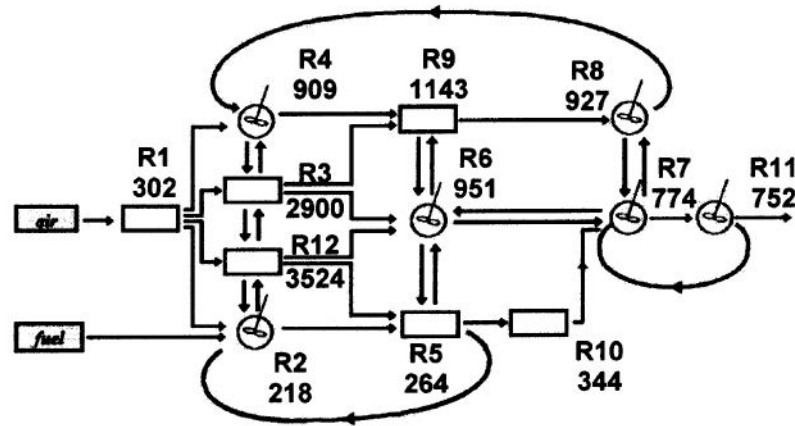


**Figure 2-14:** Reactor network considered by Falcitelli et al.[25]

The CRN was solved by DSMOKE software. The results from this study showed that the CFD temperature field was affected by radiative boundary conditions and the local oxygen concentration field was highly correlated to the chemical reactions sub-model used in the CFD simulation. On the other hand the RNA method was found to be sensitive towards even slight changes in the CFD field.

Marco Mancini in 2006[34] conducted the research on Moderate or Intense Low-oxygen Dilution (MILD) (Moderate and Intensive Low Oxygen Dilution) combustion on the IFRF furnace with reactor network approach to analyze NO<sub>x</sub> formation and destruction with emphasis on examining whether the current mathematical models can predict the characteristics of the MILD combustion technology. The author concluded that the calculations of the CRN showed excellent agreement between the species concentrations measured (experimentally) in the furnace and those predicted by the CRN.

In the recent studies on the CFD-CRN models, Nguyen Park in 2013 [28], investigated a industrial combustor for predicting the NO<sub>x</sub> emissions produced by the system with analyzing the effects of equivalence ratio, swirl angle and fuel ratio. The fuel used in the modeling was methane. The overall fuel-air equivalence ratio was varied from 0.5 to 0.7, the swirl angles of 30, 45, and 60 degrees were used and the fuel-air mixture ratio was varied from 0 to 10 % of the injector flow rate.

The authors used STAR-CCM software (version 4.02) for performing the CFD simulations. In the CFD simulations, the k-epsilon model was taken to capture turbulence and for combustion reaction analysis the Eddy-break-up (EDC) combustion model was selected.

For the CRN development, CHEMKIN software was used with GRI 3.0 as the chemical kinetic mechanism. The industrial combustor was divided into six zones based on the flow

temperature, velocity, and the chemical species concentrations from the CFD simulation, the extracted network can be shown as:-

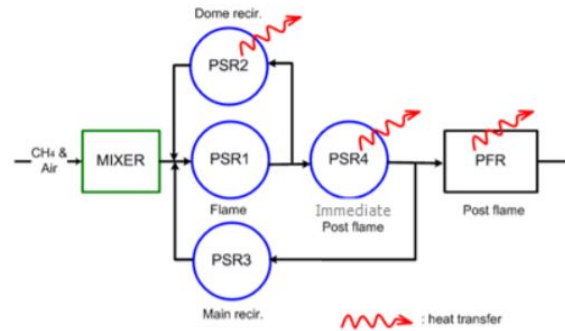


**Figure 2-15:** Reactor network considered by Nguyen and Park[28]

The major observations/results by authors were that, the reliability of CFD simulations was an important parameter for producing CRN models for the industrial combustor. Furthermore, the NO<sub>x</sub> results predicted by CRN model were in good agreement with the experimental data.

The swirl had a minimal effect on the NO<sub>x</sub> emissions but the lowest NO<sub>x</sub> concentrations were found at swirl vane angle of 45 degree also, the NO<sub>x</sub> emission tend to increase with an increase in the pilot fuel ratio.

Cuoci, Frassoldati et al.in 2012 [5] presented a very detailed study on the prediction of NO<sub>x</sub> emission in combustion system where they employed a kinetic post processing (KPP) technique to the CFD simulations of turbulent flames in complex geometries, for CFD study they used RANS models with global kinetic mechanisms. Then a network of ideal perfectly stirred reactors (PSRs) was extracted from the CFD simulation on the basis of flow, temperature and composition fields.

The temperature and mass flow rates were assumed to be constant during the post processing operation, then a detailed kinetic mechanism was introduced in the CRN model and then this network was solved by using Newton's global method. A pictorial representation of this numerical procedure can be seen in the figure below.

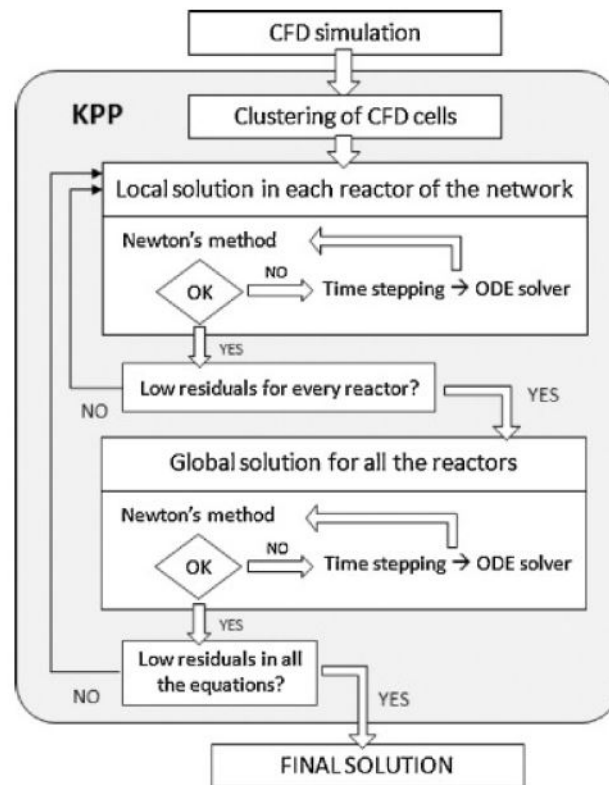


**Figure 2-16:** Numerical procedure proposed by Cuoci et al.[5]

In the study, three axis-symmetric turbulent non-premixed jet flames were investigated for validating the KPP technique. The figure shows the table for the details of investigated flames.

Flame Type	CFD Modeling Approach		KPP Approach
	Kinetic Scheme	Turbulence model	Kinetic Scheme
CO/H <sub>2</sub> Flame	PolimiH2CO1201	Standard k-e model	PolimiH2CO1201NOx
H <sub>2</sub> /He Flame	PolimiH2CO1201	Standard k-e model	PolimiH2CO1201NOx
CH <sub>4</sub> /H <sub>2</sub> /N <sub>2</sub> Flame	DRM22	Standard k-e model	GRI 3.0

**Figure 2-17:** Details of the investigated flames.

The unique aspect of this procedure was that very large network of reactors (order of 100,000) can be solved with complex flow field patterns (like re-circulations, multiphase flows etc). Also a combustor operating in MILD conditions was modeled for estimating the Nitrogen oxides (NO<sub>x</sub>) concentrations by employing this procedure [5]. The results of the study showed good agreement with the experimental data, which proved that KPP technique is a reliable tool for emission prediction studies. But from the study, some limitations of the KPP procedure were highlighted and that were the high computational time and requirement of more accurate /better clustering algorithms.

From the above paragraphs, we saw the applications of algorithms like SFIRN and RNA to construct CRN models from the CFD simulations but these algorithms are suitable for small network analysis only, if network of hundred or thousand reactors are needed for emission prediction or if a designer tends to perform probabilistic modeling and uncertainty quantification studies then these algorithms becomes unfeasible. Furthermore, even if the algorithms like KPP technique are able to construct big reactor networks the computational time and effective clustering becomes an issue.

Thus, for tackling these limitations Yousefian, Bourque and Monghan, 2019 [52] proposed a study in which they presented a systematic CRN construction method constructed from the CFD database which is then solved in Python environment for determining the NO<sub>x</sub> emission from the SCANDIA flame D. For this the authors used Python 3.5 with PCA (Principal Component Analysis) and K-means approaches to construct and solve CRN model. In this study the results of the steady-state CFD simulation were exported using Enight case gold format to Python, the data exported from the CFD solver (Ansys Fluent) was the co-ordinate information of cells, velocity components, temperature, density, mass fraction of species and cell volumes, Additionally, the mass fluxes through the faces of cells was also exported and to export the mass fluxes the authors wrote and used a UDF (user defined function) in Ansys Fluent.

Then this exported data was read in Python 3.5 and Scikit-learn package was used to implement PCA, K-means and Agglomeration clustering methods in Python, to construct the CRN model then the CRN model was solved using Cantera solver in Python environment with GRI-Mech.3 for detailed chemistry. The calculated exit temperature and mass fraction of NO species showed good correspondence with the experimental data with an accuracy of 5.6 % for the calculated NO mass fraction [52]. Thus the authors concluded that CRN approach is a competent tool for NO<sub>x</sub> emission prediction, with less computational time and reliable results.

Apart, from investigating the conventional combustion systems like gas turbines, industrial burner, boilers etc on their thermal performance, the next stage is to optimize their performance. This optimization task can be achieved by using alternate fuels, improving the combustor geometry or by applying new combustion concepts[44].

We limit ourselves to discuss the new combustion concepts to minimize the environmental impact associated with combustion systems. In recent times several novel combustion concepts like, Trapped Vortex Combustor (TVC), Lean Direct Injection (LDI) and Flameless Combustion (FC) have been developed and applied on gas turbine combustors[44]. However, flameless combustion (Flameless Combustion (FC)) is the most competent candidate for achieving low NO<sub>x</sub> emissions from the combustors [44]. Now, we can articulate the developments in CFD-CRN approach to predict pollutant emissions with flameless combustion as the background.

Perpignan, Sampat and Rao in 2019 [45], proposed an approach to model the pollutant emissions from a small-scale combustor by using CFD-CRN approach. The selected small scale

combustor was examined in detail by Verissimo et al.[7] on its operational, combustion, and emission characteristics, thus reliable data was available for CFD-CRN model validation. The combustor operated in flameless combustion regime with non-premixed combustion mode and consisted of a cylindrical combustion chamber with a central air jet surrounded by 16 fuel jets in the burner head.

For the Computational Fluid Dynamics (CFD) simulations the authors used Reynolds-Averaged Navier-Stokes (RANS) approach with two different combustion models namely, Eddy Dissipation Model (EDM) (Eddy Dissipation Model) and Flamelet Generated Manifolds (FGM) (Flamelet Generated Manifolds), two combustion models were applied to compare the performance of simulations and the fluid flow solver chosen was Ansys Fluent. Then the CFD simulations were used to extract a Chemical Reactor Network (CRN) model by using user defined clustering criteria. The important part of this study was that the authors used a novel tool know as AGNES (Automatic Generation of Networks for Emission Simulation), developed by department of aerospace engineering, TU Delft, to cluster the computational cells (from CFD simulation) and solve the extracted CRN.

For clustering the computational cells, AGNES used a “Breadth First Search (BFS)” algorithm, which clusters the cells based on the clustering criterion predefined by the user, here the authors used various clustering criteria to test the sensitivity of the clustering criterions on the final results. The clustering criterions used were temperature, velocity direction, fuel tracer variable and reaction progress variable. The temperatures and mass flows between the reactors in the CRN were assigned based on the CFD results[45]. For temperature assignment, averaged static temperatures were used and the mass flow between the reactors was corrected by using the inflow and outflow boundary conditions.

In the extracted CRN, all reactors were modeled as perfectly stirred reactors and no turbulence fluctuations were taken into account in the CRN, after CRN construction, detailed chemical mechanisms were introduced to the CRN. Here, the authors used GRI 3.0 and GRI 2.11 mechanisms for investigating the effect of different mechanisms on predicting NO<sub>x</sub> concentrations[45]. Then the CRN was solved using two levels of Cantera solver. Here, Cantera is used as a local and global solver. The local solver treats each reactor independently, whereas the global solver treats all the reactors simultaneously as a single system. In the figure below, we can see the work flow of AGNES to solve the CRNs.

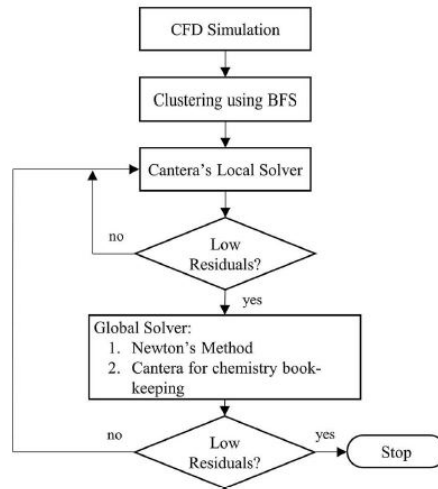


**Figure 2-18:** Schema chart for AGNES tool [45]

The results showed that the clustering criteria had a significant influence on the obtained results of CO and NO<sub>x</sub> concentrations. The use of AGNES significantly improved the NO<sub>x</sub> predictions as compared with the CFD results and showed reasonable agreement with the experimental data. Additionally, GRI 2.11 represented the prompt NO<sub>x</sub> pathways better than GRI 3.0 mechanism. Also, In the CFD simulations, the FGM model predicted better NO<sub>x</sub> values than EDM model[45]. Thus, the authors concluded that the AGNES tool can be applied to efficiently construct and solve the CRNs from the CFD simulation for a combustor operating in the flameless combustion regime with suitable accuracy for CO and NO<sub>x</sub> emission prediction with low cost.

### 2-5-5 CRN solvers.

Based on the above sections (2.4.3 and 2.4.4), we can infer that the researchers have used diverse CRN solvers for solving the CRN model. We can generally group the solvers into three categories namely, (a) commercial, (b) open-source, (c) internal/private use only. The selection of the CRN solver depends on the availability of the solver, cost of the solver and type of analysis required by the researcher/designer.

In the category of commercial solvers, Chemkin, is the most preferred commercial CRN solver. However, there are two versions of Chemkin available namely:- (a) Chemkin-Pro and (b) Chemkin. Chemkin-Pro is the most advanced version of Modern Chemkin solvers based on solution speed, solution accuracy and ability to handle large mechanisms efficiently. In recent times, software known as ENERGICO is also used in literature; ENERGICO automatically splits the flow field extracted from the CFD simulation based on predefined criteria and constructs CRNs. After the construction of CRN model by using ENERGICO, Chemkin solver can be used to introduce a detailed chemical mechanism in the CRN and then solve the CRN model. This approach is referred as CFD-ENERGICO-Chemkin approach[32].

In the category of open-source solvers, Cantera is the most preferred option. It is an open-source suite for solving problems involved with chemical kinetics, thermodynamic and transport processes[32]. The temperature of each reactor in the CRN is obtained by solving the energy equation for each reactor, this makes Cantera unwanted for fast calculations. Also, Cantera ignores the turbulence-chemistry interaction in the CRN. Apart from Cantera, people have also used KPP and KPPSMOKE softwares in the literature, both of them are also open-source. KPP takes the temperature and flow-field characteristics from the CFD simulations as the input for constructing a CRN, then it solves the set of mass balance equations in the CRN with detailed chemistry[32]. KPP does not solve the energy equation for the CRN and the temperatures for the reactors in the CRN are directly imported from the CFD results. KPP solver is known for its high solving speed with capability of solving large network of reactors (upto 1000 reactor elements).

Software like Automatic Generation of Networks for Emission Simulation (AGNES) belongs to the category of internal/private use CRN solvers. These solvers are used for internal research only, but can be commercialized or be granted open access after full development. AGNES is developed by the department of aerospace engineering of TU Delft, The Netherlands for constructing and solving CRNs extracted from CFD simulations for gas turbine combustors operating in flameless combustion regime.

## 2-5-6 Conclusions.

From the presented literature survey, we can conclude that CRN approach is a very popular and effective tool for modeling the combustion process in the combustors with very detailed chemical mechanisms. CRN approach has aided significantly in performance analysis and design development process of gas turbine combustors, which was a difficult optimization task to perform with zonal combustion modeling or by doing experimental studies.

One dimensional or quasi one dimensional approaches for constructing CRN model like (a) network approach or (b) component modeling approach are effective approaches for doing emission prediction studies on combustors with very less computational time and cost, These approaches are useful for conducting “initial conceptual design studies” on combustor performance[32] as these approaches neglect detailed flow field calculation.

Additionally, CFD has supplemented the CRN approach in a significant way, as through CFD we can compute complex fluid flow phenomenon's which can then be used to construct CRNs. Based on CFD there are two ways to construct CRNs, the first method is by analyzing the flow field patterns predicted by CFD and then dividing the flow field into homogenous zones, here the partitioning of flow field is done by user's decision. The second approach is by using mathematical algorithms to automatically detect the homogenous zones and then construct CRN out of it, this approach is more reliable and efficient than the first approach. Based on the literature survey we can now present the advantages of the CRN approach with the limitations and challenges encountered in the CRN approach, as:-

### Advantages

1. An effective tool for predicting pollutant emission concentrations from industrial combustion systems with less computational time and cost associated.
2. Enables the analysis of detailed chemistry in real time (Real Time (RT)-CRN) thus can be used as a combustion process control tool.
3. Sensitivity analysis can be conducted on the combustion process, to determine which parameter has a maximum or minimum effect on the pollutant emission.
4. CRN are also used in development of reduced order chemical mechanisms.

### Limitations

1. As the effect of turbulence – chemistry interaction is not considered in the CRN approach, this limits the accuracy of thermal NO<sub>x</sub> emission predictions.
2. The results for minor species emission predictions highly depends on the strategy employed for flow field partitioning.
3. The ideal chemical reactors (PSR, Plug Flow Reactor (PFR), Partially Stirred Reactor (PaSR), MIX) in the CRN are zero or one-dimensional thus, effects of flow disturbances are neglected. This might inhibit the user/designer to handle all the relevant turbulent flame regimes.

### Challenges

1. Implementation of CRN method to practical combustion systems needs software development, as the available open source codes do not contain all state-of-the-art features like PaSR reactor.
2. New variants of CRN method needs to be developed in order to handle partially pre-mixed flames.

---

# Chapter 3

---

## Theory

Modeling of turbulent combustion must address turbulence model, chemistry and turbulence-chemistry interaction. In literature we find two widely used mathematical formulations used to obtain the statistical properties of turbulent flows namely Reynolds averaged Navier-Stokes (RANS) models, which can further have different schemes based on two-equation Eddy viscosity model and Reynolds stress models, and Large Eddy Simulation (Large Eddy Simulation (LES)) models[37].

Modeling of turbulent reacting flow in the RANS and LES approaches involves as important subproblems the closure of the Reynolds stress, the closure of the turbulent flux and the closure of the mean chemical source term (turbulence-chemistry interaction). In this chapter we first consider the closure of the Reynolds stress and next we present two specific approaches to the closure of the mean chemical source term: steady diffusion flamelet (SDF) model and flamelet generated manifold (FGM) model. Provided the chemical mechanism contains appropriate  $\text{NO}_x$  chemistry these approaches provide a prediction for  $\text{NO}_x$  emissions. But as an alternative, because  $\text{NO}_x$  is only present in very small concentration and does not influence the density and the flow field,  $\text{NO}_x$  predictions can also be obtained via post-processing. This is explained in the last two sections of this chapter. The main sources for this chapter are the ANSYS Fluent Theory guide [19] and the lecture notes of the TU Delft course AE4262, Combustion for propulsion and power, academic year 2020-2021.

### 3-1 Turbulence model

In this work we use the  $k-\epsilon$  turbulence model, with standard wall function. The  $k-\epsilon$  model is based on two assumptions. First, the turbulent transport and dissipation of turbulent energy progresses with the identical timescale, known as dissipation time scale[55], and Secondly, the model presupposes isotropy, As a single turbulent viscosity is used to model all Reynolds stresses[55]. The  $k-\epsilon$  model has good performance in confined flows where the Reynolds shear stresses are dominant. This includes a wide range of flows with industrial engineering applications[37].

The  $k-\epsilon$  model contains the mean continuity equation and the mean momentum equation plus two extra transport equations to close the Reynolds stress tensor. For the case of variable density flow the density weighted averaging is used rather than Reynolds averaging. The velocity is split in density weighted mean value and fluctuation as

$$U_i = \tilde{U}_i + u_i'' \quad (3-1)$$

The mean continuity equation:

$$\frac{\partial}{\partial t} \langle \rho \rangle + \frac{\partial}{\partial x_j} (\langle \rho \rangle \tilde{U}_j) = 0 \quad (3-2)$$

Here  $\langle \rho \rangle$  denotes the Reynolds averaged density. The mean momentum equation (here written with neglect the effect of the laminar viscosity but in the actual simulations that was also taken into account):

$$\frac{\partial}{\partial t} (\langle \rho \rangle \tilde{U}_i) + \frac{\partial}{\partial x_j} (\langle \rho \rangle \tilde{U}_j \tilde{U}_i) = \langle \rho \rangle g_i - \frac{\partial \langle p \rangle}{\partial x_i} - \frac{\partial}{\partial x_j} [\langle \rho \rangle \widetilde{u_i'' u_j''}] \quad (3-3)$$

The closure hypothesis for the Reynolds stress tensor:

$$-\langle \rho \rangle \widetilde{u_i'' u_j''} = \mu_t \left( \frac{\partial \tilde{U}_i}{\partial x_j} + \frac{\partial \tilde{U}_j}{\partial x_i} \right) - \frac{2}{3} \delta_{ij} \left( \langle \rho \rangle \tilde{k} + \mu_t \frac{\partial \tilde{U}_k}{\partial x_k} \right) \quad (3-4)$$

Here  $\tilde{k}$  is the density weighted turbulent kinetic energy:

$$\tilde{k} = \frac{1}{2} \widetilde{u_i'' u_i''} \quad (3-5)$$

and  $\mu_t$  is the turbulent viscosity given by:

$$\mu_t = C_\mu \langle \rho \rangle \frac{\tilde{k}^2}{\tilde{\epsilon}} \quad (3-6)$$

where  $\tilde{\epsilon}$  is the rate of dissipation of . Turbulent kinetic energy and its dissipation rate are obtained from two additional transport equations:

$$\frac{\partial}{\partial t} (\langle \rho \rangle \tilde{k}) + \frac{\partial}{\partial x_j} (\langle \rho \rangle \tilde{U}_j \tilde{k}) = \frac{\partial}{\partial x_j} \left( \frac{\mu_t}{\sigma_k} \frac{\partial \tilde{k}}{\partial x_j} \right) + P_k - \langle \rho \rangle \tilde{\epsilon} \quad (3-7)$$

and

$$\frac{\partial}{\partial t} (\langle \rho \rangle \tilde{\epsilon}) + \frac{\partial}{\partial x_j} (\langle \rho \rangle \tilde{U}_j \tilde{\epsilon}) = \frac{\partial}{\partial x_j} \left( \frac{\mu_t}{\sigma_\epsilon} \frac{\partial \tilde{\epsilon}}{\partial x_j} \right) + C_{\epsilon_1} \frac{\tilde{\epsilon}}{\tilde{k}} [P_k] - C_{\epsilon_2} \langle \rho \rangle \frac{\tilde{\epsilon}^2}{\tilde{k}} \quad (3-8)$$

Here  $P$  represents the production rate of  $\tilde{k}$ :

$$P_k = -\langle \rho \rangle \widetilde{u_i'' u_j''} \frac{\partial \tilde{U}_i}{\partial x_j} \quad (3-9)$$

The standard values of the model constants in these equations are  $C_\mu = 0.09$ ,  $C_{\epsilon_1} = 1.44$ ,  $C_{\epsilon_2} = 1.92$ ,  $\sigma_k = 1.00$ ,  $\sigma_\epsilon = 1.30$ ,  $\sigma_t = 0.70$ . For the simulation of cylindrical set the modified value  $C_{\epsilon_1} = 1.6$  is recommended and has been used in this study.

## 3-2 Models for turbulence-chemistry interactions

The averaged equation for the species mass fractions is given by

$$\frac{\partial}{\partial t}(\langle \rho \rangle \tilde{Y}_\alpha) + \frac{\partial}{\partial x_j}(\langle \rho \rangle \tilde{U}_j \tilde{Y}_\alpha) = \frac{\partial}{\partial x_j} \left( (\langle \rho \rangle \mathcal{D}_\alpha + \frac{\mu_t}{\sigma_\phi}) \frac{\partial \tilde{Y}_\alpha}{\partial x_j} \right) + \langle \rho \rangle \tilde{S}_\alpha(\phi) \quad (3-10)$$

Here  $\alpha$  is an index referring to the different species and  $\mathcal{D}$  is the laminar diffusivity. The turbulent flux has been closed with the gradient diffusion assumption, but the mean chemical source term still appears as unclosed term. Many models have been proposed in the literature to close this term. Here we shall elaborate the steady laminar flamelet model and the flamelet generated manifold model because they will be used in the simulations performed in this work. In both cases we first describe the model in words and then provide the model equations.

### 3-2-1 Steady diffusion flamelet model

In the laminar flamelet model for non-premixed combustion it is assumed that the relation between different species concentrations is the same as can be found in a representative laminar flame. Considering a specific laminar flame, namely the counterflow diffusion flame the general species transport equations in three-dimensional space can be transformed to a one-dimensional equation with mixture fraction as independent variable. The relation between mixture fraction and variables describing the thermochemical state of the mixture (species mass fractions and temperature) found in the laminar flame are assumed to hold also in other flames. One additional parameter appears describing the straining of the flame front by the flow field, namely the scalar dissipation rate.

In the case of turbulent flame the turbulent fluctuations have to be taken into account. In the model only the fluctuations of the independent variables (mixture fraction and scalar dissipation rate have to be specified.) The most common approach is to use an assumed shape of the PDF of mixture fraction (beta-function), fully characterised by the value of the mean and the variance. To use this approach an extra equation has to be solved for the variance of mixture fraction. Fluctuations in scalar dissipation rate are neglected.

The procedure followed in the laminar flamelet model then consists of two steps. The first step is the creation of a flamelet library, the second is the used of the table in computations of application flames. The first step has two sub-steps, first the calculation of solutions of the flamelet equations for a range of scalar dissipation rate values and second the averaging of these solutions with the assumed PDF as weight factor. This leads to a lookup table with as independent variables mean and variance of mixture fraction and mean scalar dissipation rate. The most relevant independent variables contained in the table are mean density (needed in the transport equations) and mean temperature and mean species mass fractions (needed for validation by comparison with experiment)

In the calculation of a turbulent flame the mean and variance of mixture fraction are obtained from model transport equation. The mean scalar dissipation rate is obtained from an algebraic relationship with the turbulent frequency obtained from the k- $\epsilon$  model and the variance of mixture fraction. Since in the flamelet model approach there is not need to solve the equation for the mean species mass fractions, the closure of the source term in those equations no

longer appears. If required the mean source term can be obtained in post-processing using the expression for the source term and the PDF of mixture fraction.

The mathematical equations forming the flamelet model first of all consist of definition of mixture fraction, species and temperature equations in mixture fraction space (flamelet equations). The mixture fraction is defined to be the mass present locally which originally is coming from the fuel stream. So it has value 1 in the fuel stream and value 0 in the air stream. It can be based on a physical quantity such as carbon element mass fraction. Denoting this physical quantity as 'unnormalised' mixture fraction  $Z_{un}$ , the mixture fraction is given by

$$Z = \frac{Z_{un} - Z_{un,air}}{Z_{un,fuel} - Z_{un,air}} \quad (3-11)$$

(The mixture fraction reported in the experimental database is computed from measured mass fractions of main species.)

The unsteady flamelet equation for species is given by

$$\rho \frac{\partial Y_\alpha}{\partial \tau} = \frac{1}{2} \rho \chi \frac{\partial^2 Y_\alpha}{\partial Z^2} + \rho S_\alpha \quad (3-12)$$

Here the scalar dissipation rate is defined by

$$\chi = 2D \left\langle \frac{\partial Z}{\partial x_i} \frac{\partial Z}{\partial x_i} \right\rangle \quad (3-13)$$

Equal diffusivity  $D$  of all species was assumed. The unsteady flamelet equation for temperature is given by

$$\rho \frac{\partial T}{\partial \tau} = \frac{1}{2} \rho \chi \frac{\partial^2 T}{\partial \xi^2} - \frac{1}{c_p} \sum_{\alpha=1}^N h_\alpha \rho S_\alpha + \frac{1}{2c_p} \rho \chi \left\{ \frac{\partial C_p}{\partial Z} + \sum_{\alpha=1}^N C_{p\alpha} \frac{\partial Y_\alpha}{\partial Z} \right\} \frac{\partial T}{\partial Z} \quad (3-14)$$

In order to be able to solve these equations an expression for the scalar dissipation rate must be provided. An approximate expression is used characterised by the value of scalar dissipation at the the location where the mixture has the stoichiometric composition:

$$\chi_{st} \approx \frac{a}{\pi} \exp \left\{ -2[\text{erfc}^{-1}(2Z_{st})]^2 \right\} \quad (3-15)$$

Here  $a$  is a characteristic value of strain rate (velocity gradient) and  $\text{erfc}$  is the complementary error function. A range of flamelets can be considered by varying the strain rate or equivalently the scalar dissipation rate. This leads to a set of flamelets varying between low strain (close to equilibrium) and high strain (up to extinction).

In building a library of steady flamelet solutions the unsteady term containing the time derivative is set to zero.

In turbulent flow the transport equations for mean and variance of mixture fraction are solved and mean values of dependent quantities are calculated using a PDF. Model equations for mean and variance of mixture fraction can be found in the note "Analysis of FGM transport equations" by D. Roekaerts added to this thesis.

### 3-2-2 Flamelet generated manifold model

Also the FGM method is based on the idea that the local states in many flames can be described using properties of an representative set of laminar flames. Similar to the steady flamelet model, the states from pre-computed counterflow diffusion flames are used as source for useful relationships. The same flamelet equations as used in the flamelet model are used. But now also information on chemical evolution in time retrieved from the flamelets. In order to do so a progress variable is identified, in such a way that in the flamelet library for each set of values of mixture fraction and progress variable there is only one possible state and all thermochemical properties are uniquely defined as function of mixture fraction and progress variable. A typical choice, also used in this work, is a linear combination of the main combustion products  $\text{CO}_2$  and  $\text{H}_2\text{O}$ . In stead of using scalar dissipation rate as second independent variable in the flame property tabulation, next to mixture fraction, now the progress variable is the second independent variable. The main difference is that the progress variable is a chemically reacting variable and by storing its chemical source term in the lookup table the chemical evolution in other flames can be calculated. A complication arises from the fact that steady burning flamelets do not provide states with low value of progress variable. For this reason the flamelet library is extended with an unsteady extinguishing flamelet. It described the evolution of a flamelet at the extinction strain rate extinguishing to the non-burning state.

Again a two step procedure is needed in building the table. Solving flamelet equations and building the FGM table as function of mixture fraction and progress variable.

Next, introducing an assumed PDF for the mixture fraction and progress variable. It has been found that for ease of tabulation, but also for making good assumptions on the PDF it is necessary to introduce a scaled progress variable. For every value of mixture fraction the progress variable in general takes values between a minimum and a maximum. By referring to these extreme values a scaled progress variable is defined. The mixture fraction and the scaled progress variable can be assumed to be statistically independent. Then the joint PDF of both is the product of a PDF for each of them. For mixture fraction as before a beta-function PDF is assumed. Also the PDF of scaled progress variable can be assumed to be a beta-function. Then four extra equations have to be solved: model equations for the mean and variance of mixture fraction and for mean and variance of progress variable.

The transport equations for the mean and variance of unscaled progress variable follows can be derived in relatively straightforward manner from the transport equations for the species mass fractions. If these transport equations are solved one also needs the algebraic relations between mean and variance of unscaled progress variable and mean and variance of scaled progress variable in order to be able to do a lookup in the FGM table. Alternatively transport equations for the mean and variance of scaled progress variable can be solved and then the resulting values can be used directly to retrieve properties from the FGM table. The latter procedure is used in ANSYS-Fluent. It should be pointed out however that the equations used in ANSYS-Fluent do not contain an extra term that arises due to the transformation from unscaled to scaled progress variable. This is further documented in a note by D. Roekaerts added to this thesis.

Since in the FGM approach there is not need to solve the equation for the mean species mass fractions, the closure of the source term in those equations no longer appears. If required the

mean source term of any species can be obtained in post-processing using the expression for the source term and the PDF of mixture fraction. But the FGM approach does provide a closure for the mean chemical source term of the progress variable. This term is calculated from both the instantaneous value and the PDF of mixture fraction and progress variable and stored in the PDF table.

The flamelet model and the FGM are using the same set of laminar counterflow diffusion flames, but nevertheless lead to different predictions for the turbulent flame. The main difference between flamelet model and FGM is that the mean thermochemical composition controlled by a different variable. In the flamelet model the change of state is controlled by changes in mixture fraction and scalar dissipation rate. In the FGM model the change of state is controlled by mixture fraction and progress variable. Because changes in scalar dissipation rate and changes in progress variable are driven by different processes, differences in the predictions can arise.

The equations of the FGM model are contained in the note by D. Roekaerts added to this thesis.

### 3-3 Reactor Network Model theory

The reactor network model is a CRN tool offered by Ansys Fluent to aid the prediction of species and temperature fields in a combustion system using detailed chemical mechanism like GRImech 2.11, GRImech 3.0, San Diego mechanism etc. As, RNM tool is a post-processing tool thus it uses a converged CFD simulation to construct a reactor network, the CFD simulation can be done by using reduced/simple chemical kinetic mechanisms like DRM19, EDM etc. Also, RNM tool is only capable to utilize steady-state RANS solution or time averaged unsteady CFD solution to construct a reactor network, as the solution of the reactor network is not coupled backward to the flow field [19]. The RNM tool constructs a reactor network by considering the clustering criteria imposed by the user on the system under analysis. The default clustering criteria used by the RNM tool is based on temperature and mixture fraction, so the temperature and mixture fraction values predicted by the CFD simulation will be used to cluster the computational domain into a network of perfectly stirred reactors.

The construction of a reactor network is initiated by specifying the number of reactors  $N_{reactor}$ , that should be used to agglomerate the computational cells, this is user specification although the default value for  $N_{reactor}$  is 50. Then a clustering criterion is introduced in the RNM tool, as discussed before the default clustering criteria is based on temperature and mixture fraction values, but RNM tool allows the user to change the clustering criteria by applying a custom field function.

After that the next step is to solve the acquired reactor network formed after clustering is performed, this is accomplished by calculating the mass flux matrix ( $m$ ) from the fluxes between cells in the CFD simulation. The matrix component  $m_{ij}$  represents the mass flux from reactor  $i$  to reactor  $j$  [19]. Also, the mass fraction of  $k^{th}$  species is mathematically represented by the equation below:

$$\sum_{j=1, j \neq i}^{N_{reactor}} m_{ij} Y_k^j - m_i Y_k^i = V_i \omega_k^i + S_k^i \quad (3-16)$$

Here,  $V_i$  is the volume of the reactor (i), and  $\omega_k^i$  is the  $k^{th}$  species reaction rate in the  $i^{th}$  reactor and any other mass source term eventually present is represented by  $S_k^i$  [19]. On the other hand, the net mass flux from reactor i to other reactors is mathematically given by:

$$m_i = \sum_{j=1, j \neq i}^{N_{reactor}} m_{ij} \quad (3-17)$$

The dimension of the system of equations 3-4 is given by  $N_{reactor} \times N_{species}$  where  $N_{reactor}$  is the number of reactors in the reactor network and  $N_{species}$  is the number of species present in the chemical mechanism that is applied in the RNM tool. The solution calculated by the RNM tool can be viewed in the result tab in the fluent software and can be post-processed by plotting contours of temperature field and desired species mass fractions or the results can also be analysed by plotting the graphs for physical variables (temperature and species mass fraction) with respect to the radial profiles for the combustion system.

### 3-4 Ansys NOx post-processor theory

Ansys fluent offers an additional possibility to the user to model the pollutant emissions from the combustion system. The pollutant formation can be modelled by using NO<sub>x</sub> post-processing tool after using a detailed chemical kinetic mechanism. The thermal, prompt and fuel NO<sub>x</sub> formation can be modelled by using the NO<sub>x</sub> post-processor. For calculations the post-processor uses the rate models developed by the Dept. of fuel and energy at the Leeds University [19].

For the prediction of NO<sub>x</sub> levels, Fluent solves a transport equation for NO species. If the fuel contains fuel bound nitrogen species, then Fluent solves extra transport equations for the relevant intermediate species like HCN, NH<sub>3</sub>. This is not needed in the case considered in this work. The NO<sub>x</sub> is post-processed from a converged CFD simulation, thus the results of the NO<sub>x</sub> post-processor depend on the accuracy and reliability of the CFD simulation/baseline solution. In most cases the NO<sub>x</sub> post-processor can predict the global trends of NO<sub>x</sub> variation but the exact quantity of NO<sub>x</sub> cannot be predicted [19].

Now, we can present the governing equations that are solved by Ansys Fluent. For predicting the NO concentrations, Fluent solves the mass transport equation for NO species, the diffusion, convection, production and consumption of NO species is accounted for in the formulation. The convection terms in the governing equation accounts for the effect of residence time on the NO<sub>x</sub> mechanisms. As, in our case we only consider the prompt and thermal NO<sub>x</sub> mechanism thus only the transport equation of NO species is needed and it is given by[19]:-

$$\frac{\partial}{\partial t}(\rho Y_{NO}) + \nabla \cdot (\rho \vec{v} Y_{NO}) = \nabla \cdot (\rho \mathbf{D} \nabla Y_{NO}) + S_{NO} \quad (3-18)$$

In RANS this is the transport equation for the mean mass fraction (averaging symbols were omitted in this equation).  $\mathbf{D}$  is the effective diffusion coefficient, sum of laminar and turbulent contribution.  $S_{NO}$  is the mean source term which is calculated by using different NO<sub>x</sub> mechanisms. An option to include influence of turbulent fluctuations through a PDF of either

mixture fraction or temperature is optional. In the present study as discussed before only thermal and prompt mechanisms are considered thus the NO source terms for both thermal and prompt mechanism are presented below respectively as:

$$S_{thermal,NO} = M_{w,NO} \frac{d[NO]}{dt} \quad (3-19)$$

Here  $[NO]$  denotes concentration and  $M_{w,NO}$  represents the molecular weight of NO in kg/mol. The molar NO production rate  $\frac{d[NO]}{dt}$  is calculated by the expression:

$$\frac{d[NO]}{dt} = 2k_{f,1}[O][N_2] \frac{(1 - \frac{k_{r,1}k_{r,2}[NO]^2}{k_{f,1}[N_2]k_{f,2}[O_2]})}{(1 + \frac{k_{r,1}[NO]}{k_{f,2}[O_2]k_{f,3}[OH]})} \quad (3-20)$$

Where,  $k_{f,1}$ ,  $k_{f,2}$  are the rate constants and  $k_{r,1}$ ,  $k_{r,2}$  are the reverse rate constants. For the prompt mechanism the source term is given by:

$$S_{prompt,NO} = M_{w,NO} \frac{d[NO]}{dt} \quad (3-21)$$

Where,  $\frac{d[NO]}{dt}$  is given by:-

$$\frac{d[NO]}{dt} = k_{pr}[O_2]^a[N_2][FUEL] \exp -E_a/RT \quad (3-22)$$

In equation 3-22,  $E_a = 251151$  J/mol,  $a$  is the oxygen reaction order,  $R$  is the universal gas constant and  $p$  is the pressure.

### 4-1 Introduction

The test case for our study is a bluff-body stabilized flame known as HM1 flame. The initial experimental studies on HM1 flame were done at the University of Sydney by Dally et al. [11]. The availability of the data motivated other researchers to contribute more on the modelling aspects of this flame. It has been included as a benchmark flame in the category of turbulent non-premixed jet flames at the TNF workshop. A detailed description of the HM1 flame can be found in the documentations prepared by TNF workshop [41]. The HM1 flame contains 50 percent  $H_2$  and 50 percent  $CH_4$  by volume as its fuel composition. The fuel jet is supplied through a fuel pipe having a diameter of 3.6 mm. The fuel pipe ends in the centre of a cylindrical bluff body having outer diameter 50 mm. The oxidizer (air) flow is added laterally of the bluff-body in co-flow fashion. In our study the exit velocity of the fuel jet is 118 m/s while the mean velocity of the co-flow air stream is 40 m/s.

When the fuel jet and air streams meet and mix a non-premixed turbulent flame is formed. This mixing with products in combustion in the wake of the bluff-body acts as a stabilizing agent to the flame. Figure 4–1 shows the HM1 flame.



**Figure 4-1:** Image of HM1 flame. [41]

## 4-2 Measurement technique

In this section we present the measurement techniques that were employed by the research groups at the University of Sydney and Sandia national laboratory for measuring the velocity data and thermo-chemical data for the HM1 flame. The thermo-chemical measurements were taken at the Turbulent Diffusion Flame Lab at the combustion research facility (CRF) of Sandia Lab., while the flow field measurements were done at the University of Sydney. This measured data is freely available at the website of the TNF workshop [41]. We have used this data to validate our numerical simulations. For the validating the velocity field we have used the data corresponding to HM1 flame with fuel jet velocity of 118 m/s and air coflow velocity of 40 m/s the name of the data file used was "b4f3-a-s1.dat", this statement is important to make because in literature, people have also utilized another set of data known as Flame HM1E for validating there velocity field, although flame HM1E is analogous to HM1, just the inlet velocities are different the reason for existence of HM1E data set is related to the inability of the wind tunnel at the university of Sydney to generate a uniform 40m/s coflow (Maximum was 35m/s) [41] and for validating the temperature and species mass fractions we used the data measured by spontaneous Raman/LIF technique.

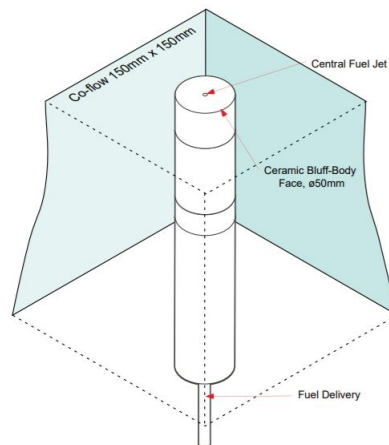


**Figure 4-2:** Representation of the bluff-body burner [41]

Figure 4-2, represents the geometry of the bluff-body burner, now we can discuss the experimental setup used for the measurements, for velocity measurement the LDV technique was used to measure the axial and radial velocity components by using two Argon-ion laser beams of 5 Watts and two photomultiplier tubes with color filters were used to collect the scatter from the Argon-ion lasers. The received output was then filtered and passed through two one-dimensional frequency counters. On the other hand the measurement of mixture fraction for non-reacting bluff-body jet is performed by using Raman/Rayleigh scattering to obtain concentration of the main species. Laser Induced Fluorescence (LIF) is used to obtain the radical species OH. The acquired data for mixture fraction is estimated to have an error of less than 5.7 percent without considering the systematic errors associated with the measurements. For more detailed explanation on experimental setup, the reader is referred to the studies performed by A.R.Masri et al. [35],[18].

The experimental data were obtained along horizontal sections in the domain. The radial profiles at which measurements were made are  $x/D = 0.3, 0.6, 0.9, 1.3, 1.8$  and  $2.4$  for the scalar data and  $x/D = 0.1, 0.26, 0.6, 0.9$  and  $1.3$  for the velocity fields. Figure 4-3 shows the geometrical location of the radial profiles. The model predictions will be compared with these measured data.

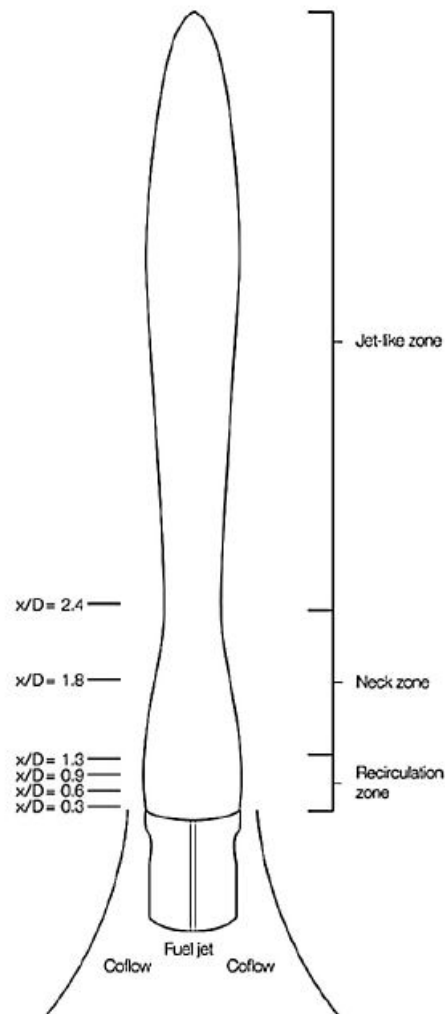


**Figure 4-3:** Radial profiles for scalar data validation. [15]

### 4-3 CFD set-up

This section describes the computational details of the numerical simulations performed on the test case of HM1 flame. All the numerical simulations were performed by using Ansys Fluent, version 19 R3. For the simulations a two-dimensional geometry was prepared, figure 4-4 shows the schematic of the geometry, we assumed the computational domain to be two dimensional and axis-symmetric in nature due to the cylindrical symmetry of the burner. The dimensions of the computational domain are represented in the following table.

**Table 4-1:** Geometrical dimensions

Dimension	Value
Burner diameter	25 mm
Height of bluff-body	50 mm
Fuel Jet inlet	1.8 mm
Length of domain	800 mm
Width of domain	100 mm

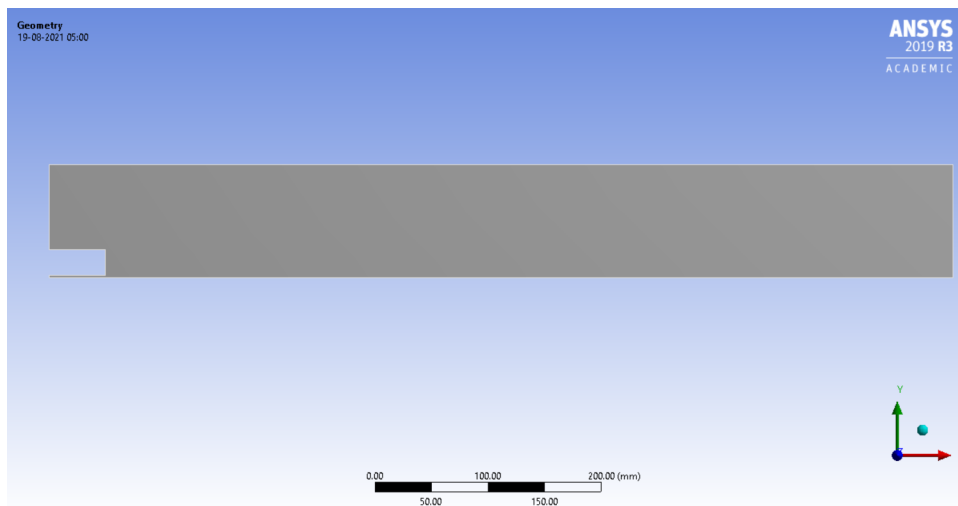


**Figure 4-4:** Representation of computational domain

For the described geometrical domain a computational mesh was constructed. The constructed mesh was a structured mesh with an inflation layer on the surface of the bluff-body and additional refinement close to the region near to the bluff-body. The basic details on the mesh are given in table 4-2. After the mesh was made the mesh quality was also assessed, table 4-3 provides the details for the mesh quality.

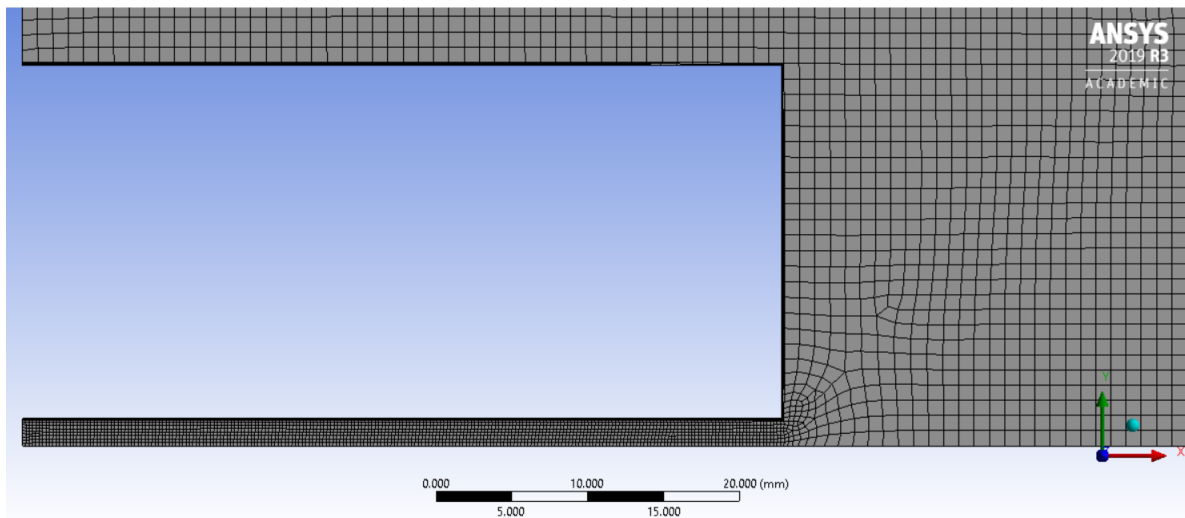
**Table 4-2:** Mesh characteristics.

Nodes	87413
Elements	86585
Minimum edge length	1.8 mm

**Table 4-3:** Mesh quality.

Average orthogonal quality	0.99884
Average aspect ratio	1.0553
Average skewness	$5.683510^{-3}$

Figure 4-5 shows the schematic of the computational mesh, in this figure an enlarged view of the region close to the bluff-body is presented for better visualization.

**Figure 4-5:** Enlarged view of mesh

After the mesh construction, the solution set-up was initiated in which the boundary conditions for temperature and inlet velocities were set. The turbulence was modeled by modified  $k-\epsilon$  model, where the  $C_{\epsilon 1}$  parameter was changed from 1.44 to 1.60. Furthermore, the combustion was modeled by selecting the FGM model and steady diffusion flamelet model independently. The chemical mechanism used for the simulations was Gas Research Institute (GRI) 2.11 mechanism. In total six simulations were performed, figure 4-6 shows the breakdown of the simulations. In the simulations performance of both the combustion models are assessed and also the performance of the post-processing tools, namely reactor network model (RNM) tool and Ansys  $\text{NO}_x$  post-processor tool are assessed for predicting the  $\text{NO}$  concentrations.

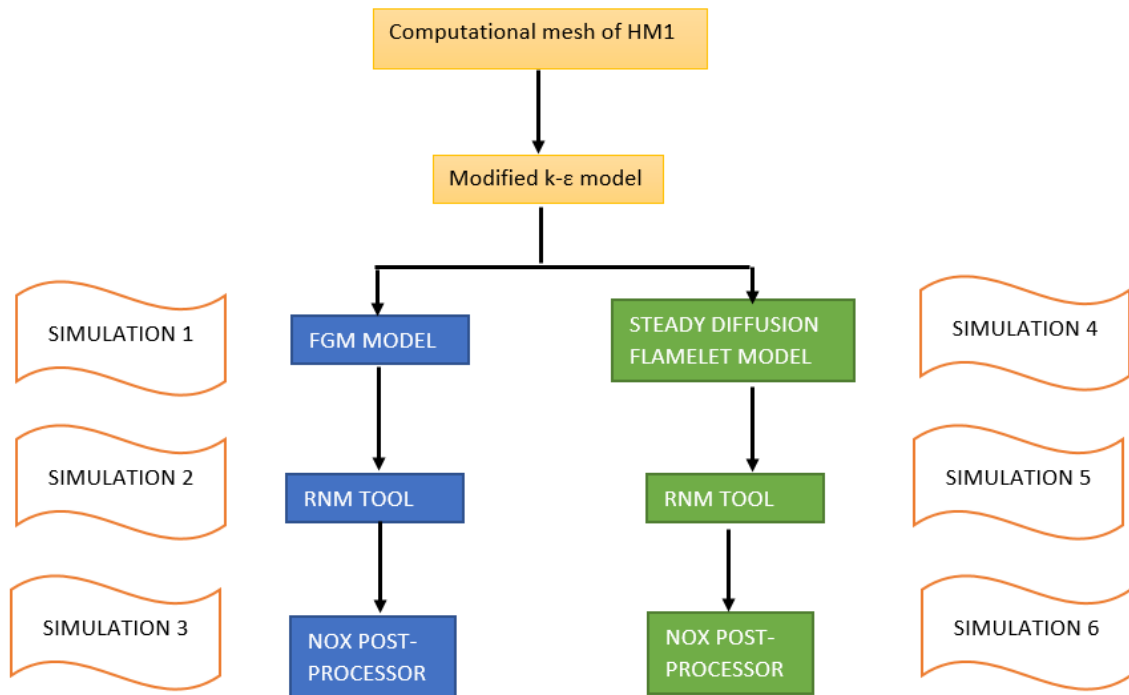


Figure 4-6: Breakdown of the numerical simulations

## 4-4 Grid independence study

Subsequently, a grid independence study was done after the first CFD solution with FGM model was completed, for selecting the most reliable mesh for the modeling study. For the grid independence study the Richardson extrapolation method was selected, figure 4-8, shows the graphs obtained during the mesh study, we took three grid resolutions and then used them to calculate the exact solution (for particular physical variable) by using Richardson extrapolation method, the details of the three grid configurations are shown in table 4-4.

Here, we selected the physical variable as mass weighted average of the temperature, CO<sub>2</sub>, N<sub>2</sub> and CH<sub>4</sub>. The first grid resolution was taken as 1 mm (element size) this also becomes our coarse mesh resolution, and then we took our refinement ratio as "0.5", thus the second resolution would be 0.5 mm (element size) thus it would be our medium mesh resolution and so on.

The extrapolation method provides an estimate of the exact solution for each physical variable by using the formula

$$\phi_{exact} = \phi_{fine} - \frac{\phi_{medium} - \phi_{fine}}{r^p - 1} \quad (4-1)$$

Where,

$$p = \frac{\ln(\frac{\phi_{coarse} - \phi_{medium}}{\phi_{medium} - \phi_{fine}})}{\ln(r)} \quad (4-2)$$

And, r is the refinement ratio.

A grid convergence index (GRI) between two levels is defined as

$$GCI = \frac{F_s}{(r^p - 1)} \left| \frac{\phi_2 - \phi_1}{\phi_1} \right| \quad (4-3)$$

where  $F_s$  is an empirical factor which is not important in the final step, namely based on three successive levels of refinement the asymptotic range of convergence is obtained from formula 4-4:

$$Conv = \frac{GCI_{mediumcoarse}}{r^p \cdot GCI_{finemedium}} \quad (4-4)$$

As per theory if the value predicted by formula 4-4 i.e the value for the asymptotic range of convergence is close to unity, then the exact solution calculated is grid independent and we obtained for all our selected physical variables, value approximately equal to unity,

After, the grid independence study we observed the graphs in figure 4-7 and noted that the biggest difference for the predicted physical variable was coming from the change from coarse to medium mesh configuration. Also, the difference between the predicted values for physical variables is very minute between the fine and medium mesh configurations thus we selected the medium mesh configuration as our mesh for the simulations.

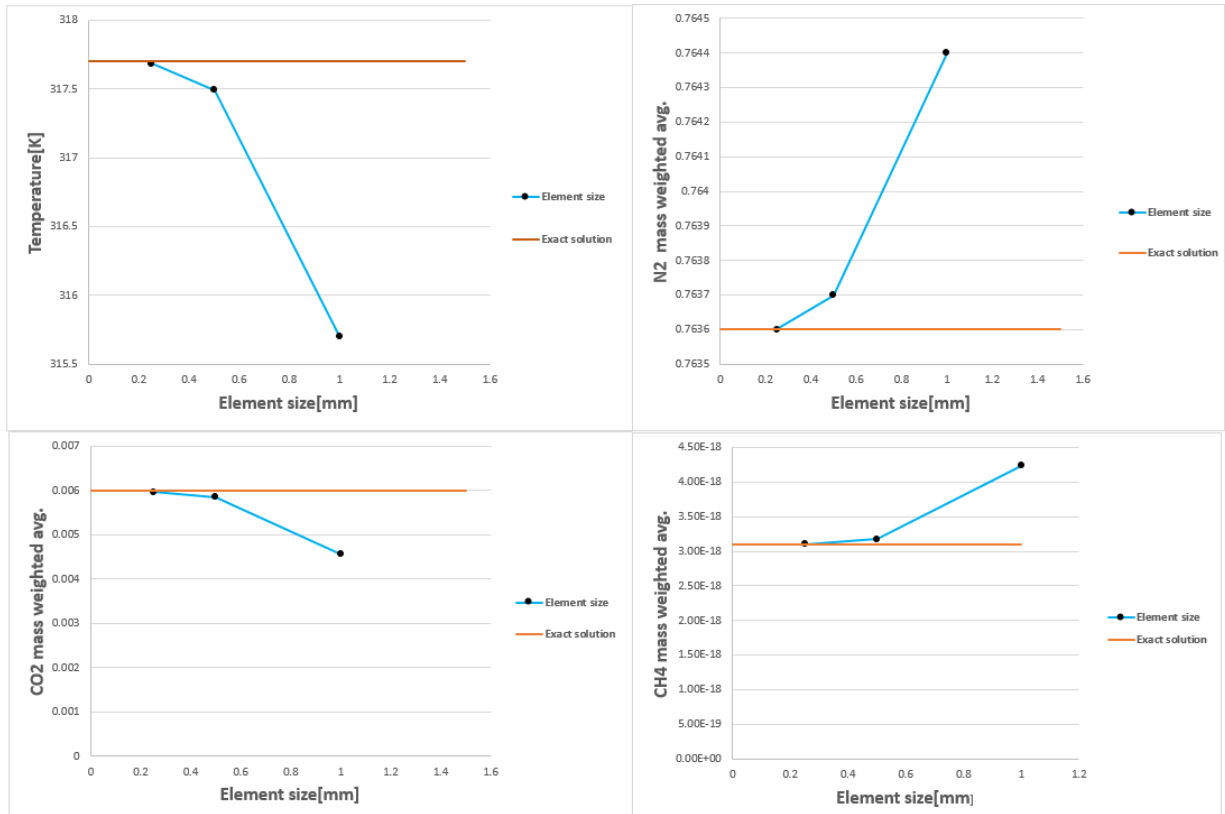


Figure 4-7: Grid independence test

Table 4-4: Grid resolutions for Richardson extrapolation.

-	Grid resolution 1	Grid resolution 2	Grid resolution 3
Element size	1 mm	0.5 mm	0.25 mm
Mesh nodes	21265	87413	340848
Mesh elements	20863	86585	339250

---

# Chapter 5

---

## Results

In this chapter, we present the acquired results of the simulation after getting the solution from Ansys Fluent 19-R3 for the HM1 flame test case, the results were post processed in Ansys CFD post-processor ( ver.19 R3). The chapter is divided into two sections, the first section deals with the observations of the results and the second section deals with the analysis of the results.

### 5-1 Observations of the Results.

This section describes the comprehensive observations that were made on the basis of the results, here we present the results for the velocity field, temperature field and major and minor species concentrations, the results are pictorially represented by using graphs where the curves are shown for data acquired through the usage of FGM model and steady diffusion flamelet model also the acquired curves for velocity and thermo-chemical properties (eg. temperature etc.) are validated by comparing them to the experimental data.

#### 5-1-1 Velocity Field

Figure, 5-1 shows the curves of the U-component of the velocity field for the HM1 flame. As, discussed before HM1 is a jet flame, thus the fuel is supplied through the center jet of the burner and the air enters through the circular space outside the center jet pipe in a coflow fashion. Due to the interaction of the fuel jet and coflow of air, two vortices are formed at the top of the bluff-body, this region is also termed as the inner re-circulation zone of the flame, this re-circulation zone has the approximate length of  $x/D \approx 1.5$  [17], which is also clearly verified by our simulation results.

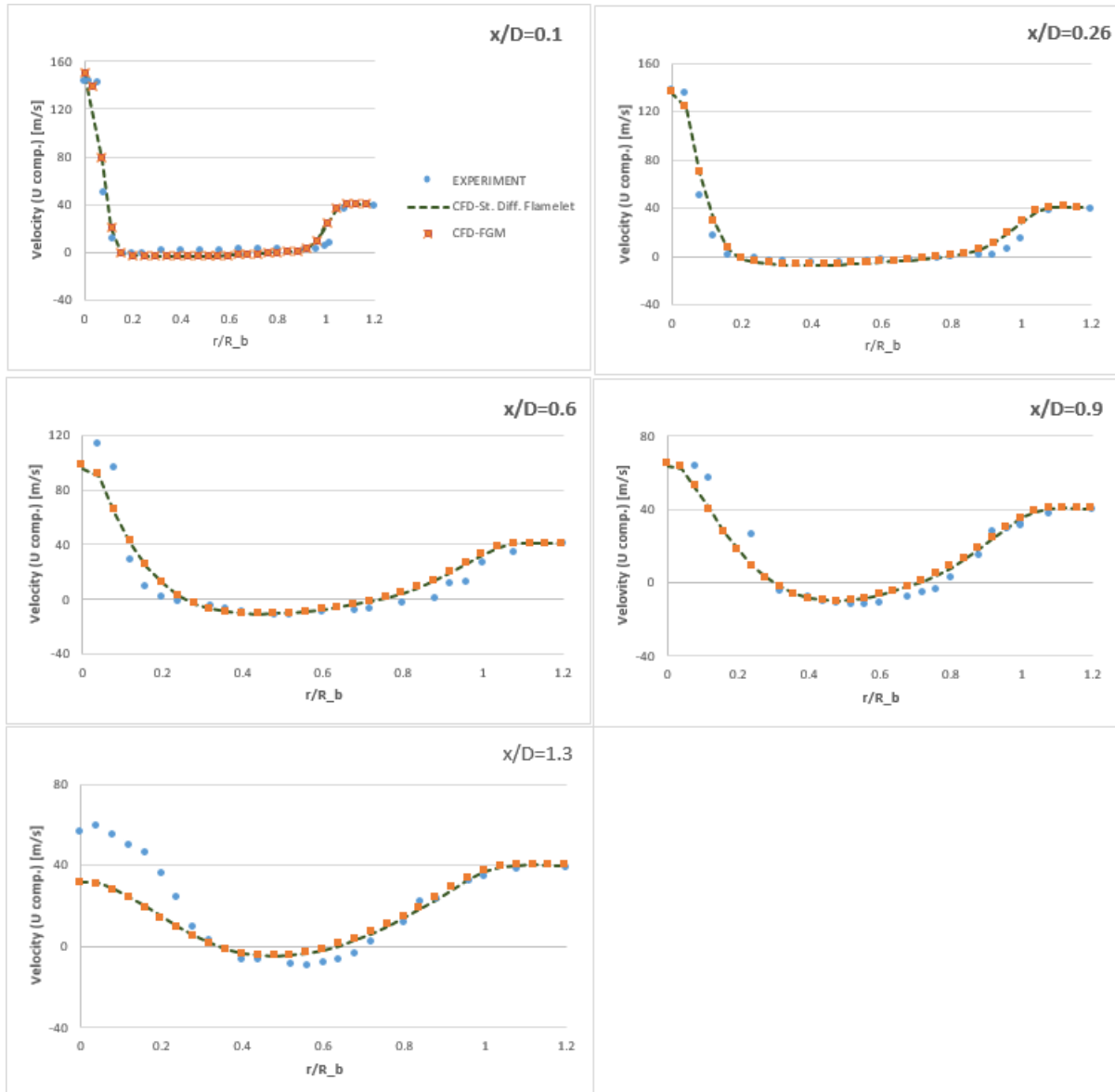


**Figure 5-1:** Radial profiles of U-component of velocity.

This re-circulation zone can be clearly seen in figure 5-2, this is also the region where the mixing between the fuel and air is initiated, after which the combustion process begins, the two re-circulations can also be visualized by making a contour of the velocity vector (Figure 5-3) and velocity magnitude (Figure 5-4). This re-circulation zone also stabilizes the flame.

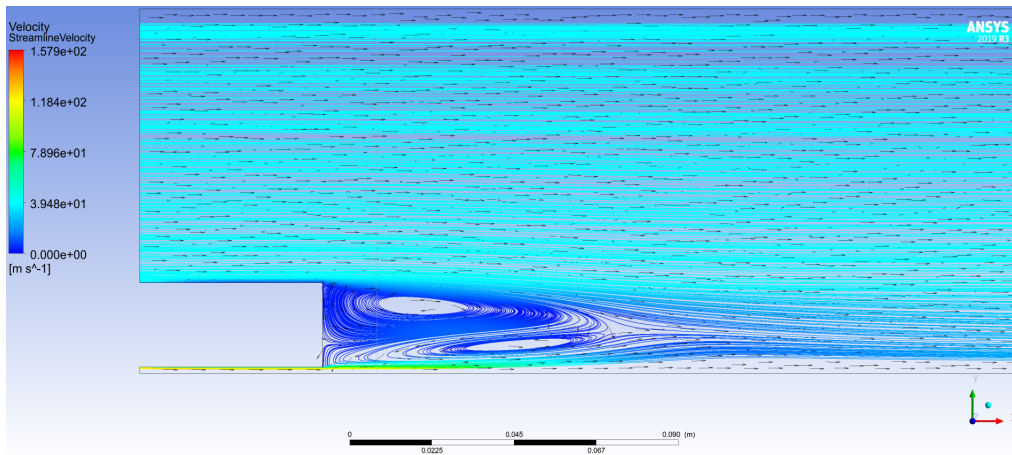


Figure 5-2: Contours for streamlines for velocity

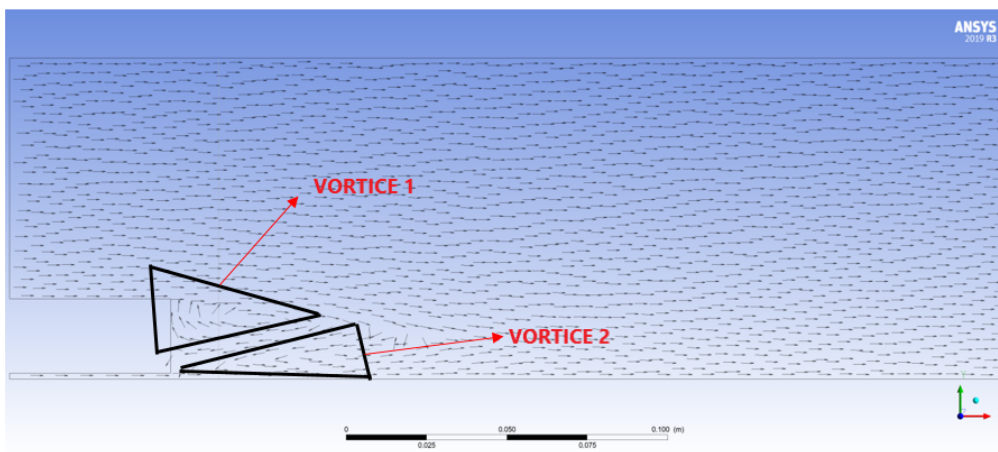


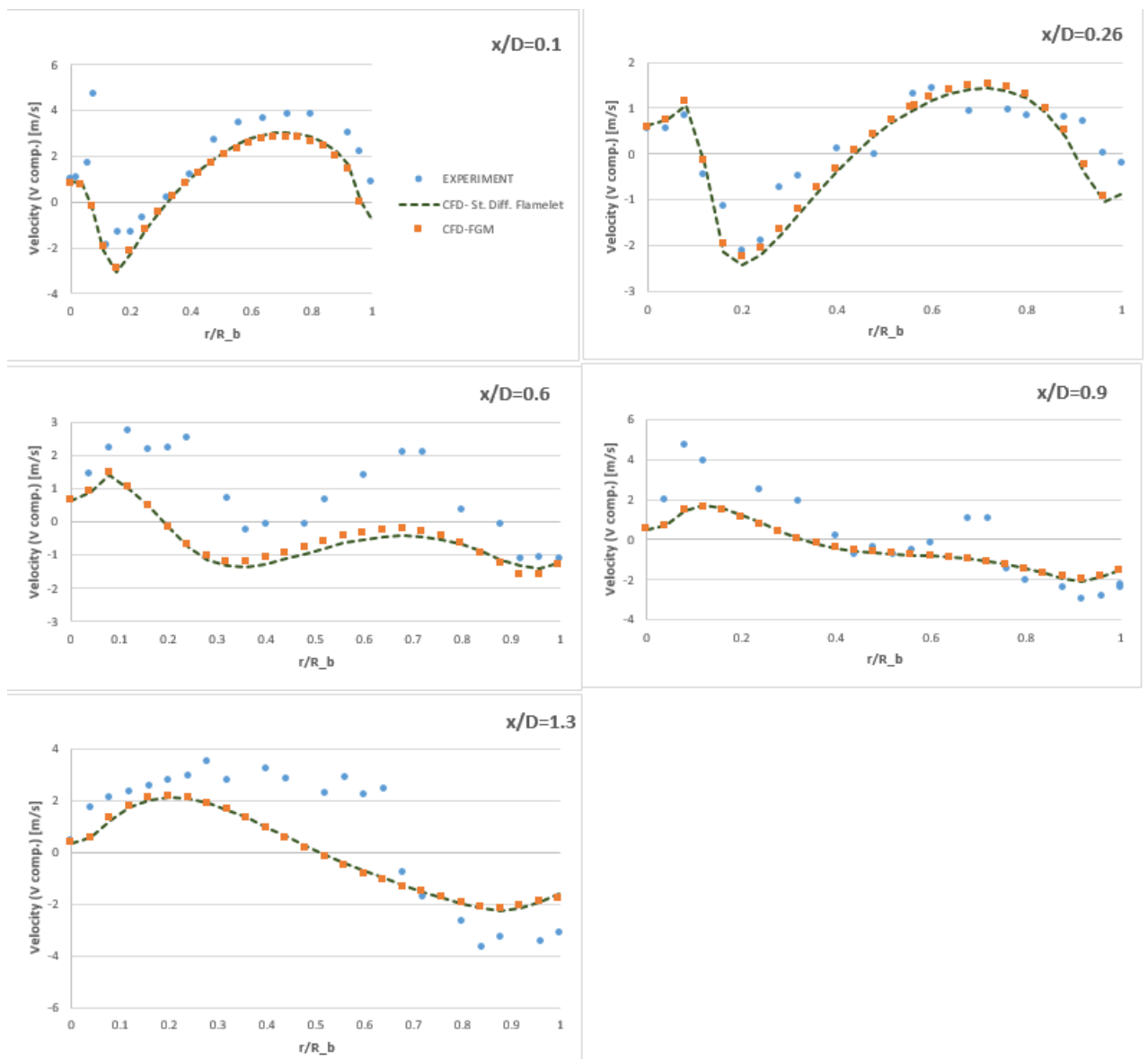
Figure 5-3: Contour for velocity vector



Figure 5-4: Contour for velocity magnitude.

Figure 5-5, represents the V-component of the velocity field. From the graphs of both the

components of the velocity field i.e. U and V components, we observe that both the combustion models namely FGM model and the steady diffusion flamelet model predicts the results in an identical manner, in most of the graphs the results from the two combustion model overlap each other, with a good agreement (trendwise) with the experimental data. However, some deviation from the experimental results is seen in the U component's profile,  $x/D = 1.3$  and in the V-components profiles  $x/D = 0.6, 0.9$  and  $1.3$ , but these deviations are not uncommon and previous investigations on HM1 flame have also reported this observation [17][13][8], these deviations can be further investigated by using different turbulence models to gain more insights on the deviations.



**Figure 5-5:** Radial profiles of V-component of velocity.

### 5-1-2 Temperature and Mixture Fraction.

Figure 5-6 represents the mean temperature profiles. We can clearly observe that both the combustion model FGM and steady diffusion flamelet model predicts the same temperature profile till  $x/D = 0.9$  after this there is a difference in peak temperature predictions between the two models. The steady diffusion flamelet model predicts the peak temperature with a very good agreement with the experimental data, on the other hand FGM model also predicts the temperature profile with reasonably good agreement with experimental data but it under-predicts the peak temperatures after  $x/D = 0.9$ . For the global visualization of the temperature field, figure shows the temperature contours for the FGM Model.

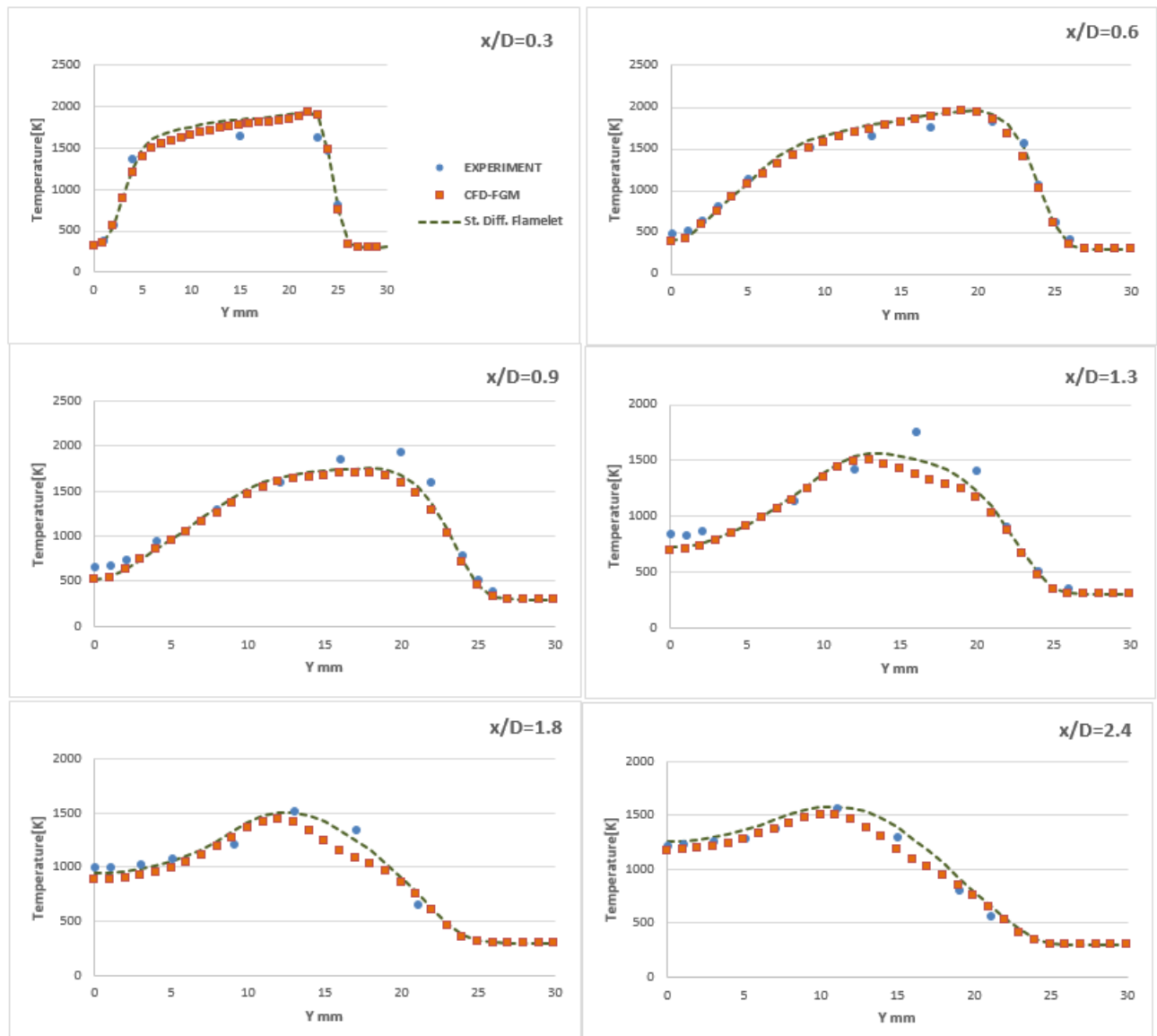
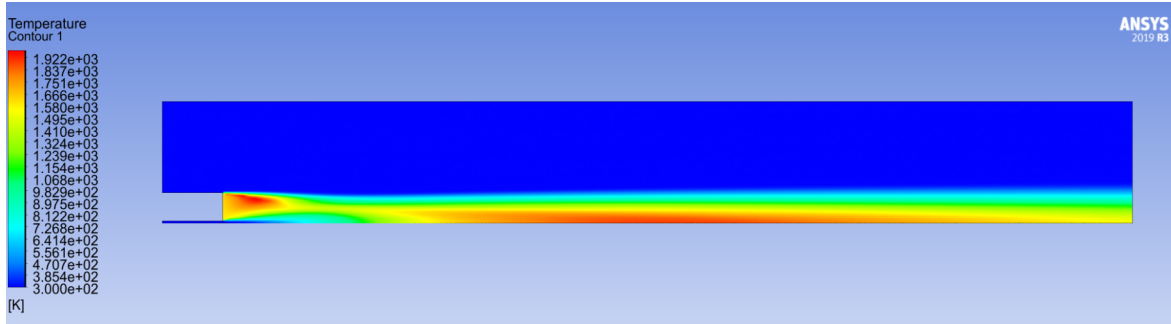


Figure 5-6: Radial profiles of the mean temperature

Also, at locations,  $x/D = 0.3$  and  $x/D = 0.6$  there is a little over-prediction of the peak temperatures by both the combustion models. In the literature we find that this deviation from the experimental data has been attributed to the uncertainty in the coflow boundary condition [17], especially the observed deviation seen at the locations close to the bluff-body is due to this uncertainty.



**Figure 5-7:** Contour of temperature for FGM model.



**Figure 5-8:** Contour of mixture fraction for FGM model.

Furthermore, figure 5-8 shows the contour for mixture fraction (for FGM model) and figure 5-9 represents the mean mixture fraction curves for both the combustion models, we can observe that at all radial locations the mixture fraction results predicted by both of the models overlap each other. Although there is a minor under-prediction of mixture fraction for the locations  $x/D = 1.3, 1.8$  and  $x/D = 2.4$ , this deviation has been reported in previous studies of Roekaerts et al [12], Ravikanti et al [17] and Kempf et al. [9]. However a study performed by Raman et al. [48] reported that it is possible to improve these deviations of mixture fraction at locations  $x/D = 1.3, 1.8$  and  $x/D = 2.4$  by using LES for simulating the flow field with a recursive filter-refinement procedure.

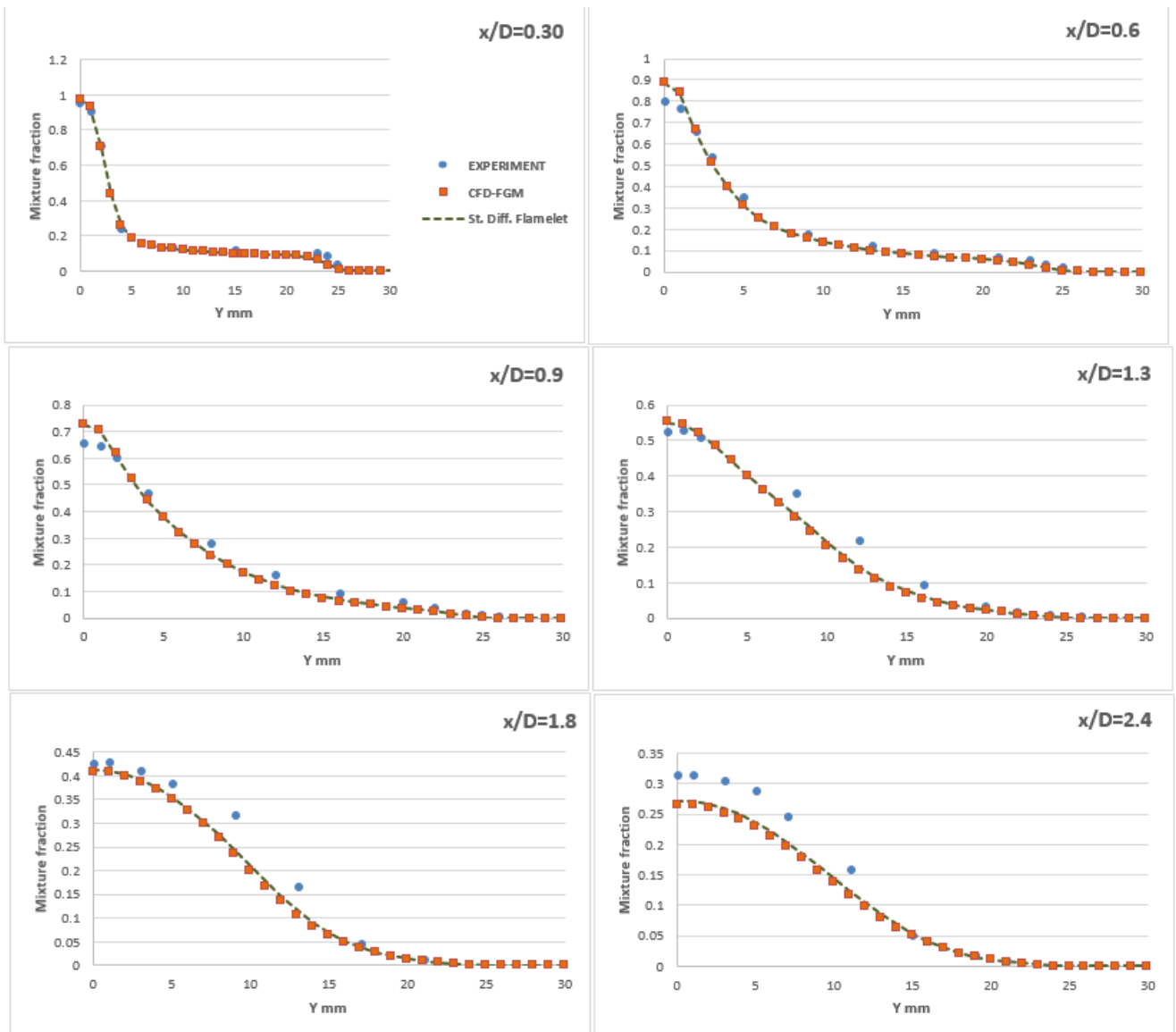


**Figure 5-9:** Radial profiles of the mean mixture fraction.

Also, figure 5-10 represents the rms values of the mixture fraction at different radial locations, in this figure we observe that the results predicted by the simulations have some deviations from the experimental data. In this figure we also observe that the results predicted by both combustion models overlap each other, which is expected as the governing equation for mixture fraction is same for both the combustion models.

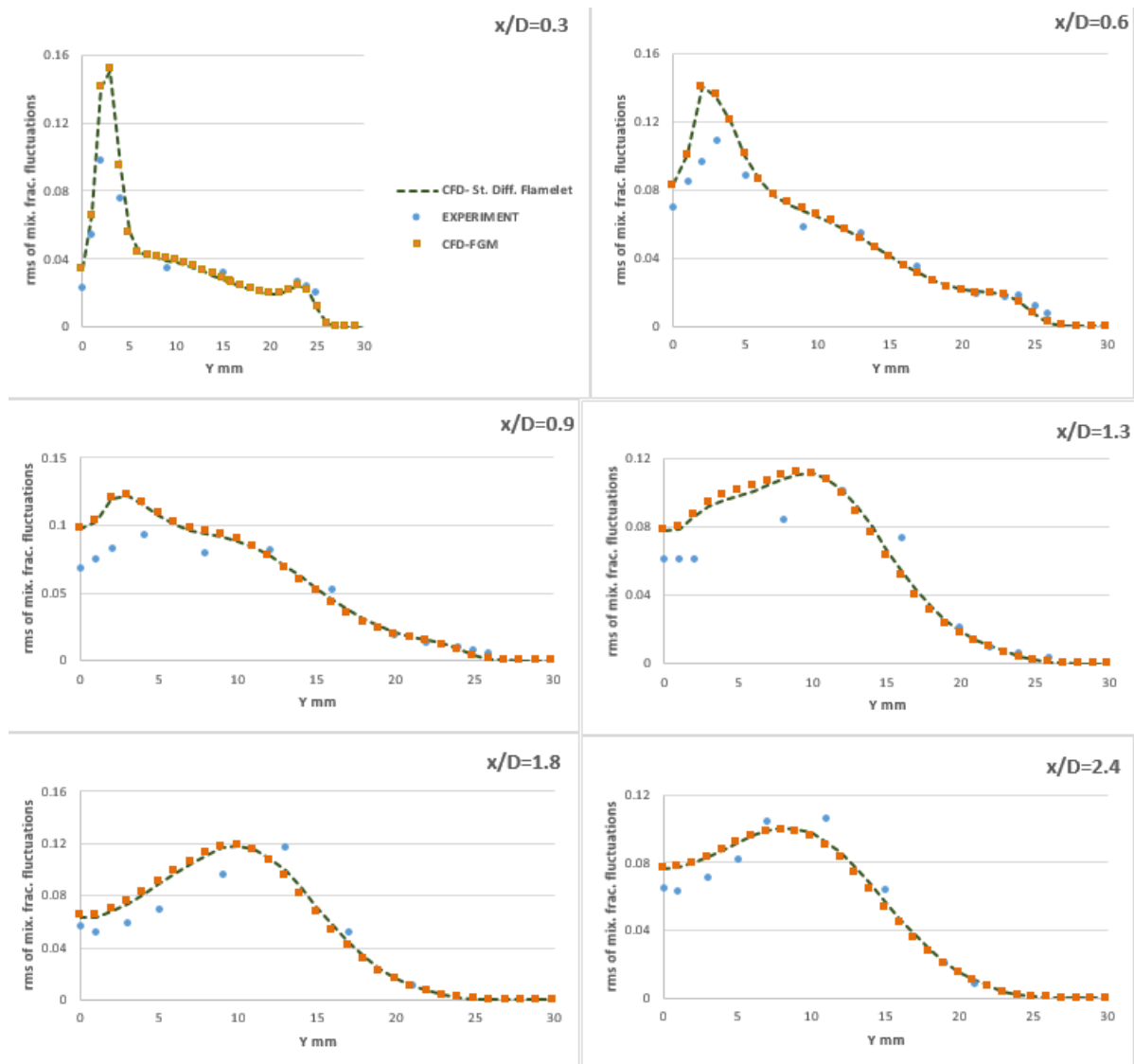


Figure 5-10: Radial profiles of rms of the mixture fraction.

### 5-1-3 Major species profiles.

Here, we present the profiles for the major species of the combustion namely,  $H_2O$  and  $CO_2$ . Figure 5-11 represents the radial profiles of  $H_2O$ . The results in figure 5-11 shows a good agreement with the experimental data, but for locations  $x/d = 0.9$  and  $x/d = 1.3$  we observe a minor under-prediction in  $H_2O$  mass fraction, from the figure we can state that steady diffusion flamelet model predicts better than the FGM model, but the difference in the results of FGM and steady diffusion flamelet model are not very significant. The acquired  $H_2O$  predictions are analogous to the results of Ravikanti et al.[17] and Verma et al.[13].

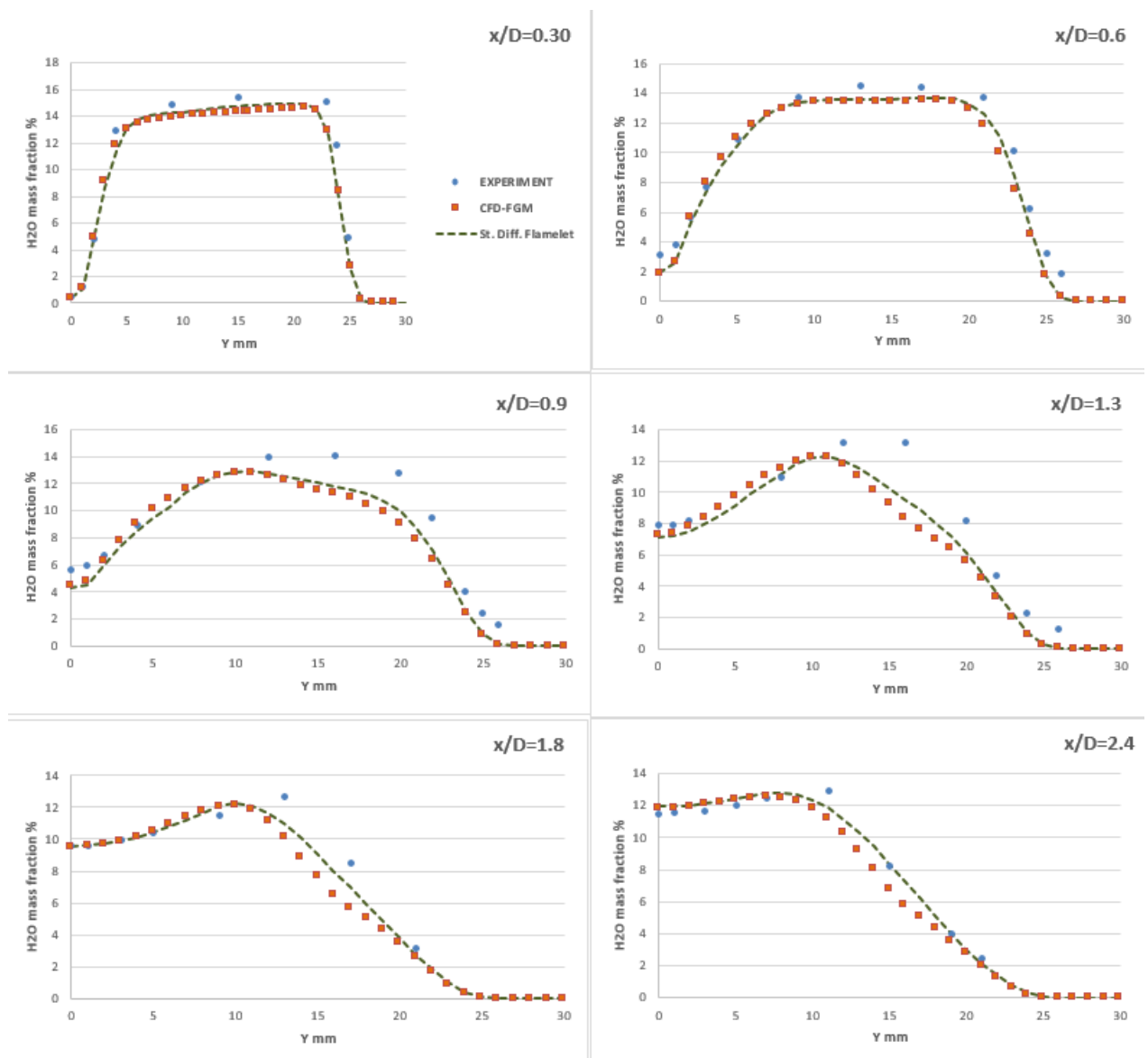
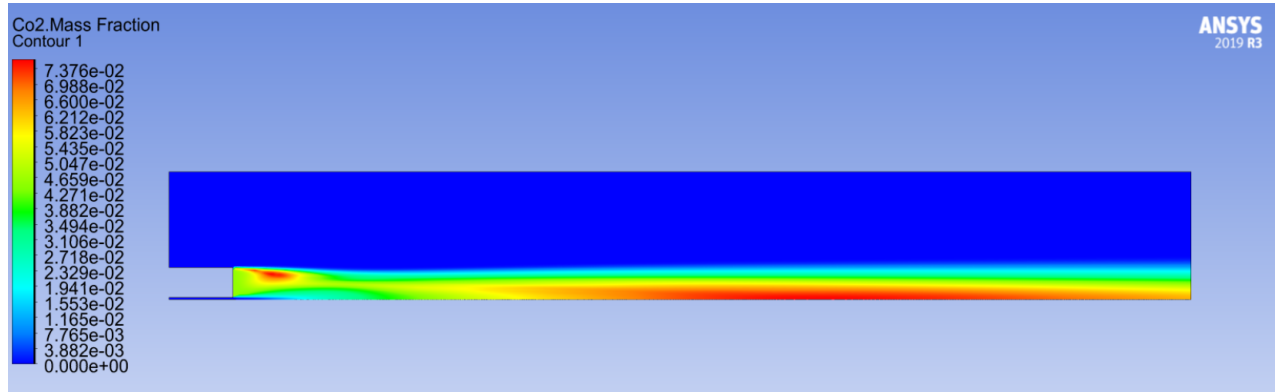
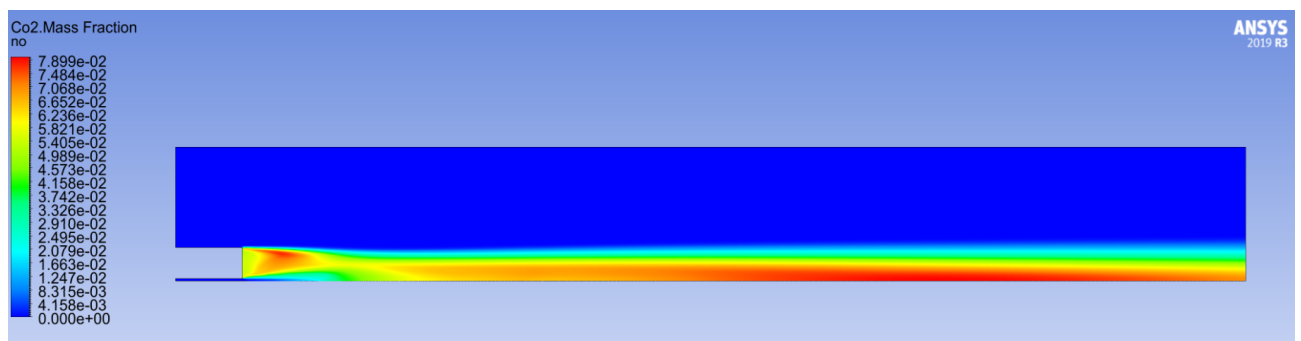


Figure 5-11: Radial profiles of  $H_2O$  mass fraction.

Figure 5-12 and 5-13, represents the the contours of  $\text{CO}_2$  mass fraction for FGM and steady diffusion flamelet model respectively.



**Figure 5-12:** Contour of  $\text{CO}_2$  for FGM model.



**Figure 5-13:** Contour of  $\text{CO}_2$  for SDF model.

From the contours of  $\text{CO}_2$  we can clearly observe that the FGM model under-predicts the  $\text{CO}_2$  levels than the steady diffusion flamelet model, this behaviour is also clearly repeated in figure 5-14, where the radial profiles of  $\text{CO}_2$  are reported. From the radial profiles of  $\text{CO}_2$  we can note that better agreement to experimental data is achieved by steady diffusion flamelet model than the FGM model, although both of these combustion models do not have full agreement with the experimental data, this observations has been also reported by Dally et al.[11] and Ravikanti et al.[17] one of the reason for this is the uncertainty in the co-flow boundary condition which acts as an obstacle for achieving exact predictions from the simulations for  $\text{CO}_2$  and OH mass fractions [17].

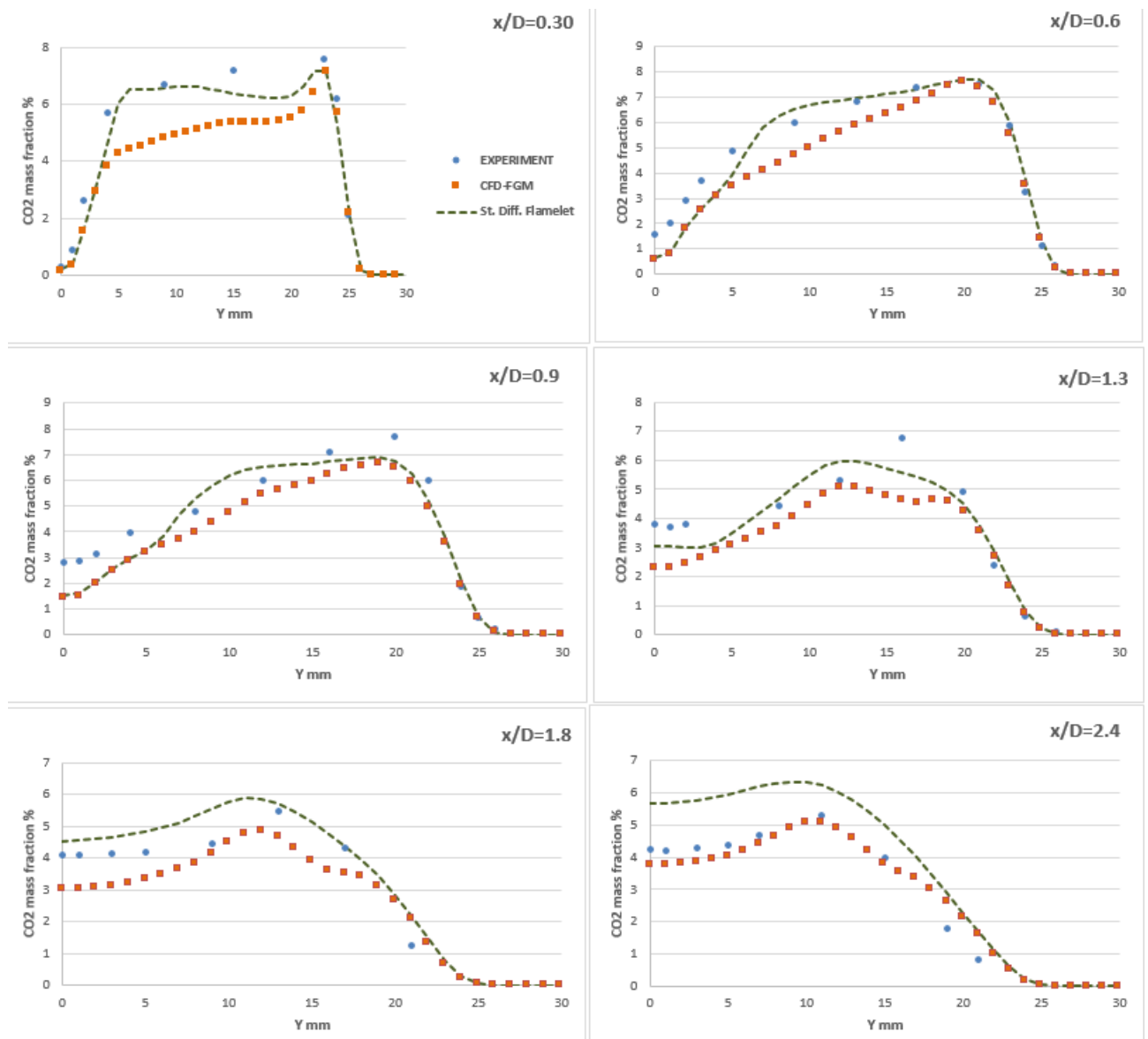
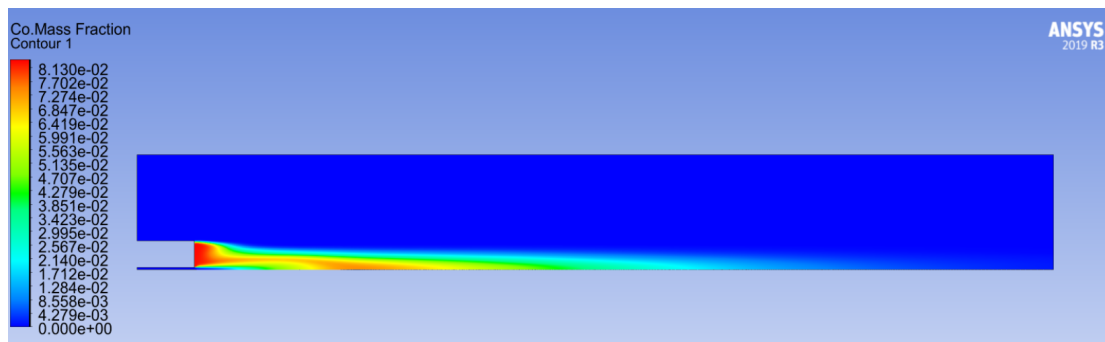


Figure 5-14: Radial profiles of CO2 mass fraction.

### 5-1-4 Minor species profiles

In this segment we report the results for the minor species of the combustion namely the mass fractions of OH, CO and NO species. First we present the contours of CO specie for FGM and steady diffusion flamelet model respectively. From the contours below we can observe that the FGM model predicts higher levels of CO mass fraction, specifically in the region close to bluff-body.



**Figure 5-15:** Contours of CO for FGM model

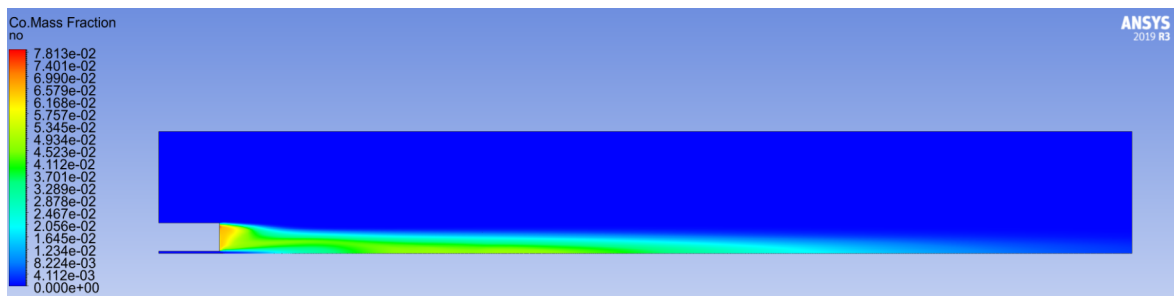


**Figure 5-16:** Contours of CO for SDF model

Furthermore, figure 5-17, represents the radial profiles of CO at different axial locations, from this figure we can clearly observe that the FGM model consistently over-predicts the CO concentrations for all axial profiles. On the other hand the steady diffusion flamelet model predicts results that are in good agreement with the experimental data.

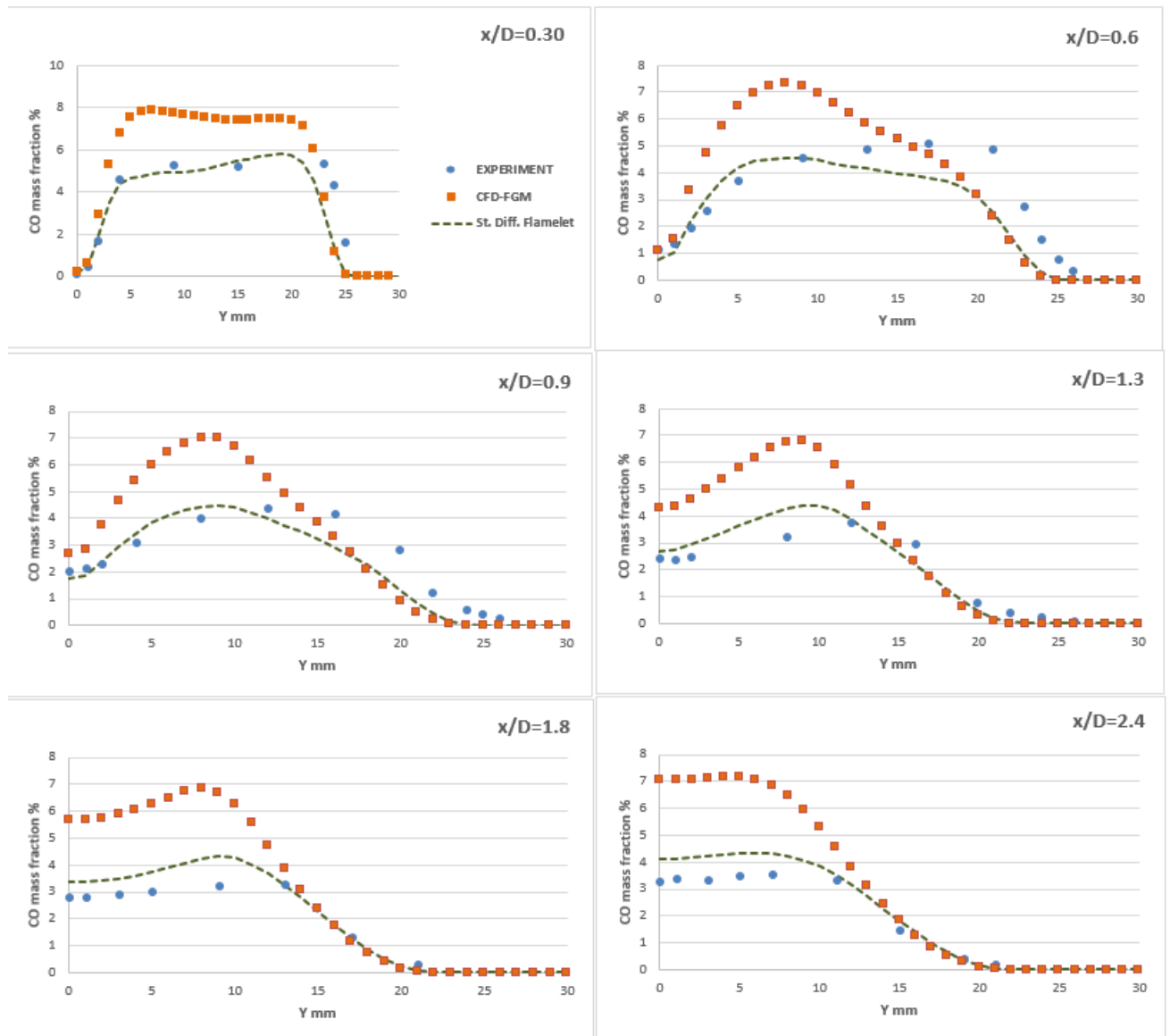


Figure 5-17: Radial profiles of CO mass fraction.

Figure 5-18, represents the radial profiles for OH mass fraction, here we observe that the FGM model consistently under-predicts the OH concentrations, while the steady diffusion flamelet model over-predicts the OH levels.

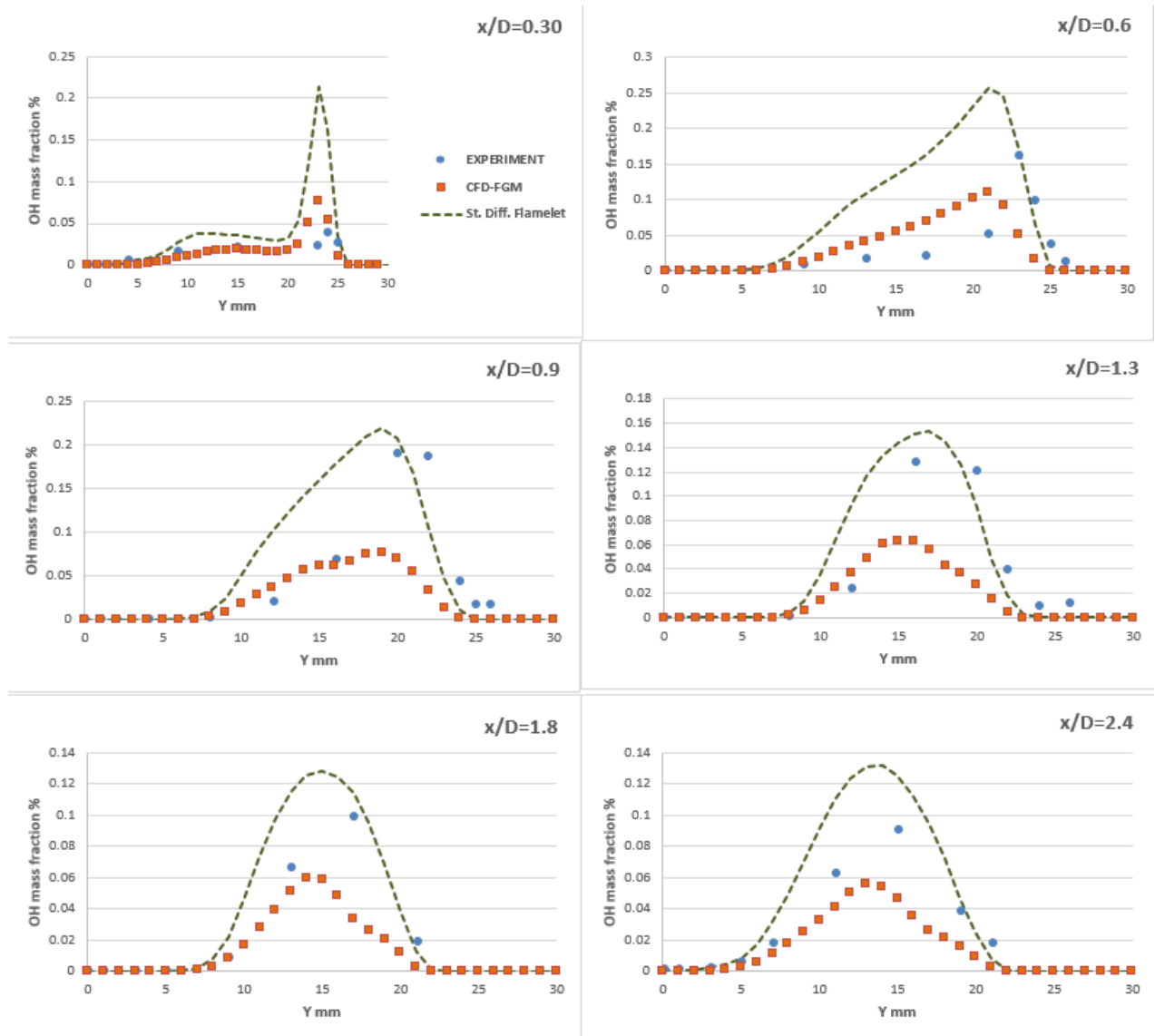
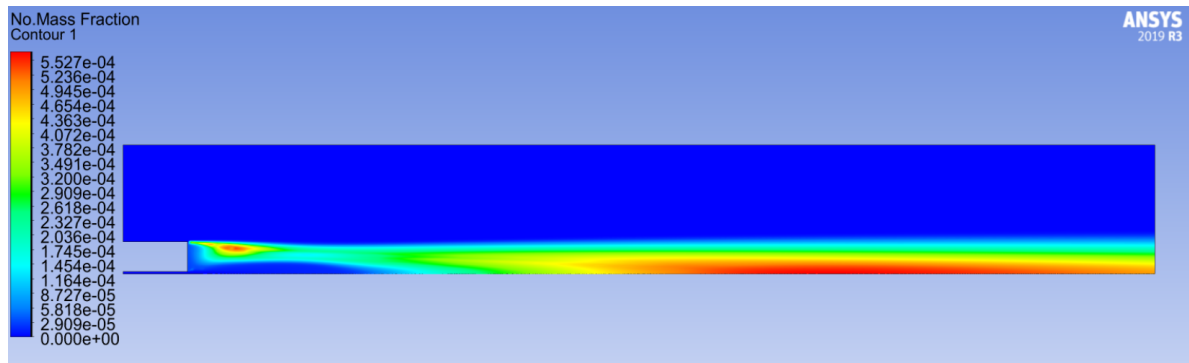
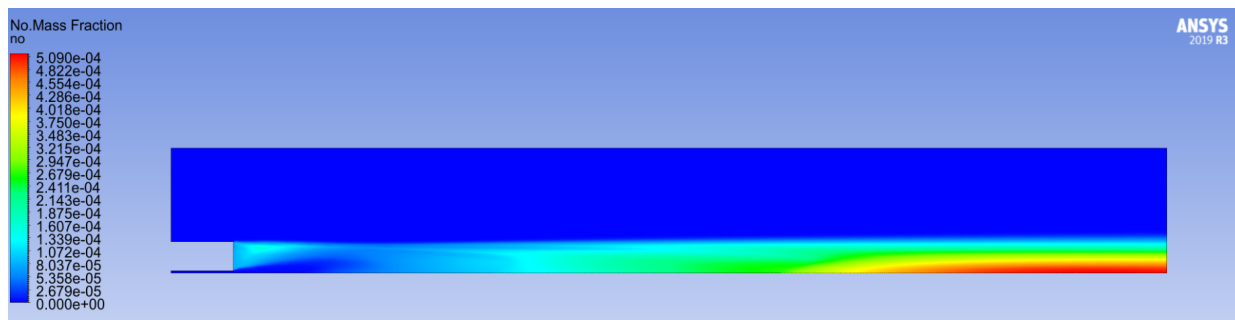


Figure 5-18: Radial profiles of OH mass fraction.

Now, we present the results for NO mass fraction profiles, but first we can consider the contour figures 5-19 and 5-20 for a comprehensive view on the performance of the combustion models. From the contour figures we can observe that the FGM model predicts the NO levels much higher than the steady diffusion flamelet model, especially at the region close to the bluff-body and at farfield ( $x/D > 2.4$ ).



**Figure 5-19:** Contour of NO for FGM model



**Figure 5-20:** Contour of NO for SDF model

Figure 5-21, represents the NO radial profiles for different axial locations, from the graphs we can note that FGM model over-predicts the NO concentrations by a large margin with respect to the experimental data, the steady diffusion flamelet also over-predicts the NO levels but with a small margin with a trendwise similarity to the experimental data, clearly steady diffusion flamelet model performs better than FGM model for NO mass fraction predictions.

The over-prediction in the results for both the combustion models can be caused due to exclusion of radiation model in the simulation. Ravikanti et al. [16] have reported that however the effect of radiation model inclusion is insignificant on the results of major species but the incorporation of radiation model can show improvements in the NO predictions.

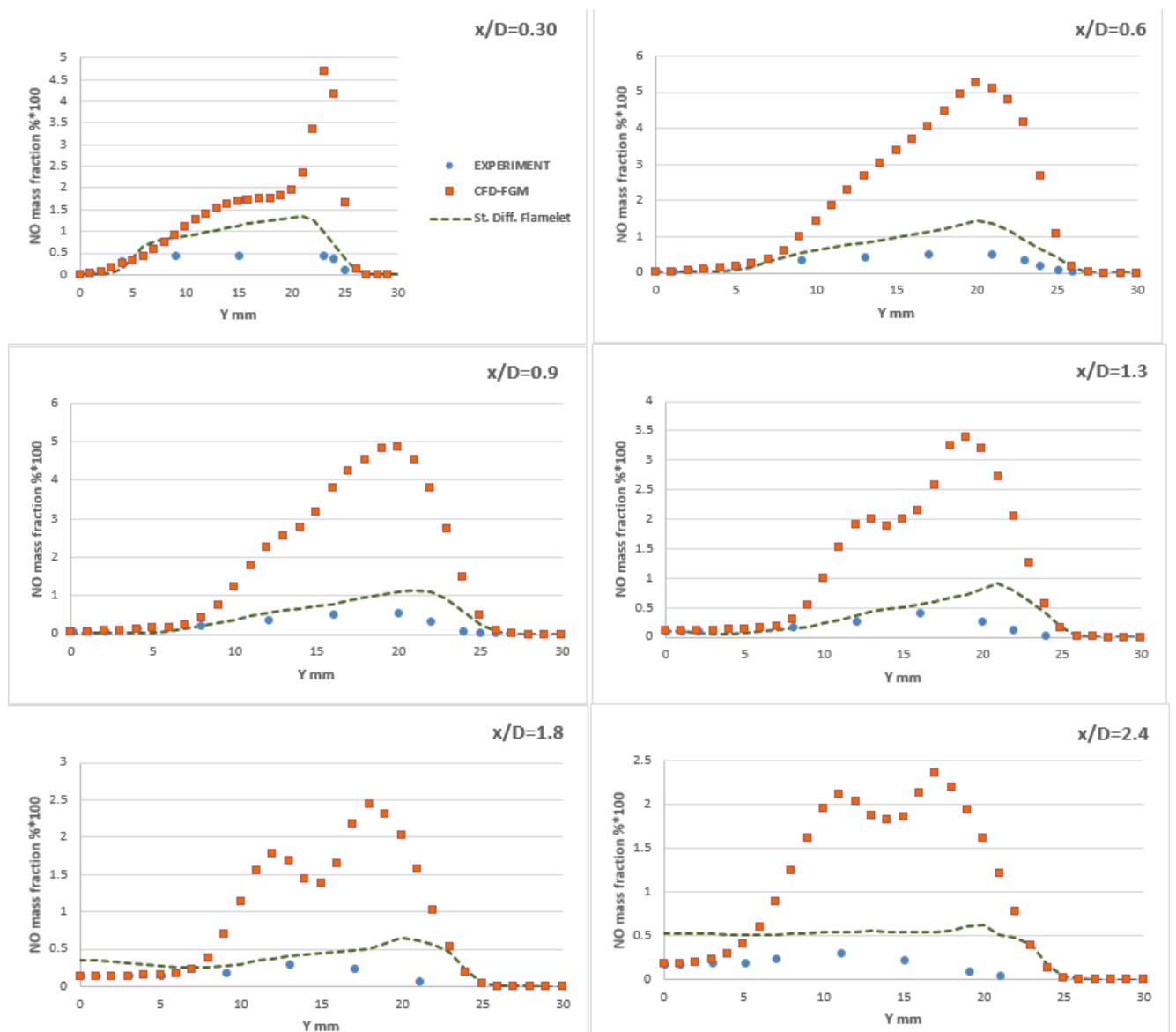


Figure 5-21: Radial profiles of NO mass fraction.

### 5-1-5 Performance of post-processing tools on $\text{NO}_x$ predictions.

#### Reactor Network Model (RNM)

As, we can infer from the above section that the  $\text{NO}$  mass fractions were over-predicted by the present modeling approaches, thus we employ extra tools to see if we can achieve better prediction capabilities for  $\text{NO}$  specie. For the present study, we have selected two post-processing tools namely reactor network model (RNM) and Ansys  $\text{NO}_x$  post processor, both of these tools are integrated with Ansys Fluent software platform. We initiate our study on a converged solution with FGM model, as the combustion model, thus the flow field predicted by the FGM model will be taken as the input for predicting the pollutant emissions by RNM.

The RNM tool, provides us with an option to use the temperatures predicted by the CFD simulation or to re-calculate the temperature field, where it solves the equation of state to recalculate the temperatures, although the temperature predicted by the CFD simulations are reliable, we used the option to solve the temperature equation, to see the difference in results (if any). Then we used temperature and mixture fraction as our clustering criteria with GRI 2.11 mechanism in the RNM tool to predict the  $\text{NO}_x$  concentrations.

For the RNM calculations, 100 reactors were specified to represent the computational domain, where each reactor represents a PSR. After, 200 iterations the solution was converged. Figures 5-22 and 5-23 shows the contours acquired by RNM tool.

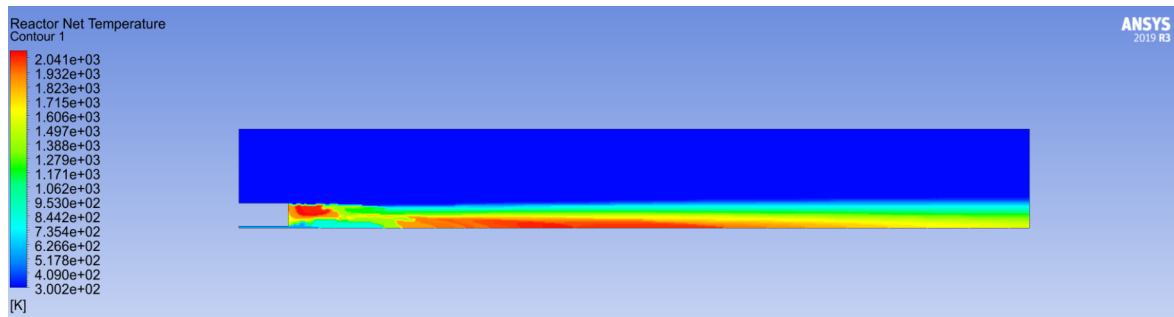
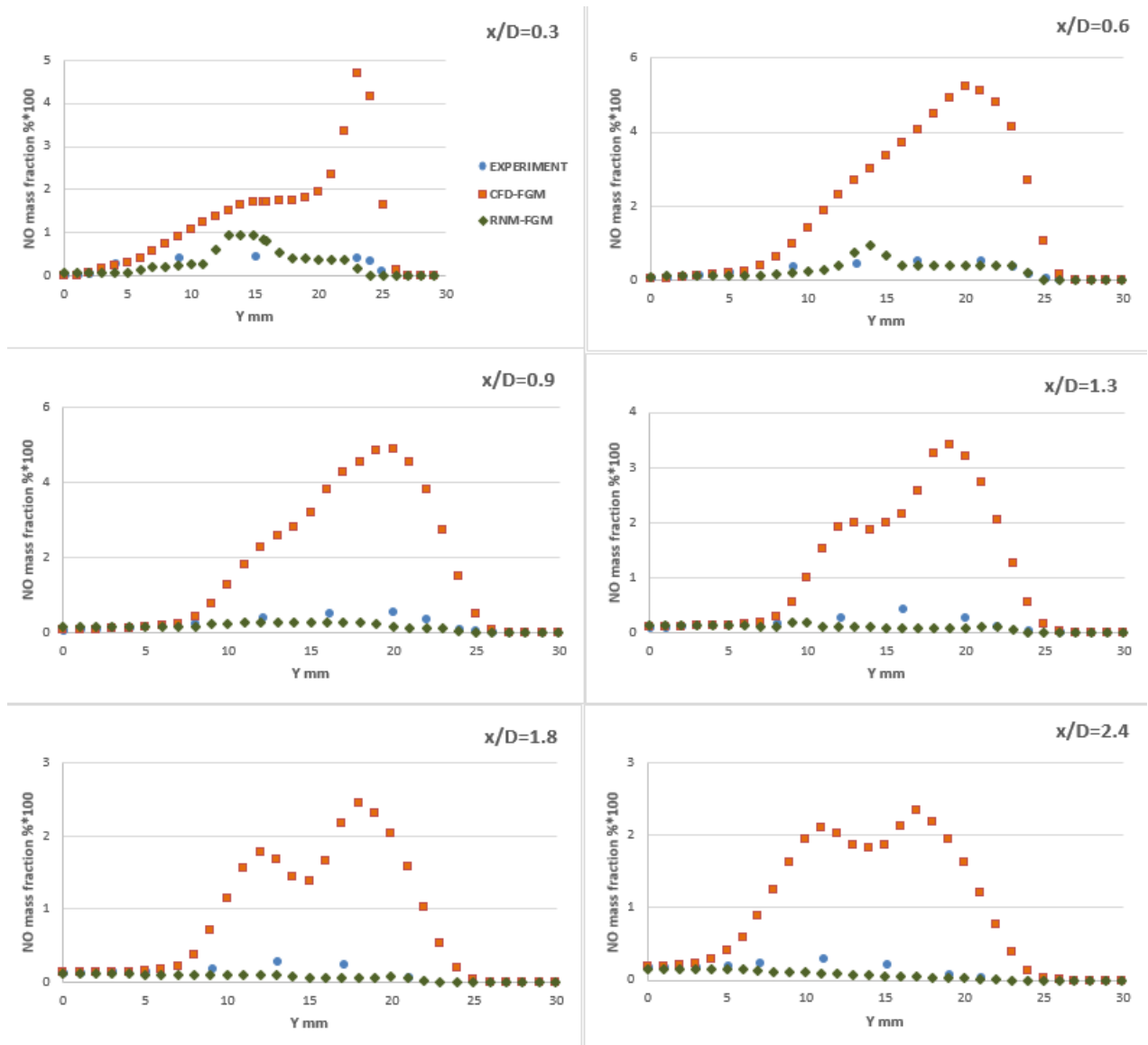


Figure 5-22: Temperature profile by RNM tool.



Figure 5-23:  $\text{NO}$  profile by RNM tool.

From the contour plots we can observe that the contour of temperature is approximately similar to the contour profile of temperature predicted by the FGM model, thus solving the equation of state, has very minimal effect on the temperatures predicted by RNM tool. Although we see a significant difference in the NO mass fraction contours predicted by FGM model and RNM tool. Further to expand on this observation we can consider figure 5-24 , where the radial profiles predicted by FGM model and RNM tool are compared at different axial locations.



**Figure 5-24:** Radical profiles of NO mass fractions with RNM model.

From the graphs in figure 5-24, we can clearly state that the RNM tool produces good agreement with respect to experimental data for  $x/D = 0.3$  and  $x/D = 0.6$ , However for the farfield profiles like  $x/D = 1.8$  and  $x/D = 2.4$ , we note minor under-predictions in the predicted values of NO.

For a robust assessment on the efficacy of RNM tool to predict minor species concentration reliably, we compared the CO profiles predicted by FGM model and RNM tool with the experimental data. The case of CO profiles was taken as CO is also a minor species and is much easier to predict reliably than  $\text{NO}_x$  concentrations [10]. Figure 5-25 represents the radial profiles of CO at different axial locations, from the figure we can observe that RNM tool significantly under-predicts the CO levels. This under-prediction can be attributed to the clustering criteria used for building the CRN.

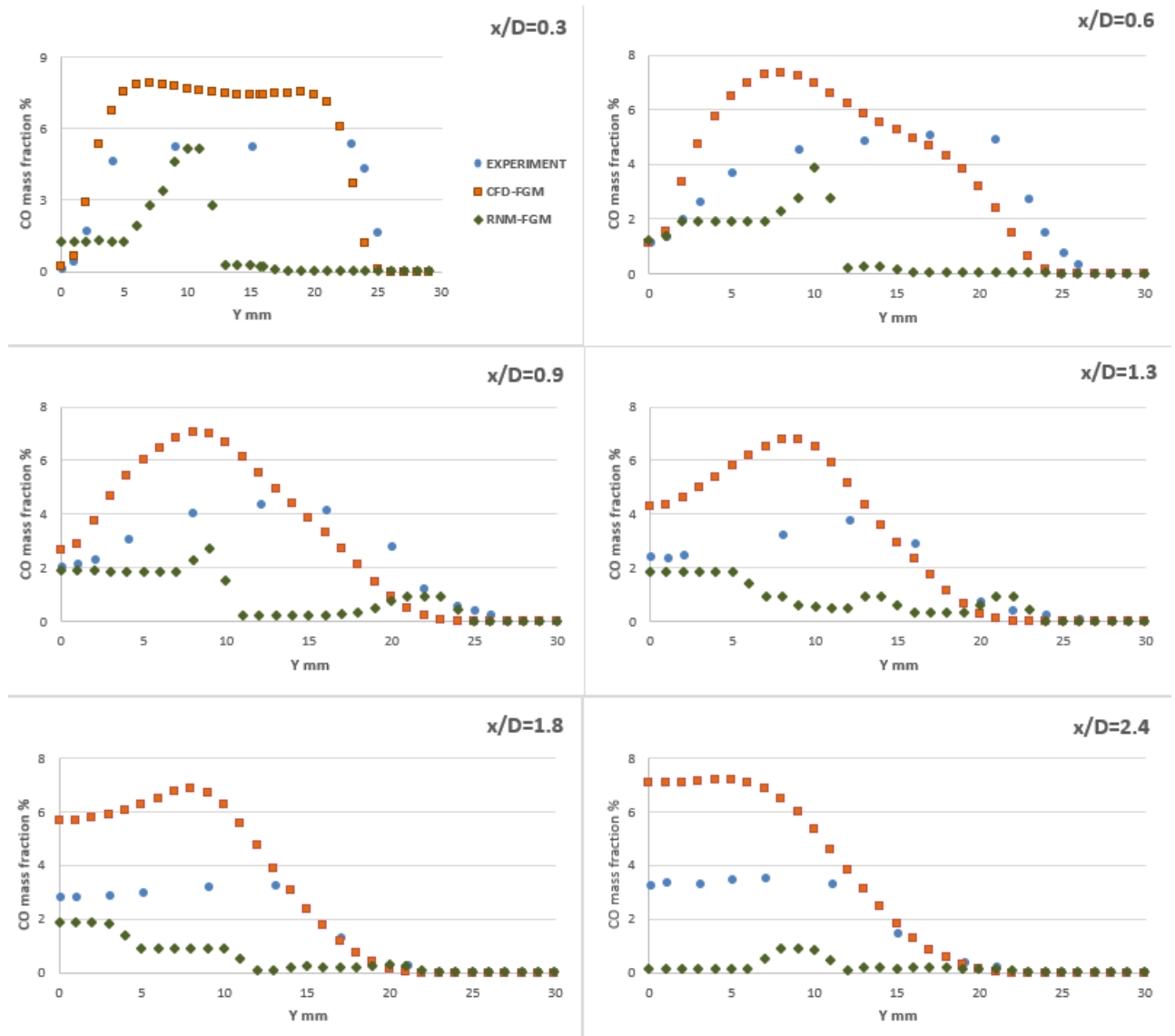
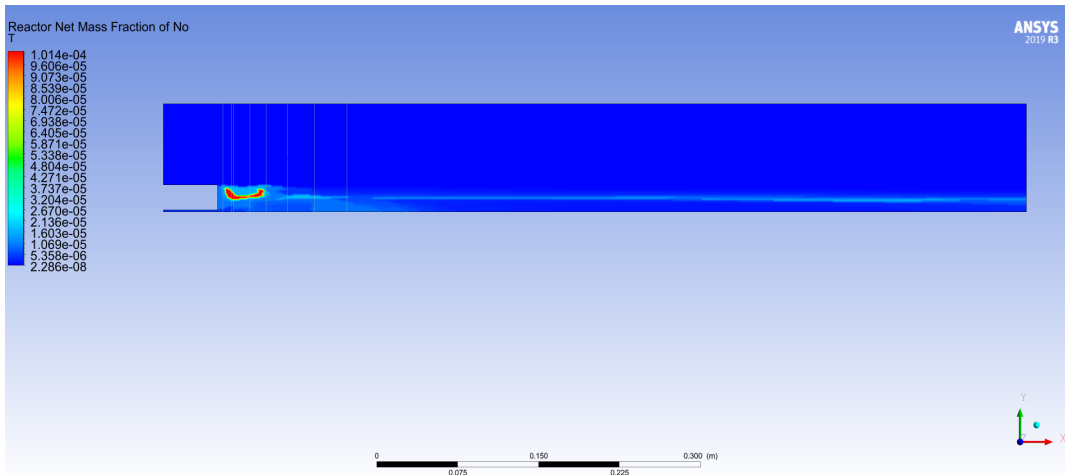
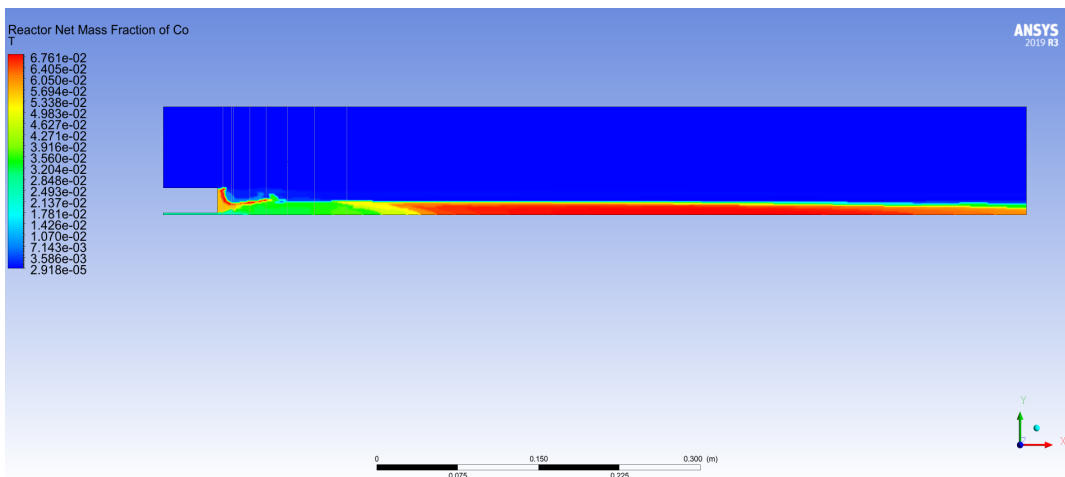


Figure 5-25: Radical profiles of CO mass fractions with RNM model.

Following the utilization of RNM tool to post-process the data for CFD calculations with FGM model we extended the scope of RNM tool by initiating a study on a converged solution with steady diffusion flamelet model, as the combustion model, thus the flow field predicted by the SDF model will be taken as the input for predicting the pollutant emissions by RNM tool. Figures 5-26 and 5-27 represents the contours of NO and CO mass fractions predicted by the RNM tool respectively, in this simulation also we selected our clustering criteria based on temperature and mixture fraction with 100 reactors to form a reactor network including GRI 2.11 mech. as the chemical mechanism.



**Figure 5-26:** Contours of NO mass fraction predicted by RNM for SDF model as baseline



**Figure 5-27:** Contours of CO mass fraction predicted by RNM for SDF model as baseline

Furthermore, we plotted the radial profiles of NO levels predicted by RNM tool at different axial locations and compared it with the radial profiles predicted by steady diffusion flamelet model, figure 5-28 shows this comparison.

From figure 5-28, we can clearly observe that the RNM tool consistently under-predicts the NO concentrations for farfield larger than and including  $x/D = 0.9$  as compared to the experimental data, while the SDF model consistently over-predicts the NO concentrations for all axial locations. One more observation is noted for the radial distance, from the figure 5-28 we observe that after the radial distance of  $y = 10$  mm the performance of RNM tool gets worse for the all the axial locations but a significant diversion from the experimental data is seen for  $x/D = 0.3$  and  $0.6$ .

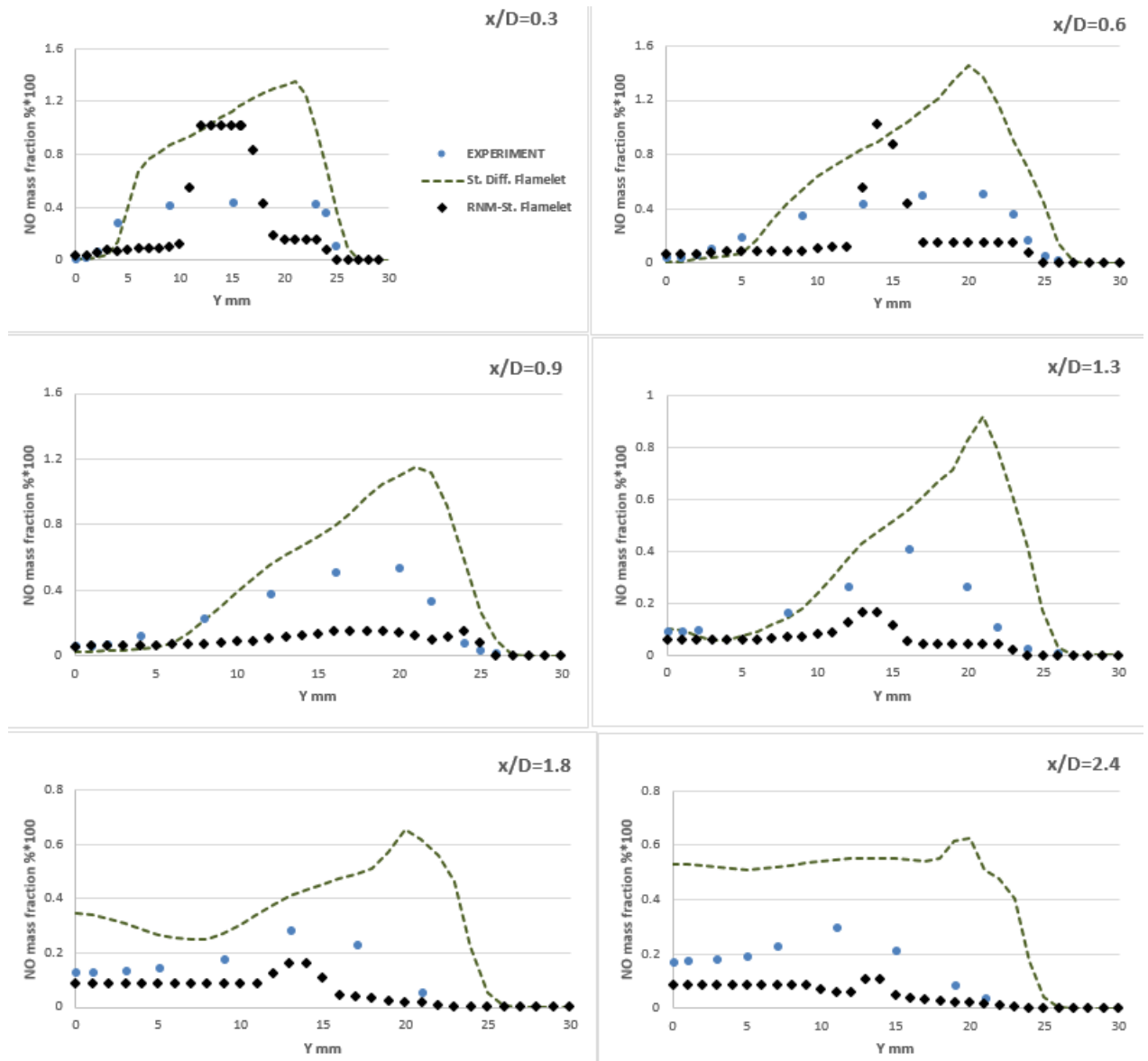


Figure 5-28: NO profiles with RNM tool for SDF model

The CO mass fractions were also predicted by using the RNM tool for the steady diffusion flamelet model and compared with the experimental data and (baseline) steady diffusion flamelet model, figure 5-29 reports the predictions of RNM tool. From figure 5-28 we observe that the predictions of CO levels get worse around radial profile of  $y = 10$  mm for all axial locations. For axial profiles  $x/D = 1.3, 1.8$  and  $2.4$  we observe a step-wise response in the predictions of CO mass fraction by RNM tool.

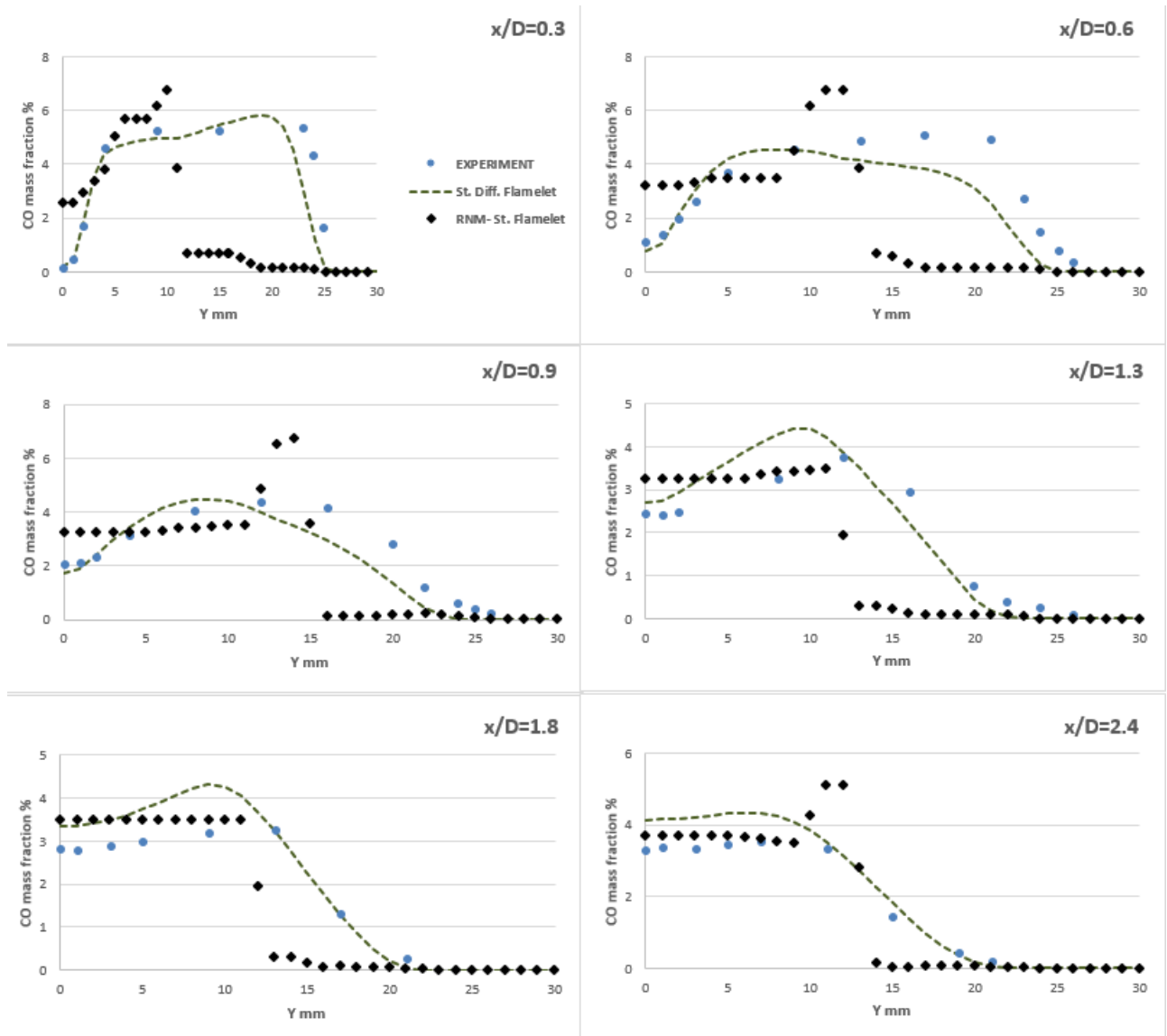
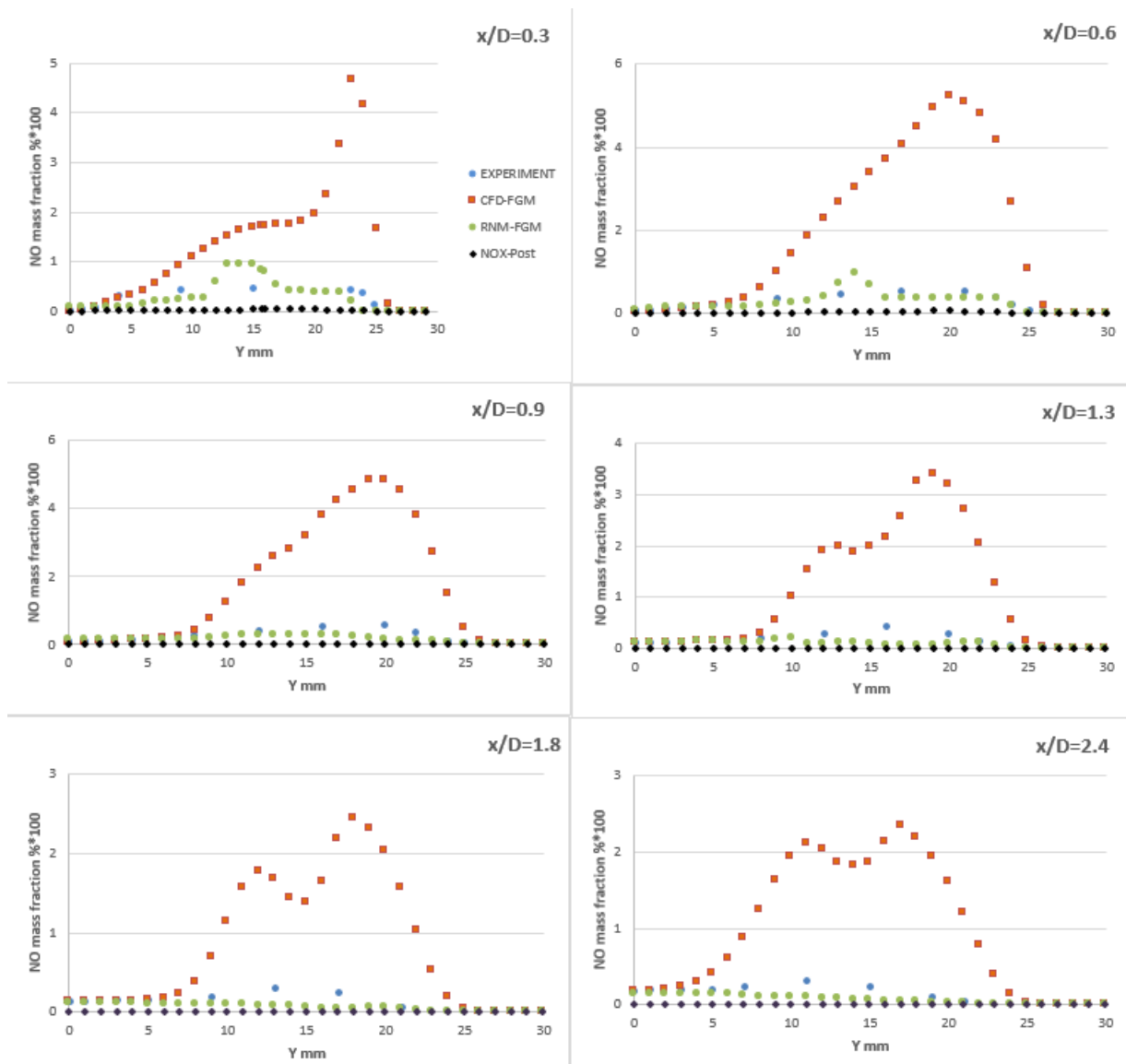


Figure 5-29: CO profiles with RNM tool for SDF model

**Ansys NO<sub>x</sub> post-processor**

Furthermore, we employ the next post-processing tool to predict the NO<sub>x</sub> concentrations. In the NO<sub>x</sub> post-processor we have the option for modeling the thermal, prompt, and fuel NO<sub>x</sub> formations. In our case we have enabled the thermal and prompt NO<sub>x</sub> formation mechanisms. For this the NO<sub>x</sub> post-processor solves an additional transport equation for NO species based on the given flow field and combustion solution predicted by the combustion model, in figure 5-30 we used FGM model to acquire the baseline solution with GRI 2.11 mechanism and after the convergence of results, NO<sub>x</sub> post-processor was "switched on" by selecting thermal and prompt mechanisms. Figure 5-30 represents the radial profiles acquired for the NO<sub>x</sub> post-processor at different axial locations, in the figure we can compare the results predicted by the RNM tool, NO<sub>x</sub> post-processor, FGM model with the experimental results.



**Figure 5-30:** Radical profiles of NO mass fractions with RNM model and NOx post processor.

From figure 5-30, we can clearly observe that the  $\text{NO}_x$  post-processor consistently under-predicts the NO levels with comparison to the experimental results for all axial locations, this observation is not uncommon as similar results for  $\text{NO}_x$  post-processor were reported by Stagni et al. [10]. The same observation was recorded by us from the simulation with SDF model as the background. However the  $\text{NO}_x$  post-processor is computationally very fast in reporting  $\text{NO}_x$  concentrations, we achieved convergence at 100 iterations for post-processing the  $\text{NO}_x$  mass fraction results. This swiftness in results is possible because the  $\text{NO}_x$  post-processor decouples the NO transport equation from the species equations.

## 5-2 Discussion and analysis

In this section we present our analysis on the observations of the results. The section is divided into two parts, the first part deals with the analysis on the performance aspects of the combustion models for predicting NO levels and the second part consists of the analysis of the post-processing tools on their performance in pollutant predictions.

### 5-2-1 Performance of combustion models

In this segment we discuss the performance of FGM model and SDF model in predicting the NO concentrations. As, we have already discussed the general observation on the results produced by these model with reference to the experimental data.

In general the FGM model highly over-predicts the NO levels and the SDF model also over-predicts the NO levels but in minor amount. There are multiple reasons why these deviations can happen:-

1. As, from the results (figure 5-6) , we observed that the temperature field was over predicted by both of these models for  $x/D = 0.3$  and  $0.6$ , these axial locations corresponds to the nearfield in the computational domain which is near to the re-circulation zone, consisting of two vortices. This re-circulation zone is classified by high temperature and large residence times thus resulting in high NO formation. If temperature is over-predicted in this region it will lead to a significant over-prediction in NO species mass fraction also.
2. In the present study, we have used adiabatic treatment for the flamelet model without including any radiation model, thus the heat loss downstream of the flame is not accounted, which can cause over-prediction in the predicted temperatures consequently over-predicting the NO levels.
3. From figure 5-18, we also observed that both the combustion models over-predicted the Hydroxyl radical (OH) mass fraction for axial locations  $x/D = 0.30$  and  $0.60$ , which was expected because the temperature was also over-predicted for the same axial locations and as thermal or Zeldovich mechanism is the  $NO_x$  producing mechanism in these axial locations due to high temperatures, it will lead to a over-prediction of NO species because OH radical levels are over-predicted.

### 5-2-2 Performance of post-processing tools

In the presented study, we have performed simulations with two post processing tools namely RNM tool and Ansys  $NO_x$  post processor, below we give an analysis on each of them:-

#### Reactor Network Model (RNM) post-processing tool

We have performed two simulation using RNM tool, the first simulation has the baseline solution with FGM model and the second simulation has the baseline solution with steady

diffusion flamelet model and the concentrations of NO and Carbon Monoxide (CO) species were reported from these simulations.

The NO concentrations predicted by RNM tool with FGM model as baseline solution, are in good agreement with the experimental data however for SDF model as baseline solution the NO predictions are consistently under-predicted by the RNM tool. This deviation in the results is related to the clustering criteria selected during the simulations.

If we infer figure 5-22, where the predicted temperature contours are shown by RNM tool, we observe that region wherefrom the air enters the computational domain and all the downstream region after that has a temperature of approximately 300 K, this observation is not unphysical but it causes serious problems while clustering process to form reactor network. As our clustering criteria depends on temperature and mixture fraction, thus the whole region (as described above) with 300 K is assumed as a single Perfectly Stirred Reactor (PSR) by the RNM tool, this causes energy unbalances causing inexact predictions of NO concentrations. This observation is also verified if we carefully look at the radial profiles of the NO levels, as we approach near to the wall of bluff-body the deviations in the NO predictions starts to occur due to energy unbalances, the similar observation is also extended towards the deviation in the predicted CO concentrations by RNM tool.

If we discuss the solution speed of RNM tool it is computationally very fast to produce results. For both of our simulations 200 iterations were performed by the RNM tool within 10 minutes per simulation. Thus this is an advantage of the RNM tool.

### **Ansys NO<sub>x</sub> post processor**

Ansys NO<sub>x</sub> post processor was used to post-process the NO mass fraction data, after performing the CFD simulation with FGM model and SDF model. Figure 5-30, clearly shows that the Ansys NO<sub>x</sub> post processor consistently under-predicts the NO levels.

One reason for this discrepancy is that, we have implemented the thermal and prompt NO<sub>x</sub> mechanisms directly in the simulations without using a user defined function (UDF).

Also as we can infer from the theory [19], the Ansys NO<sub>x</sub> post processor is not a stand-alone software, which means that it relies on the combustion solution predicted by the combustion model and as, we have already discussed that the combustion models did not exactly predict the results for NO concentrations thus, it can be expected that the results produced by NO<sub>x</sub> post processor will also not be more precise than that predicted by the combustion models.

Although, the consistent under-prediction by the tool is recorded in the literature [10] were similar trends were reported but the exact cause for this under-prediction is still unclear.

# Conclusion and recommendations

## Conclusions

The thesis report presented the modelling approaches for predicting the NO concentrations from the bluff-body stabilized HM1 flame. Numerical investigations were performed on two combustion models to assess their efficacy to predict the NO mass fractions, we compared the steady diffusion flamelet model with the flamelet generated manifold model for both major and minor species with a special focus to assess their performance on NO predictions. In chapter one of the thesis project we defined the research questions for the project. Now, as we have presented the results we can evaluate the research questions by providing a response to them.

1. For the first research question, we can state that both of combustion models used in the thesis work namely FGM model and SDF model were capable to model the TCI in a satisfactory way but SDF model performed better than FGM model.
2. By the literature study, we can state that using a detailed chemical mechanism corresponds to better predictions of the thermo-chemical properties of the combustion system (here HM1 flame) and the GRI 2.11 mechanism is recommended to model practical combustion systems.
3. For the third question we can state that using post-processing tools with simple formulation did not improve the NO levels predicted by the CFD simulations.

Below we have stipulated our main remarks from the study:-

1. The comparison between FGM model and Steady Flamelet Model (SDF) was conducted with GRI 2.11 chemical mechanism and k-  $\epsilon$  model, which is also the novelty of the study as this kind of comparison has not been reported in the literature. From the results, we can conclude that the steady diffusion model showed better agreement with the experimental data than the FGM model. Although both models over-predicted the NO concentrations.

2. The overall performance of the steady diffusion flamelet model (including the predictions of mixing field, temperature field, and major and minor species) corresponds to a clear agreement with the results reported by Ravikanti et al. [17] and the performance of the FGM model is qualitatively analogous to the results reported by Mauro et al. [8] but our study present the FGM results in a better way than Mauro et al.
3. To improve the  $\text{NO}_x$  predictions, two post-processing tools were also employed in the present study. The computational speed to attain a converged solution for both of the post-processing tools was very good, and that is an advantage of these tools. However in the case of Reactor Network Model (RNM) tool there were some deviations in the predictions of NO levels but still it did capture the global trend with respect to the experimental data but in case of Ansys  $\text{NO}_x$  post-processor the results were not so encouraging as it highly under-predicted the NO levels.

### Recommendations

1. A comparative study needs to be performed between the FGM model and the non-adiabatic flamelet model to assess their distinctions in NO predictions.
2. A study is open to investigate the precise form of the equations for mean and variance of the scaled progress variable.
3. The coflow boundary condition needs to be studied in more detail by using different model formulation and mesh construction, for achieving better predictions from the simulations.
4. More rigorous studies need to be conducted with the RNM tool by using multiple clustering criterion's for the CRN construction to get better insights on the performance of the RNM tool on NO concentration predictions.
5. It was observed that relatively simple formulations for  $\text{NO}_x$  calculation by post-processing tools do not perform well. It remains open whether more detailed formulation using a CRN with many more reactors can give better predictions.

---

# Appendix A

---

## **FGM transport equations**

The appendix is written by Prof. em. Dr. Dirk Roekaerts for supporting the work presented in the thesis.

## Analysis of FGM transport equations

In the FGM approach to turbulent flame modelling the mixture fraction and the progress variable are considered to be fluctuation quantities and in the model they are described by their one-point PDF, the probability density function for values taken at one point in space.

In the presumed PDF approach one describes the PDF by an assumed mathematical shape characterised by the values of first and second moments (mean and variance).

The instantaneous values of all needed thermochemical quantities are tabulated as function of mixture fraction and progress variable based on results of calculated flamelets. The mean values of all needed thermochemical quantities are calculated performing the integration of instantaneous values over all possible values of mixture fraction and progress variable with the PDF as weight factor. The mean values then are also tabulated and are used in the turbulent flame calculation.

An extra complication arises from the fact that it is useful to formulate the model in terms of a progress variable that is normalized on the interval [0,1]. It has been found to be useful for two reasons. First, it is practical for tabulation when the independent variables of the table all have a range [0,1]. Second, scaled variables are found to be statistically independent to a greater degree than unscaled variables. The assumption of statistical independence of mixture fraction and scaled progress variable simplifies the difficulty of finding a good assumed shape for the joint PDF and will be an important part of the model formulation.

It is the purpose of this note to explain the implications of the switch from original definition of progress variable (unscaled progress variable) to normalized progress variable (scaled progress variable) for the model equations.

### Relation between statistical moments of unscaled and scaled progress variable

In FGM for non-premixed and partially premixed combustion the independent variables are mixture fraction and progress variable. The progress variable most often is a linear combination of species, constructed in such a way that its value changes monotonously when traversing the flame and the relation between values of thermochemical quantities and a pair of values of mixture fraction and progress variable are unique and reveal the relevant processes with sufficient detail. Here it is assumed that an appropriate unscaled progress variable  $Y_c$  has been found.

For tabulation purposes the scaled progress variable is introduced. It is defined by

$$c = \frac{Y_c - Y_{c\min}}{Y_{c\max} - Y_{c\min}}$$

Here “min” and “max” refer to the minimal value and maximal value of unscaled progress variable. In the case that the fuel or oxidiser do not contain any of the species contributing to the progress variable, for every value of mixture fraction its minimal value is 0 and the scaled progress variable then becomes

$$c = \frac{Y_c}{Y_{c\max}(Z)}$$

The maximal value of unscaled progress variable could vanish at  $Z=0$  and  $Z=1$  and the scaling would be mathematically ill-undefined but in these cases  $c$  is set 0 by definition and not by the transformation equation. The relations between the independent variables  $Z$  and  $c$  and other thermodynamic variables are stored in the FGM table.

In turbulent flow the mixture fraction and the progress variable are fluctuating and in the model this is described using their probability density function.

Density weighted mean properties of any thermodynamic quantity that can be included in the table can then be calculated from

$$\tilde{Y}_k = \int_0^1 \int_0^1 Y_k^{fgm}(z, c) \tilde{P}_{z,c}(z, c) dz dc$$

Making the assumption that the mixture fraction and the scaled progress variable are statistically independent the joint PDF reduces to the product of the marginal PDF of mixture fraction and the marginal PDF of scaled progress variable.

$$\tilde{Y}_k = \int_0^1 \int_0^1 Y_k^{fgm}(z, c) \tilde{P}_z(z) \tilde{P}_c(c) dz dc$$

A standard approach is to make the assumption that both marginal PDFs take the form of a beta-function. This mathematical function is depending on two parameters, that can be related to the mean and variance.

### Transport equations for mixture fraction and unscaled progress variable

Because both mixture fraction and progress variable are linear combinations of species mass fractions, their laminar transport equations can be derived from the transport equations of species mass fractions. This leads to relatively simple equations only in the case all species can be assumed to have equal diffusivity. Let us assume first that this assumption can be made. For generality we keep however a different notation for laminar diffusivity of mixture fraction  $D_Z$  and laminar diffusivity of progress variable  $D_{Y_c}$ . Further on we shall however use that they are assumed to be equal.

Using standard averaging approaches and modelling assumptions, model equations for mean and variance of mixture fraction and unscaled progress variable can be derived. They are given by:

Equation for mean mixture fraction

$$\frac{\partial}{\partial t} \bar{\rho} \tilde{Z} + \frac{\partial}{\partial x_i} (\bar{\rho} \tilde{v}_i \tilde{Z}) = \frac{\partial}{\partial x_i} \left( \bar{\rho} \bar{D}_{eff} \frac{\partial}{\partial x_i} \tilde{Z} \right)$$

with  $\bar{\rho} \bar{D}_{eff} = \bar{\rho} \bar{D}_Z + \frac{\mu_t}{\sigma_Z}$

Equation for variance of mixture fraction

$$\frac{\partial}{\partial t} \bar{\rho} \widetilde{Z''^2} + \frac{\partial}{\partial x_i} (\bar{\rho} \tilde{v}_i \widetilde{Z''^2}) = \frac{\partial}{\partial x_i} \left( \bar{\rho} \bar{D}_{eff} \frac{\partial}{\partial x_i} \widetilde{Z''^2} \right) + 2 \bar{\rho} \bar{D}_{eff} \frac{\partial \tilde{Z}}{\partial x_i} \frac{\partial \tilde{Z}}{\partial x_i} - C_{\phi, Z} \bar{\rho} \frac{\varepsilon}{k} \widetilde{Z''^2}$$

In preparation of the discussion of the equation for scaled progress variable below we note that the last term is a model term obtained by the following closure assumption:

$$2 \bar{\rho} \bar{D}_{eff} \left( \frac{\partial \tilde{Z}}{\partial x_i} \right) \left( \frac{\partial \tilde{Z}}{\partial x_i} \right) = C_{\phi, Z} \bar{\rho} \frac{\varepsilon}{k} \widetilde{Z''^2}$$

Equation for mean unscaled progress variable

$$\frac{\partial}{\partial t} \bar{\rho} \tilde{Y}_c + \frac{\partial}{\partial x_i} (\bar{\rho} \tilde{v}_i \tilde{Y}_c) = \frac{\partial}{\partial x_i} \left( \bar{\rho} \bar{D}_{eff, c} \frac{\partial}{\partial x_i} \tilde{Y}_c \right) + \bar{\rho} \tilde{S}_{Y_c}$$

with  $\bar{\rho} \bar{D}_{eff, c} = \bar{\rho} \bar{D}_{Y_c} + \frac{\mu_t}{\sigma_{Y_c}}$

Equation for variance of unscaled progress variable

$$\frac{\partial}{\partial t} \bar{\rho} \widetilde{Y_c''^2} + \frac{\partial}{\partial x_i} (\bar{\rho} \tilde{v}_i \widetilde{Y_c''^2}) = \frac{\partial}{\partial x_i} \left( \bar{\rho} \bar{D}_{eff, c} \frac{\partial}{\partial x_i} \widetilde{Y_c''^2} \right) + 2 \bar{\rho} \bar{D}_{eff, c} \frac{\partial \tilde{Y}_c}{\partial x_i} \frac{\partial \tilde{Y}_c}{\partial x_i} - C_{\phi, Y_c} \bar{\rho} \frac{\varepsilon}{k} \widetilde{Y_c''^2} + 2 \bar{\rho} (\widetilde{S_{Y_c} Y_c} - \tilde{S}_{Y_c} \tilde{Y}_c)$$

In these equations several model constants appear, Schmidt numbers with standard value 0.9

$$\sigma_Z = \sigma_{Y_c} = 0.9$$

and constants controlling the variance decay rate with standard value 2

$$\phi_Z = \phi_{Y_c} = 2$$

It should be recalled that the recommended values of these constants are case dependent.

### Calculation of mean values when transport equations of mixture fraction and unscaled progress variable have been obtained

In order to be able to calculate mean values it is necessary to obtain the mean and variance of scaled progress variable (appearing in the PDF) from the mean and variance of unscaled progress variable.

When mixture fraction and scaled progress variable are statistically independent these relations are (considering the case with  $Y_{cmin}=0$ ):

$$\tilde{Y}_c = \tilde{c} \tilde{Y}_{cmax}$$

$$\widetilde{Y_c''^2} = \left( \widetilde{c^2} - \tilde{c}^2 \right) \widetilde{Y_{cmax}^2} + \left( \widetilde{Y_{cmax}^2} - Y_{cmax}^2 \right) \tilde{c}^2$$

$$\widetilde{Y_c''^2} = \left( \widetilde{c''^2} \right) \widetilde{Y_{cmax}^2} + \left( \widetilde{Y_{cmax}''^2} \right) \tilde{c}^2$$

Note that the mean values of maximal unscaled progress variable and the square of the maximal unscaled progress variable can be obtained from

$$\tilde{Y}_{c_{\max}} = \int_0^1 Y_{c_{\max}}(z) \tilde{P}_Z(z) dz$$

$$\overline{Y_{c_{\max}}^2} = \int_0^1 Y_{c_{\max}}^2(z) \tilde{P}_Z(z) dz$$

To use these equations the maximum of unscaled progress variable must be tabulated and the averaging formula has to be applied.

### Transport equation for the mean of scaled progress variable

It would be convenient to directly solve the transport equations for mean and variance of scaled progress variable and such equations have been used in the literature. But it should be pointed out that these contain some extra terms, compared to what is obtained by simply replacing  $Y_c$  by  $c$ .

The equation for mean and variance of scaled progress variable can be obtained by substitution the definition of scaled progress variable and working out the equations. But to understand the origin of extra terms it is better to do the transformation from unscaled progress variable to scaled progress variable in the laminar equations, then split variable in mean and fluctuation and do the averaging of the equations. Next find out which terms are small in the limit of large Reynolds number and can be left out and finally propose closure models for the unclosed terms. This is a tedious procedure that has been presented in full in the Appendix of the PhD thesis of Marco Derksen [1] (University Twente) for the more general case including enthalpy loss. Here we recall only the key points leading to the final form of the equations.

The extra source term arising from the diffusion term in the laminar form of the transport equation for scaled progress variable is (contained in Equation B.9 in [1]):

$$\rho S_{ST} = \left[ \frac{1}{Y_{c_{\max}}} \frac{\partial^2 Y_{c_{\max}}}{\partial Z^2} \right] \rho c D \left( \frac{\partial Z''}{\partial x_i} \right) \left( \frac{\partial Z''}{\partial x_i} \right)$$

We now assume that the laminar diffusivity of mixture fraction and unscaled progress variable are equal and have value  $D$  and that also their turbulent Schmidt numbers are equal.

The factor between angular brackets is only function of mixture fraction and following the assumption made above is statistically independent of the scaled progress variable  $c$ . Statistical properties of the factors containing the gradient of the density weighted fluctuation of mixture fraction are not described by the PDF of mixture fraction and progress variable and their average is unclosed. But a similar expression was already present in the derivation of the equation of variance of mixture fraction

and we apply the same closure here. This leads to the following expression for the mean of the extra source term in the equation for mean scaled progress variable: (Note that the factor between angular brackets was assumed to be statistically independent of the quantity that was replaced by a closure assumption.)

$$\overline{\rho S_{ST}} = \bar{\rho} \widetilde{S_{ST}} = \left[ \frac{1}{Y_{c\max}} \frac{\partial^2 Y_{c\max}}{\partial Z^2} \right] \tilde{c} \frac{1}{2} C_{\phi,Z} \bar{\rho} \frac{\varepsilon}{k} \widetilde{Z}''^2$$

The source terms of scaled and unscaled progress variable are related by

$$\tilde{S}_c = \frac{1}{\widetilde{Y}_{c\max}} \tilde{S}_{Y_c}$$

The final equation of mean scaled progress variable therefore is:

$$\frac{\partial}{\partial t} \bar{\rho} \tilde{c} + \frac{\partial}{\partial x_i} (\bar{\rho} \tilde{v}_i \tilde{c}) = \frac{\partial}{\partial x_i} \left( \bar{\rho} \bar{D}_{eff,c} \frac{\partial}{\partial x_i} \tilde{c} \right) + \bar{\rho} \tilde{S}_c + \bar{\rho} \widetilde{S_{ST}}$$

the source term due to the scaling transformation is linear in the mean scaled progress variable and is proportional to the product of the variance of mixture fraction and the second derivative of  $Y_{c\max}$  with respect to mixture fraction. In a situation with no mixture fraction fluctuations, the term vanishes. Indeed, in that case the unscaled progress variable statistics evolves in conditions with a certain fixed maximum and effects of changes in the maximum at other values of mixture fraction are of no importance. The extra term also vanishes when the change of maximum of unscaled progress variable with mixture fraction is linear. In that case the effects of fluctuations towards higher and lower mixture fraction cancel out. But when there is a nonlinear dependence of the maximum of unscaled progress variable as function of mixture fraction, there is an effect. This situation arises in the stoichiometric zone where combustion products typically contributing to the progress variable can reach the highest value. Since the second derivative of  $Y_{\max}$  is negative in this region the source term is negative. Gradients in the mean mixture fraction are the main source of variance of mixture fraction. So when the stoichiometric zone is lying in a region with high mixture fraction gradient, some effects can be expected.

### Transport equation for the variance of scaled progress variable

Source terms appearing in the equation for the mean progress variable, also lead to a source term in the equation for the variance of progress variable. It is already known is that the contribution due to the chemical source term is given by

$$2\overline{\rho S_{Y_c}'' Y_c''} = 2\bar{\rho} \widetilde{S_{Y_c}'' Y_c''} = 2\bar{\rho} \left( \widetilde{S_{Y_c}'' Y_c''} - \tilde{S}_{Y_c}'' \widetilde{Y_c''} \right)$$

The contribution of the source term due to the scaling transformation is of the same form. The equation for the variance of scaled progress variable therefore is:

$$\begin{aligned} \frac{\partial}{\partial t} \bar{\rho} \widetilde{c}^{\prime\prime 2} + \frac{\partial}{\partial x_i} (\bar{\rho} \widetilde{v}_i c^{\prime\prime 2}) = \rho \frac{\partial}{\partial x_i} \left( \bar{\rho} \bar{D}_{eff} \frac{\partial}{\partial x_i} c^{\prime\prime 2} \right) + 2 \bar{\rho} \bar{D}_{eff} \frac{\partial \widetilde{c}}{\partial x_i} \frac{\partial \widetilde{c}}{\partial x_i} - C_{\phi, Y_c} \bar{\rho} \frac{\varepsilon}{k} (c^{\prime\prime 2}) \\ + 2 \bar{\rho} (\widetilde{S}_c c - \widetilde{S}_c \widetilde{c}) + 2 \bar{\rho} (\widetilde{S}_{ST} c - \widetilde{S}_{ST} \widetilde{c}) \end{aligned}$$

However, there is an important difference between the contribution from the chemical source term and from the scaling transformation source term. The chemical source term is a function of local properties in one point and is closed once the one-point PDF of scalar properties is known. The chemical source term due to the scaling transformation depends on the statistics of the gradient of mixture fraction and closure has to be specified. The instantaneous expression is

$$\rho S_{ST} c = \left[ \frac{1}{Y_{cmax}} \frac{\partial^2 Y_{cmax}}{\partial Z^2} \right] \rho c^2 D \left( \frac{\partial Z''}{\partial x_i} \right) \left( \frac{\partial Z''}{\partial x_i} \right)$$

The expression to be closed is

$$\bar{\rho} (\widetilde{S}_{ST} c - \widetilde{S}_{ST} \widetilde{c})$$

The first term is

$$\overline{\rho S_{ST} c} = \overline{\left[ \frac{1}{Y_{cmax}} \frac{\partial^2 Y_{cmax}}{\partial Z^2} \right] \rho c^2 D \left( \frac{\partial Z''}{\partial x_i} \right) \left( \frac{\partial Z''}{\partial x_i} \right)}$$

Invoking the assumption that the factor between square brackets is independent of the rest and the closure of the mean of the square of the mixture fraction gradient, one obtains

$$\overline{\rho S_{ST} c} = \left[ \frac{1}{Y_{cmax}} \frac{\partial^2 Y_{cmax}}{\partial Z^2} \right] \widetilde{c}^2 \frac{1}{2} C_{\phi, Z} \bar{\rho} \frac{\varepsilon}{k} \widetilde{Z}^{\prime\prime 2}$$

Using the already given closure for the second term one finally arrives at (corresponding to term 6 in Equation B.22 in [1])

$$\bar{\rho} (\widetilde{S}_{ST} c - \widetilde{S}_{ST} \widetilde{c}) = \left[ \frac{1}{Y_{cmax}} \frac{\partial^2 Y_{cmax}}{\partial Z^2} \right] \widetilde{c}^{\prime\prime 2} \frac{1}{2} C_{\phi, Z} \bar{\rho} \frac{\varepsilon}{k} \widetilde{Z}^{\prime\prime 2}$$

In the region where the factor between brackets is negative, the extra term in the variance equation is negative. It is of the same form as the modelled dissipation term and leads to an increase in the rate of dissipation of progress variable variance.



---

# Bibliography

- [1] Charles E. Baukal Jr . *Industrial Burners Handbook*. CRC Press LLC, 2003. ISBN: 0-8493-1386-4.
- [2] Vasudevan Raghavan . *Combustion Technology, "Essentials of Flames and Burners"*. John Wiley Sons Ltd., 2016. ISBN: 978-11-1924-178-2.
- [3] Shakeri A. and Mazaheri K. "Integrated procedure,using differential evolution optimization of rate parameters, for design of small and accurate multistep global chemical mechanisms." In: *Industrial Engineering Chemistry Research* 57(10) (2018), pp. 3530–3544.
- [4] Y.Levy A.A.Perpignan M.G. Talboom and A.G Rao . "Emission modeling of an inter-turbine burner based on flameless combustion". In: *Energy Fuels* 32(1) (2018), pp. 822–838.
- [5] A.Stagni et al. A.Cuoci A.Frassoldati. "Numerical Modeling of NO<sub>x</sub> Formation in Turbulent Flames Using a Kinetic Post-processing Technique". In: *Energy and Fuels* (2013), 1104–1122.
- [6] Lefebvre A.H. and Ballal D.R. *Gas Turbine Combustion: Alternative Fuels and Emissions*. Vol. 3 rd. 2010.
- [7] A.M.A. Rocha A.S. Verissimo and M.Costa. "Operational, Combustion, and Emission Characteristics of a Small-Scale Combustor." In: *Energy Fuels* 25 (2011), pp. 2469–2480.
- [8] A. Di Mauro et al. "Modelling Aspects in the Simulation of the Diffusive Flame in A Bluff-Body Geometry." In: *Energies* 14 (2021).
- [9] A. Kempf et al. "Large-eddy simulation of a bluff-body stabilised nonpremixed flame." In: *Combust. Flame* 114 (2006), pp. 170–189.
- [10] A. Stagni et al. "A fully coupled, parallel approach for the post-processing of CFD data through reactor network analysis." In: *Computers and Chemical Engineering* 60 (2014), pp. 197–212.
- [11] B.B. Dally et al. "Instantaneous and mean compositional structure of a bluff-body stabilized nonpremixed flame." In: *Combust. Flame* 114 (1998), pp. 119–148.

- [12] G. Li et al. "Numerical investigation of a bluff-body stabilised nonpremixed flame with differential Reynolds-stress models." In: *Flow, Turbul. Combust.* 70 (2003), pp. 211–240.
- [13] I. Verma et al. "Flamelet Generated Manifold Simulation of Turbulent Non-Premixed Bluff Body Flames." In: *Proceedings of ASME 2019* 2 (2019).
- [14] K. Liu et al. "Calculations of bluff-body stabilized flames using a joint probability density function model with detailed chemistry." In: *Combustion and Flames* (2005).
- [15] M. Hossain et al. "A combustion model sensitivity study for CH<sub>4</sub>/H<sub>2</sub> bluff-body stabilized flame." In: *Journal of Mechanical Engineering Science* 221(11) (2007), pp. 1377–1390.
- [16] M. Ravikanti et al. "Flamelet Based NO<sub>x</sub> - Radiation Integrated Modelling of Turbulent Non-premixed Flame using Reynolds-stress Closure." In: *Flow Turbulence Combustion* 81 (2008), pp. 301–319.
- [17] M. Ravikanti et al. "Laminar flamelet model prediction of NO<sub>x</sub> formation in a turbulent bluff-body combustor." In: *Proc. IMechE Part A: Power and Energy* 223 (2008), pp. 41–54.
- [18] Masri et al. "Turbulent Nonpremixed Flames of Methane Near Extinction: Mean Structure from Raman Measurements." In: *Combust. Flame* 71 (1988), pp. 245–266.
- [19] *Ansys Fluent theory guide (Release 15.0)*. URL: <http://www.pmt.usp.br/academic/martoran/notasmodelosgrad/ANSYS%5C%20Fluent%5C%20Theory%5C%20Guide%5C%2015.pdf>.
- [20] Falcitelli M. et al. Benedetto D. Pasini S. "NO<sub>x</sub> emission prediction from 3-D complete modelling to reactor network analysis". In: *Combustion Science and Technology* 153(1) (2000), pp. 279–294.
- [21] S.L. Bragg. "Application of Reaction Rate Theory to Combustion Chamber Analysis". In: *Aeronautical Research Council, London*. (1953).
- [22] Gauthier J. Charest M. and Huang X. "Design of a lean premixed prevaporized can combustor". In: *ASME Turbo- Expo 2006: Power for Land, Sea, and Air, American Society of Mechanical Engineers* (2006), pp. 781–791.
- [23] Ferraris G.B. et al. Cuoci A. Frassoldati A. "The ignition, combustion and flame structure of carbon monoxide/hydrogen mixtures". In: *International Journal of Hydrogen Energy* 32(15) (2007), pp. 3486–3500.
- [24] *DIRECTIVE (EU) 2015/2193 OF THE EUROPEAN PARLIAMENT AND OF THE COUNCIL*. URL: <https://eur-lex.europa.eu/legal-content/EN/TXT/PDF/?uri=CELEX:32015L2193&from=EN..>
- [25] Pasini S. Falcitelli M. and Tognotti L. "Modelling practical combustion systems and predicting NO<sub>x</sub> emissions with an integrated CFD based approach". In: *Computers Chemical Engineering* 26(9) (2002b), pp. 1171–1183.
- [26] Frassoldati A. Faravelli T. and Ranzi E.. "Kinetic modeling of the interactions between NO and hydrocarbons in the oxidation of hydrocarbons at low temperatures". In: *Combustion and Flame* 132(1/2) (2003), pp. 188–207.
- [27] Plion P. Fichet V. Kanniche M. and Gicquel O. "A reactor network model for predicting NO<sub>x</sub> emissions in gas turbines". In: *Fuel* 89(9) (2010), pp. 2202–2210.

- [28] Nguyen Thanh Hao and Park Jungkyu. “CRN Application to Predict the NO<sub>x</sub> Emissions for Industrial Combustion Chamber.” In: *Asian Journal of Applied Science and Engineering* 2(2) (2013), pp. 9–26.
- [29] Novosselov I.V. and Malte P.C. “Development and application of an Eight-Step global mechanism for CFD and CRN simulations of lean-premixed combustors”. In: *Journal of Engineering for Gas Turbines and Power* 130(2) (2008), p. 21502.
- [30] F.A.Lammers J.A.van Oijen and L.P.H.de Goey. “Modeling of complex premixed burner systems by using flamelet-generated manifolds”. In: *Combustion and Flame* 127(3) (2001), pp. 2124–2134.
- [31] U.Maas J.Warnatz and R.W.Dibble . *Combustion, Physical and Chemical Fundamentals, Modeling and Simulation, Experiments, Pollutant Formation*. Springer, 2006. ISBN: 10 3-540-25992-9.
- [32] Ommi F. Khodayari H. and Saboohi Z. “A review on the applications of the chemical reactor network approach on the prediction of pollutant emissions”. In: *Aircraft Engineering and Aerospace Technology* 92(4) (2020), pp. 551–570. DOI: [doi.org/10.1108/AEAT-08-2019-0178](https://doi.org/10.1108/AEAT-08-2019-0178).
- [33] Starik A. et al. Lebedev A. Secundov A. “Modeling study of gas-turbine combustor emission”. In: *Proceedings of the Combustion Institute* 32(2) (2009), pp. 2941–2947.
- [34] Marco Mancini. *PHD thesis, Analysis of mild combustion of Natural Gas with preheated air*.
- [35] A.R. Masri and R.W. Bilger. “Turbulent Diffusion Flames of Hydrocarbon Fuels Stabilised on a Bluff Body.” In: *Twentieth Symposium (International) on Combustion, The Combustion Institute, Pittsburgh* (1985), pp. 319–326.
- [36] James A. Miller and Craig T. Bowman. “Mechanism and modeling of nitrogen chemistry in combustion”. In: *Progress in Energy and Combustion Science* 15(4) (1989), pp. 287–338.
- [37] F. Nieuwstadt, J. Westerweel, and J. Bendiks Boersma. *Turbulence: Introduction to theory and applications of turbulent flows*. Springer, 2016. ISBN: 9783319315973.
- [38] Liu G-S. Niksa S. and R.H Hurt. “Coal conversion submodels for design applications at elevated pressures. Part I. devolatilization and char oxidation”. In: *Progress in Energy and Combustion Science* 29(5) (2003), pp. 425–477.
- [39] *Notes of CEFRC summer school-2010, Princeton University, Norberts Peters*. URL: [https://cefrc.princeton.edu/sites/cefrc/files/Files/2010%5C%20Lecture%5C%20Notes/Norbert%5C%20Peters/Peters\\_Summerschool\\_reference.pdf](https://cefrc.princeton.edu/sites/cefrc/files/Files/2010%5C%20Lecture%5C%20Notes/Norbert%5C%20Peters/Peters_Summerschool_reference.pdf).
- [40] *Office of Energy Efficiency and Renewable Energy, U.S. Department of Energy*. URL: <https://www.nrel.gov/docs/fy01osti/29676.pdf>.
- [41] *Official website of the International Workshop on Measurement and Computation of Turbulent Flames*. URL: <https://tnfworkshop.org/data-archives/bluffbod/>.
- [42] Rubin P. and Pratt D. “Zone combustion model development and use: application to emissions control”. In: *American Society of Mechanical Engineers* (1991), pp. 1–41.
- [43] Stuttaford P.J. and Rubini P.A. “Assessment of a radiative heat transfer model for gas turbine combustor preliminary design”. In: *Journal of Propulsion and Power* 14(1) (1998), pp. 66–73.

- [44] Rao AG Perpigan AAV and Roekaerts DJEM. “Flameless combustion and its potential towards gas turbines.” In: *Progress in Energy and Combustion Science* 69 (2018), pp. 28–62.
- [45] Sampat R Perpigan AAV and Gangoli Rao A. “Modeling Pollutant Emissions of Flameless Combustion With a Joint CFD and Chemical Reactor Network Approach”. In: *Frontiers in Mechanical Engineering* (2019). DOI: [10.3389/fmech.2019.00063](https://doi.org/10.3389/fmech.2019.00063).
- [46] Thierry Poinso and Denis Veynante. *Theoretical and Numerical Combustion*. Edwards, 2005. ISBN: 1-930217- 10-2.
- [47] J.J Pretorius. “A network approach for the prediction of flow and flow splits within a gas turbine combustor”. In: *University of Pretoria*. (2005).
- [48] V. Raman and H. Pitch. “Large-eddy simulation of a bluff-body stabilised nonpremixed flame using a recursive filter-refinement procedure.” In: *Combust. Flame* 142 (2005), pp. 329–347.
- [49] Denny R. Rezvani R. and Mavris D. “A design oriented semi-analytical emissions prediction method for gas turbine combustors”. In: *47th AIAA Aerospace Sciences Meeting including The New Horizons Forum and Aerospace Exposition, American Institute of Aeronautics and Astronautics* 14(1) (2009), p. 704.
- [50] Marshall A.W. Rizk N.K. Chin J.S. and Razdan M.K. “Predictions of NO<sub>x</sub> formation under combined droplet and partially premixed reaction of diffusion flame combustors”. In: *Journal of Engineering for Gas Turbines and Power* 124(1) (1999), pp. 31–38.
- [51] Mirmohammadi A. Rostami E. Ommi F. and Khodayari H. “Investigation of the effect of liquid viscosity on the primary break up lengths and droplet diameter and ligament diameter and instability of a swirling annular liquid sheet”. In: *Journal of Advanced Physics* 3(2) (2014), pp. 171–178.
- [52] G. Bourque S. Yousefian and R. Monaghan. “Systematic CFD-CRN Study of Exit NO<sub>x</sub> Emission in a Methane/Air Diffusion Flame.” In: *Proceedings of the European Combustion Meeting 2019* ().
- [53] Ommi F. Saboohi Z. and Fakhrtabatabaei A. “Development of an augmented conceptual design tool for aircraft gas turbine combustors”. In: *The International Journal of Multiphysics* 10(1) (2016).
- [54] Staffebach G.S. et al. Sengissen A.X. Giauque A.V. “Large eddy simulation of piloting effects on turbulent swirling flames”. In: *Proceedings of the Combustion Institute* 31(2) (2007), pp. 1729–1736.
- [55] *Simulation of turbulence flows*. URL: <https://web.stanford.edu/class/me469b/handouts/turbulence.pdf>. (accessed: 16.17.2020).
- [56] A.Frassoldati et al. T.Faravelli L.Bua. “A new procedure for predicting NO<sub>x</sub> emissions from furnaces.” In: *Computers and Chemical Engineering* 25 (2001), pp. 613–618.
- [57] S.R. Turns. *An Introduction to Combustion*. 1996.
- [58] *U.S. Department of Energy (DOE), Industrial Combustion Vision: A Vision by and for the Industrial Combustion Community*. URL: [https://www1.eere.energy.gov/manufacturing/industries\\_technologies/combustion/pdfs/combustion\\_roadmap2.pdf..](https://www1.eere.energy.gov/manufacturing/industries_technologies/combustion/pdfs/combustion_roadmap2.pdf..)

- 
- [59] *United States Environmental Protection Agency, Global Greenhouse Gas Emissions Data*. URL: <https://www.epa.gov/ghgemissions/global-greenhouse-gas-emissions-data>.
- [60] Shao W. et al. Wang H. Lei F. “Experimental and numerical studies of pressure effects on syngas combustor emissions”. In: *Applied Thermal Engineering* 102 (2016), pp. 318–328.
- [61] Hsiao G. et al Wang S. Yang V. “Large-eddy simulations of gas-turbine swirl injector flow dynamics”. In: *Journal of Fluid Mechanics* 583 (2007), pp. 99–122.



---

# Glossary

## List of Acronyms

<b>CFD</b>	Computational Fluid Dynamics
<b>PSR</b>	Perfectly Stirred Reactor
<b>PSR</b>	Perfectly Stirred Reactor
<b>PFR</b>	Plug Flow Reactor
<b>FGM</b>	Flamelet Generated Manifolds
<b>EDM</b>	Eddy Dissipation Model
<b>CFD</b>	Computational Fluid Dynamics
<b>CRN</b>	Chemical Reactor Network
<b>RANS</b>	Reynolds-Averaged Navier-Stokes
<b>NO<sub>x</sub></b>	Nitrogen oxides
<b>DNS</b>	Direct Numerical Simulation
<b>SDF</b>	Steady Flamelet Model
<b>RNM</b>	Reactor Network Model
<b>CO</b>	Carbon Monoxide
<b>GRI</b>	Gas Research Institute
<b>RT</b>	Real Time
<b>LES</b>	Large Eddy Simulation
<b>PaSR</b>	Partially Stirred Reactor
<b>FC</b>	Flameless Combustion
<b>MILD</b>	Moderate or Intense Low-oxygen Dilution
<b>OH</b>	Hydroxyl radical
<b>AGNES</b>	Automatic Generation of Networks for Emission Simulation

## List of Symbols

$\mathcal{D}$	Laminar diffusivity
$\dot{m}$	Mass flow rate
$\eta_k$	Kolmogorov length scale
$\rho$	Density
$\tau$	Residence time
$\tilde{\epsilon}$	Rate of dissipation
$\tilde{k}$	Density weighted turbulent kinetic energy
$k$	Kinetic energy
$l_t$	Integral length scale
$N_s$	Total number of species
$P$	Production rate
$S_{NO}$	Mean Source Term
$Z_{un}$	Unnormalised Mixture Fraction
$\chi$	Scalar Dissipation Rate
$\tilde{U}_i$	Mean velocity
$I$	Turbulence Intensity
$u''_i$	Velocity fluctuations
$U_i$	Velocity
$V$	Control volume
$Z$	Mixture Fraction